Real-time non-intrusive reed valve measurement and analysis

Peter Ralph Collins

A thesis submitted in partial fulfilment of the requirements of Oxford Brookes University for the degree of Master of Philosophy

July 1994

Acknowledgements

I would like to take this opportunity to express my gratitude to the following:

Tony Hern for his consistent support and supervision;

Dr. G. R. Bremble, Head of School and second supervisor;

Roland Broadbent for his original encouragement and assistance;

Paul Allen of the technical staff for his assistance throughout the project.

CONTENTS

ABSTRACT

An experimental and theoretical investigation has been undertaken in which a unique method of position measurement has been developed and used to study the real-time behaviour of reed valves in a two-stroke engine. This sensor has allowed the acquisition of high resolution position data, recorded during *unstable* operating conditions, in a format that is convenient for further analysis. This in turn has provided the opportunity to improve the modelling of reed valves through the development of the forcing function.

The sensor uses active infra-red to achieve non-intrusive position measurement and can be attached in close proximity to the reed valve, enabling high common mode rejection of vibration with a resolution of 0.01mm possible. The sensor underwent back to back evaluation with a recognised video stroboscopic method of reed position measurement during *stable* operating conditions, during which not only was its own integrity established, but also the limitations of the currently recognised method demonstrated. A set of comparative experiments using different reed types in a range of operating conditions were conducted, with observations on the high resolution data reported. The sensor's ability to record the continuous real-time position of a reed in unstable motion resulted in improved modelling of reed valves through a detailed examination of the forcing function and damping parameters.

Nomenclature

The following list defines general symbols, subscripts, notation and abbreviations; specific nomenclature is defined in the appropriate text.

Symbols		Units
α	Starting peak amplitude	-
ζ	Viscous damping	-
η	Structural damping	-
λ	Vibrational constant	m^{-1}
ρ	Reed density	kg/m^3
ϕ	Free vibration mode shape	-
θ	Angle	rad
χ	Arbitrary variable	-
ω_a	Radiancy above mode i	rad/s
ω_1	Radiancy at half power below ωi	rad/s
ω_2	Radiancy at half power above ωi	rad/s
ω_b	Radiancy below mode i	rad/s
A	Reed cross-sectional area	m^2
b	Width of reed	m
C	Damping constant	-
d	Height of reed	m
E	Modulus of elasticity	N/m^2
F	Forcing function	N
f	Frequency	Hz
I	Second moment of area	m^4
j	Attenuating constant	-
k	Attenuating constant	-
K	Spring constant	N/m
l	Length of reed	m
M	Mass	Kg
m	Moment	Nm
P	Pressure	N/m^2
P_{down}	Pressure downstream of reed	N/m^2
P_{off}	Preload offset	N/m^2
P_{up}	Pressure upstream of reed	N/m^2
Q	Shear force	N
t	Time	*s*
x	Distance along reed from pinned end	m
y	Reed displacement	mm
z	Principal coordinate	m

Abbreviations

A/D	Analogue to Digital converter
TDC	Top Dead Centre
ATDC	After Top Dead Centre
BDC	Bottom Dead Centre
BTDC	Before Top Dead Centre
IR	Infra Red
IEU	Instrumentation Enhancement Unit
LED	Light Emitting Diode
PC	Personal Computer
QUB	Queens University Belfast
FFT	Fourier Function Transformer

Subscripts

i	At mode i
n	At the natural frequency of oscillation

CHAPTER 1 - INTRODUCTION

1.1 GENERAL

This chapter briefly describes the history of the two-stroke engine and in particular the key aspects of development that have been important. The contemporary research is reviewed and presented in order to illustrate how the broader, more general topics, relate to those specialist subjects such as reed valves. The relevance of reed valves to current two-stroke applications is explained and some of the difficulties relating to their real-time analysis is discussed. In view of the difficulties of obtaining reliable reed position data for the analysis of their dynamic behaviour, current sensor technology is reviewed in an attempt to identify alternative approaches. Finally, the objectives of the work described in this study are presented.

1.2 THE TWO-STROKE ENGINE: A REVIEW

The invention of the two-stroke engine is generally accredited to Sir Dugald Clerk in the late nineteenth century. However the original 'three port' design (where the piston controlled the inlet, transfer and exhaust ports, and scavenging was achieved through the use of crankcase compression) was patented in 1891 by Joseph Day. Loop scavenging was patented in 1925 by the German engineer Dr. E. Schneurle and it was his design which has had a major influence on most subsequent two-stroke engine development.

Contemporary small displacement designs are based on the more recent innovations by Walter Caaden from the MZ company, who in 1959 introduced an engine with a resonant expansion chamber and disc valve induction control. The abundance of motorcycle, scooter, moped and outboard engines using similar designs is testament to the successful

automotive application of the MZ design. In addition, its ability to operate in any orientation together with its high power to weight ratio has allowed it to dominate the engine choice in hand-held power tool applications. The reasons for its successful widespread application are often masked by the perception that the two-stroke is just a simple design which is easy to develop and manufacture. Whilst this statement may be true for the fundamental power generating mechanism, the gas dynamic processes involved are extremely complex, giving rise to multifarious possible configurations and associated characteristics.

A survey of the published literature relating to gas flow in two-stroke engines revealed that unsteady flow through the entire engine was first analysed by Blair[1]. He used an approach based on the method of characteristics to predict the through flow and hence engine performance. Earlier research had treated inflow and outflow separately.[2,3] Across the last two decades analysis of the complete system has been further developed[4-6] and more recently has been revised by Blair[7] using a new approach based upon a procedural method of mesh interpolation.

The complete system can be divided into three natural areas of study:

(i) The flow of fresh charge through the carburettor and inlet manifold into the crankcase which is generally referred to as "induction".

(ii) The transfer process of fresh charge into the cylinder displacing the residual exhaust charge which is referred to as "scavenging".

(iii) The gas dynamic processes in the exhaust and expansion chamber.

Of these three, scavenging is probably the most complex as it involves the simultaneous replacement of the residual charge by the fresh charge. This would ideally happen without any mixing between the old and new charge; the old charge being expelled without any fresh charge lost into the exhaust. Ideally, perfect scavenging would occur at all speeds and throttle settings. Analysis of the scavenging processes enabled the extent to which the fresh charge successfully replaced the residual gases to be determined. It identified the amount of mixing that occurred between the two and the trapping efficiency which determined the degree of containment of the fresh charge in the cylinder. The effects of these scavenging processes affect other quantifiable parameters such as emissions and thermal efficiency. The efficient use of fuel suffers if poor scavenging with a high degree of mixing and "short circuiting" takes place.[8,9] "Short circuiting" is the term for fresh charge passing directly into the exhaust without participating in the combustion process. This represents the most wasteful use of fuel.[10] Mixing of the fresh charge and residual gases during scavenging results in poor combustion with a detrimental effect on thermal efficiency.[11]

Recent legislation and environmental issues led to more research on emissions, the prime areas of work focusing on short circuiting during scavenging,[10,12] and combustion chamber design[13]. Stratified charging was identified as one way of ensuring that fuel was not lost into the exhaust by short circuiting, because the fuel would not enter the cylinder until the end of the scavenging process.[14,15] An alternative approach was through the use of direct injection, where a fuel/air emulsion was injected into the cylinder after the exhaust port had closed.[16,17]

Research into the unsteady flow in the exhaust system formed an important area of research, not only because it defined the boundary conditions at the exhaust port (required for scavenging analysis), but also because it explained the relationship between the physical geometry of the expansion chamber and the torque characteristics of the engine.[18] The expansion chamber is constructed from two elements which fulfil two basic functions. The diverging section (the diffuser) acts as a wave converter transforming the exhausted pressure pulse travelling down the pipe into a negative pulse which is then reflected back towards the cylinder. This reflected pulse would, ideally, arrive so that it is optimally used in the scavenging of the cylinder. As the exhaust pressure front continues along the expansion chamber it reaches the converging section (the baffle), where the second function is fulfilled. Here the positive pulse is reflected without inversion so that a high pressure wave travels back along the expansion chamber and arrives at the cylinder in time to "plug" the exhaust port. This stops the outflow of fresh charge from the cylinder which is now on the compression stroke.

The gas and thermodynamic processes that are involved with these resonating pressure pulses are extremely complex. Research into this behaviour can be categorized into the pure work,[19,20] which attempted to accurately model the behaviour, and the work which derived simpler empirical relationships for determining basic expansion chamber geometries.[21,22] One branch of this predictive work focused on the acoustic consequences of expansion chamber behaviour where, through legislation, noise performance has come under scrutiny.

Another area of research has been the unsteady flow in the inlet and crankcase which is necessary for defining the boundary conditions at the transfer ports. Most studies focused on the analysis and solution of unsteady flow in the associated pipes, ducts and nozzles. [22-25]

There are other special topics associated with induction that are of interest to researchers. These include the carburation of fuel under unsteady flow conditions[26] and the use of electronic fuel injection as a method of metering the fuel/air mixture, investigation of induction-generated noise and the means of reducing it without affecting performance, [37,28] as well as the mechanisms of flow control between the inlet manifold and the crankcase.

It is these mechanisms of flow control which are of most interest in this study and are discussed in more detail in the next section.

1.2.1 TWO-STROKE INDUCTION MECHANISMS

In the contemporary small displacement designs mentioned earlier, there are three types of induction mechanism:

(i) The piston-ported system.

(ii) The disc valve system.

(iii) The reed valve system.

The simplest method of allowing fresh charge into the two-stroke engine is by the movement of the piston exposing ports in the cylinder wall which allow direct flow into the crankcase, this is called piston-porting. The timing of a piston-port is symmetric about

Bottom Dead Centre (BDC) and the port has no ability to stop reverse flow. The large port time-areas required for high power also tended to cause 'peaky' torque curves because of the poor trapping efficiency at low speed. Better control of the fresh charge is possible with the disc valve, a spring steel or phenolic disc connected to the crank, in which an aperture aligns with the inlet manifold to open the port when the crankshaft is in the desired position. The resultant port timing could be asymmetric about BDC giving a significantly improved torque curve since reverse flow is minimized. This represents a big improvement over the piston-ported configuration. However, this system of induction control still has two limitations, firstly the valve timing is fixed with respect to speed and load, and secondly the disc needs to be located on the end of the crankshaft associated to each cylinder. For multi-cylinder designs this becomes a restricting factor.

The reed valve is an automatic demand-operated valve with infinitely variable valve timing which can optimise itself to suit the fluid dynamic conditions. Reed valves have enjoyed widespread use in compressor design throughout the twentieth century and were first used in two-strokes in outboard motors. In the late seventies they were introduced into motorcycle engines. Figure 1 overleaf shows a typical reed valve, designed as a wedge-shaped block with either spring steel or composite material used for the reed petals. The reed valve functions as follows: with no pressure differential across it, the valve is kept closed by the spring stiffness of the reed. A negative pressure gradient keeps the reed closed against the sealing surface, whilst a positive pressure differential will oppose the reed stiffness and allow it to open. Once open, flow can occur through the valve.

An ideal valve would be one which opened and closed instantaneously when a positive or negative gradient was sensed. Unfortunately there is a finite time for such a valve to close, during which undesirable reverse flow may occur. Flow through the valve should have no resistance, but since the open valve forms a nozzle, the discharge coefficient is less than unity. As a result a design compromise had to be reached. To achieve high coefficients of discharge, a reed with a low spring stiffness is required. For fast closing, a reed with a high stiffness to weight ratio would be necessary.

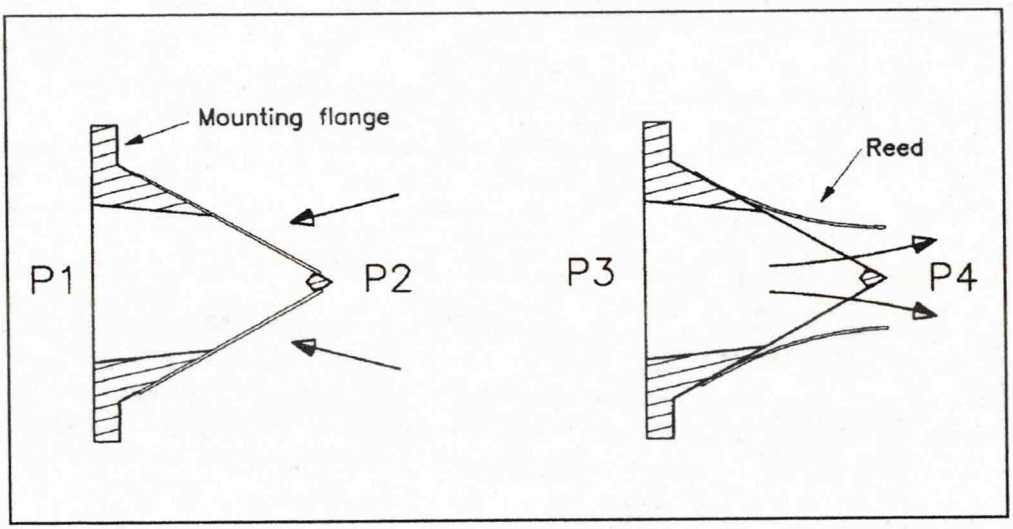

FIGURE 1 - Reed valves shown in the open and closed position. Left with pressure (P)1 less than P2, the reed valve is held closed by the spring stiffness and the pressure difference. Right with P3 greater than P4, the spring stiffness of the reed is overcome and flow through the valve will occur.

In some applications such as a reciprocating compressor there is no need to compromise the design, for example, when operating at 600 rev/min, a reed with a natural frequency of 200 Hz (12000 rev/min) would close within 4.5 degrees of engine rotation under its own

spring action. In a high speed two-stroke working at 12000 rev/min (the same as the reed's natural frequency) it would take 90 degrees to close. In practice the reed would be forced closed during the period of reverse flow.

Observation of reed valve motion in a working engine is of considerable benefit in improving the understanding of factors affecting reed performance, however, achieving this in the hostile environment of a firing engine has in the past, proved to be difficult.

1.3 REED VALVES: A REVIEW

Some of the benefits of reed valves over piston-ported designs were demonstrated by Blackwell[29] who showed that by converting piston-ported designs to reed induction he could improve the performance at both low engine speeds and at part throttle. This was of significant use in the consumer motorcycle market because by flattening the torque curve, the two-stroke motorcycle became much more rideable and therefore more commercially acceptable. Although Blackwell provided a general model for describing the unsteady flow through the engine, no specific model for the reed was included. Krieger[30] had made the first attempt to model reed valves in two-stroke engines in 1969 by considering the reed as a sprung mass with a single degree of freedom. However this did not produce a close correlation between the theoretical and experimental results. In 1967 during work on reciprocating compressors, Wambsganss and Cohen[31] considered the reed to behave as a simple cantilever.

Studies on reed valve modelling in two-stroke engines (assuming cantilever behaviour) were published by Hinds[32] and Blair[33] who built on the significant engine modelling done in Belfast earlier by Blair and Cahoon.[34] Blair and Cahoon had investigated and modelled unsteady gas flow through the induction systems of high specific output two-stroke engines, but had not included any consideration of engines that used reed valves. Together Hinds and Blair developed a mathematical model which represented the reed valve/crankcase boundary that could then be included in the general engine model. They too, considered the reed as a simple cantilever. Their investigation used an engine simulator to allow reed position to be recorded photographically using discrete photographs and high speed cine-film. Their theoretical approach took into consideration the shape of the reed as it lifts off the valve seat, and concluded that it was the superposition of the separate modes associated to the reed vibrating naturally as a cantilever beam. They concluded that the model provided a basic correlation under uncomplicated simulator conditions between predicted and pseudo-real reed position.

Blair and Hinds[33] also compared several thicknesses of steel reeds and their corresponding performance against the piston-ported design. This work showed that thin reeds "flutter" at high speeds, whilst thick reeds remain stable and that thin reeds have a good delivery ratio at low speed, unlike thick reeds whose stiffness had a detrimental effect on the flow performance. Essentially this reflected the fundamental conflict in the design parameters, i.e. high speed stability was compromised with low speed flow. They also demonstrated that if a piston-ported engine had port timing that was sufficiently conservative so as to preserve low speed performance, it could not be improved with reed valve induction.

The next significant development in reed analysis came out of the Yamaha Motor Co. Ltd., from its researchers Hata *et al.*[18] To improve part throttle performance in reed valve engines, they used a video stroboscopic technique to record reed motion in a firing engine. Their methods allowed far faster analysis of data, although it relied on stable reed operation and on the averaging of many cycles to give lift information that was representative of general reed behaviour.

This technique was used and improved specifically for reed valve research by Fleck *et al.*[35] To assist data analysis, a circle of a known diameter was used as a reference dimension against which reed lift could be compared using an imaging processing system. However, this system of reed measurement was still restricted to stable cyclic regimes, and the frequency of data was still limited by the frame speed of the video camera. This method also required manual involvement in taking measurements. An interactive imaging process was used to measure the position of the reed tip on the video monitor for every data point logged. It demonstrated the cyclic variation of the reed even under the stable operating conditions of the simulator. The "actual" lift positions showed erratic and instant position changes which would have represented reed jerks of some significant magnitudes, but there was no corresponding real-time pressure data to coincide with this lift detail (see Figure 2 overleaf). Cyclic variation would cause jitter in the stroboscopic construction of a pseudo-real lift profile. This study by Fleck *et al.*,[35] also compared performance data from a range of steel and composite reeds with both plain and tapered profiles and demonstrated for the first time that improvements in performance could be gained with the use of composite materials.

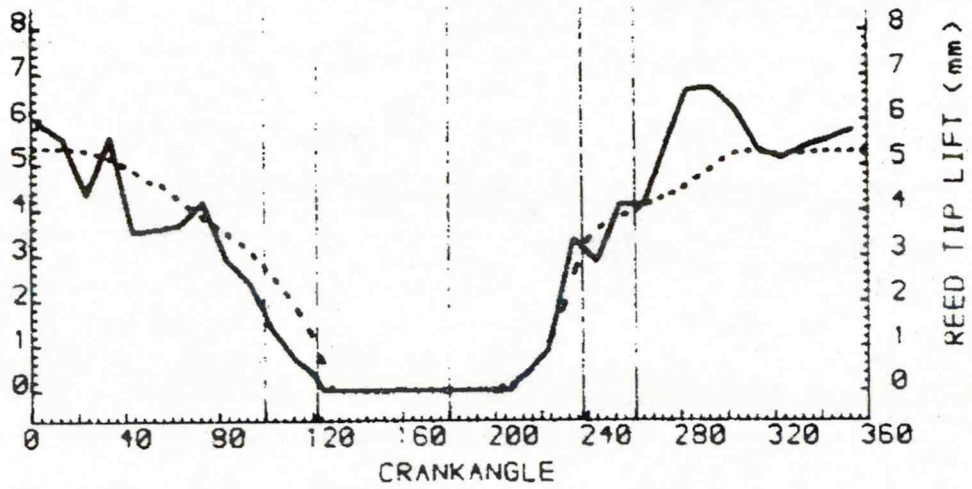

FIGURE 2 - Measured reed lift showing "instantaneous" changes in reed direction as a result of cyclic variation during stroboscopic filming. The dotted line represents the predicted reed position. (Reproduced from Fleck *et al.*[35])

In addition to the experimental work, Fleck and his co-workers made three main modifications to the theoretical model of the reed, these were:

(i) Simplification of the forcing function by considering the force on the reed to be the product of the reed area and the pressure differential across it. This was found to be as accurate as splitting the reed into incremental areas which was a method earlier developed at QUB by Hinds[32] in his Doctoral thesis.

(ii) Inclusion of algorithms to predict reed rebound from the stops.

(iii) Adjustment of the model to allow the use of tapered reeds.

The most recent work published on the function of reed valves has come from researchers working at Alpha Lancia in Italy,[36] who studied the possibility of reed valves improving the

torque characteristics of four-stroke engines by placing a reed valve assembly directly upstream from the inlet valves. This design resulted in no loss of torque within the power band and up to a 30% improvement was achieved in the mid-range torque. This was as a direct result of the reeds blocking any reverse flow during inlet and exhaust valve overlap, where previously, pollution of the inlet charge would normally have occurred. These researchers evaluated and optimised the design feasibility using a fluid-dynamic modelling package called "SASP".

1.4 POSITION SENSOR TECHNOLOGY: A REVIEW

In light of the previously described difficulties involved in obtaining reliable reed position data, it was useful to review the sensor technologies which may have been possible to adapt for direct real-time reed position measurement. The previously published methods used to measure the position of a reed valve have all been photographic techniques, where images of the reed in subsequent frames are used to construct the dynamic position profile. These are indirect methods of measurement.

A direct method of measurement would use a sensor whose output directly indicated the position of the reed. The position of the reed can be considered as a deflection or movement from a rest position. Strain gauges and accelerometers are able to measure deflection and motion but they would modify the behaviour of a delicate structure such as a reed. Proximity sensors, including laser measurement devices, can measure position without affecting any of the structures. Current systems however are generally large and expensive and although cheaper systems are available they have a limited bandwidth.

There are three main sensor technologies that are applicable for low cost proximity sensing or measurement. A good detailed review of these technologies is given by C. Loughin.[37] These are the inductive, capacitive and photo-electric sensors. Each will be briefly discussed here and the mechanisms of detection described.

1.4.1 INDUCTIVE PROXIMITY SENSORS

An inductive proximity sensor can be used to detect conductive materials in which eddy currents can be generated. A coil is energised with an alternating current, generating an associated magnetic field that emerges from the coil axis (Figure 3). If a piece of conducting material is placed near the end of such a sensor then the lines of magnetic flux induce circular eddy currents in the material. These eddy currents dissipate resistive energy which is provided by the oscillating source. As the target is brought closer to the sensor, the load current increases with the strength of the magnetic field.

A circuit that can then measure the changes in load on the system can provide a signal with a relationship between load and the distance between the target and the sensor. The sensitivity of an inductive sensor is dependent on the size and material of the target, the power of the coil and the orientation of the target to the sensor. The range of the inductive sensor is typically up to 20mm. Inductive sensors are not suited to reed valve measurement since they are sensitive to both electrostatic and magnetic fields, more generally they would not work with composite reeds.

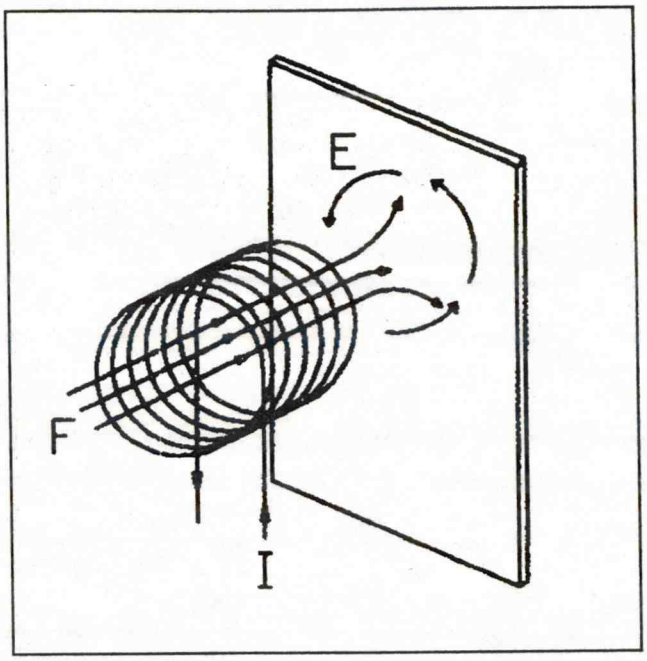

FIGURE 3 - Current (I) flowing in the coil generates a magnetic field (F) flowing through its axis. If a conductor is brought within this field circular eddy currents (E) are generated which load the coil as they dissipate resistive energy.

1.4.2 CAPACITIVE SENSORS

Capacitive sensors are similar to inductive sensors but they use a modulating electrostatic field rather than a magnetic field. They are sensitive to a wider range of materials and are useful up to 100mm. A capacitor is made up of two charge-coupled electrodes normally referred to as plates which are separated by an insulating dielectric. The capacitance changes according to the size of the plates, the distance between them and the permittivity of the dielectric. A capacitive sensor is made by energising an electrode (which forms one capacitor plate) with an ac voltage and uses the target object as the other plate, the air gap or other non-conducting fluid acts as the dielectric. Circuits then measure the capacitance of the system and can sense the target object as it approaches. The capacitance between the plates is inversely proportional to the distance between them.

Capacitive sensors are sensitive to most materials and are consequently affected by the

surrounding environment. Their sensitivity also depends on the target material, metals having ten times more capacitance per unit volume than oil or plastic. The capacitive sensor is sensitive to magnetic and electrostatic fields and changes in temperature and humidity. It is also difficult to make capacitive sensors directional. For these reasons this technology is unsuited to reed valve measurement.

1.4.3 PHOTO-ELECTRIC PROXIMITY SENSORS

Photo-electric sensors function by detecting the presence or absence of light. The material of the target is not important, only its ability to reflect or block light. The photo-electric sensor requires a transmitter and a receiver and at the time of this study, the cheapest source of which, were semi-conductor devices. The transmitters being light emitting diodes (LEDs) and the receivers photodiodes or phototransistors. The intensity of the received light is the sensed variable and it is necessary to use a modulated source or pulse code to reject the effects of strong background light. There are four basic types of photo-electric sensor, the first three, the through beam, the retro-reflective and the fixed focus are go/no go sensors in that they are intended to detect only the presence or absence of the target object. These operate by sending out a beam of light which arrives at the receiver either by continuous line of sight (the through beam), or by prismatic reflection (the retro-reflective), or by focused reflection (the fixed focused). The receiver indicates whether this light is present, which in turn determines whether a target is present or not, depending on the application. Fixed focus sensors usually worked up to 20mm, the retro-reflective up to 2m and the line of sight sensors up to 20m. The fourth type, the diffuse-reflective optical sensor, measures the amount of light reflected from the surface of the target objects (Figure 4 overleaf).

For a proximity switch a threshold is set above which the target object is recognised as being present. In this fundamental state the received signal strength is a function of the surface colour, type and size. These sensors are used extensively in process control where the variable parameters are defined, but are not directly suitable for applications where a linear relationship between sensor output and target distance is required. The large separation possible between sensor and target, coupled with flexibility of application, suggested that these sensors were the preferred choice for pursuing a linear system such as that required for the measurement of reed position.

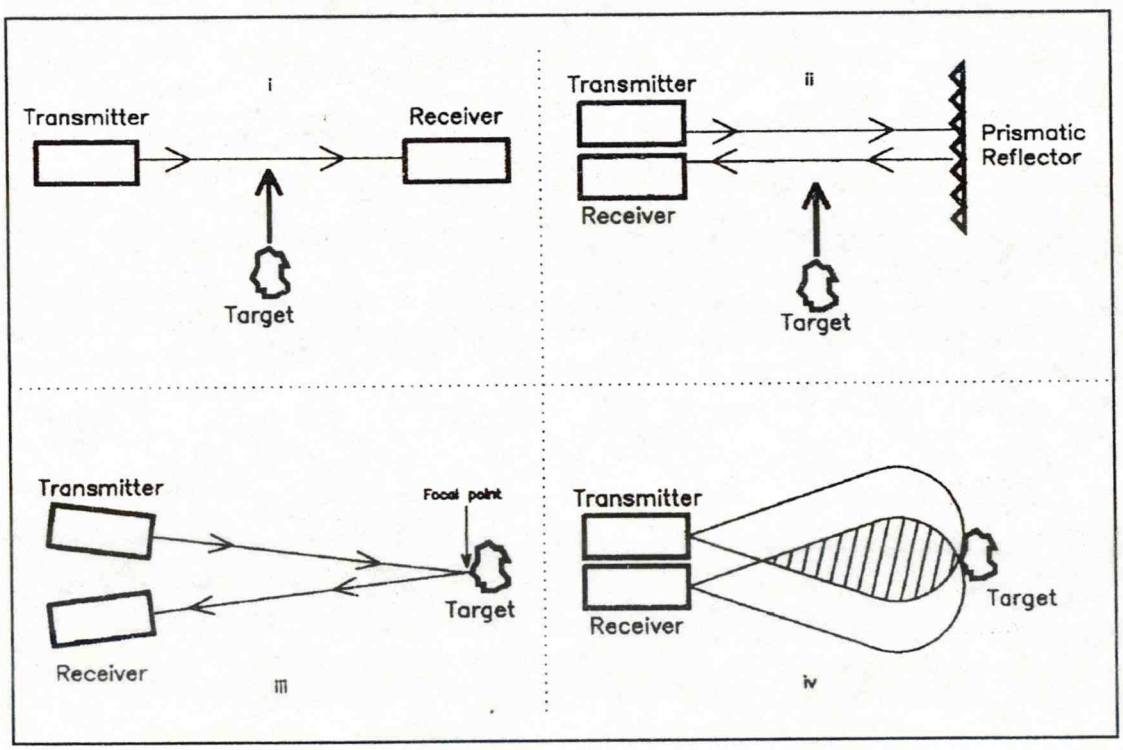

FIGURE 4 - (i) The through beam, (ii) the retro-reflective sensor, (iii) the fixed focus sensor and (iv) the diffuse-reflective sensor.

1.5 SUMMATION AND OBJECTIVES OF THIS STUDY

The survey of the literature revealed that there was room for improvement in the techniques used for reed valve position measurement. Existing techniques, while providing useful information, yielded data with a number of discrepancies. Accurate real-time measurement of reed valve motion should aid understanding of their operation, their influence on engine performance and assist in their development, especially in the unsteady operating regime if such data could be obtained.

The use of a real-time technique for position sensing that could couple directly to a data acquisition system would allow fast analysis and comparison of different designs. Automating this part of a previously time consuming activity would speed up the iterative loop in optimising the analysis of any particular reed design or the development of a reed model.

A survey of appropriate sensor technology suggests that a non-intrusive technique based upon optical proximity technology offered the most hopeful solution. A dedicated, optical based sensor system would have advantages of small size, low cost and flexibility over any proprietary system. It was also felt that such a sensor design could have subsequent commercial benefit and that this application offered a good development opportunity.

An analysis of the existing modelling techniques had shown that a critical issue in modelling reed behaviour was the establishment of the forcing function. Existing studies of reed motion use a forcing function derived from up- and downstream pressures in an

arbitrary manner. Accurate real-time reed position data in conjunction with pressure data would enable a much better understanding of the forcing function and it's effect on reed motion.

As a consequence of the previous analyses it was decided to undertake a program of work with the five main objectives summarised below:

(i) To develop a low cost position sensor capable of measuring reed position in real-time and to acquire this position data in an electronic format, suitable for subsequent computer manipulation, at a frequency of at least every one degree of crank rotation.

(ii) To validate the sensor output by comparison with a recognised procedure for measuring reed valve position.

(iii) To measure and acquire the pressure difference across the reed whilst in unstable operation so that a more accurate model of dynamic reed motion could be developed.

(iv) To use the sensor's real-time output to obtain modal damping and frequency data from out-of-engine bench tests.

(v) To use the sensor to compare the performance of different reed types in a firing engine.

CHAPTER 2

POSITION SENSOR DESIGN AND DEVELOPMENT

2.1 GENERAL

It was decided that a device for measuring reed valve position in a firing engine should include the following specification:

(i) The sensor had to be non-intrusive.

(ii) It had to be small enough to mount in the most restrictive of positions.

(iii) It had to be immune to high levels of vibration and temperature.

(iv) A wide bandwidth would be desirable to maximize its application.

As previously discussed, it was felt that this specification could be met by using an optical device. In order to pursue this approach, a review of reflective photo-electric technology was undertaken.

2.2 REFLECTIVE PHOTO-ELECTRIC REVIEW

The fundamental reflective photo-electric theory has been presented in texts such as that by Victor Noviski,[38] and the important elements and conclusions are summarised below.

If a light source radiates towards an object, there are two possible mechanisms by which the incident light will be reflected. In the first, "specular reflection", incident light is reflected at an angle equal to the incident angle but in the opposite direction. The second is known as "Lambertain reflection" after Heinrich Lambert who first characterised it. This is defined as the diffuse reflection of residual light after a surface has absorbed and dissipated some of the light energy as heat. Diffuse reflection has an intensity of reflection which is a function of the viewing angle (see Figure 5 overleaf).

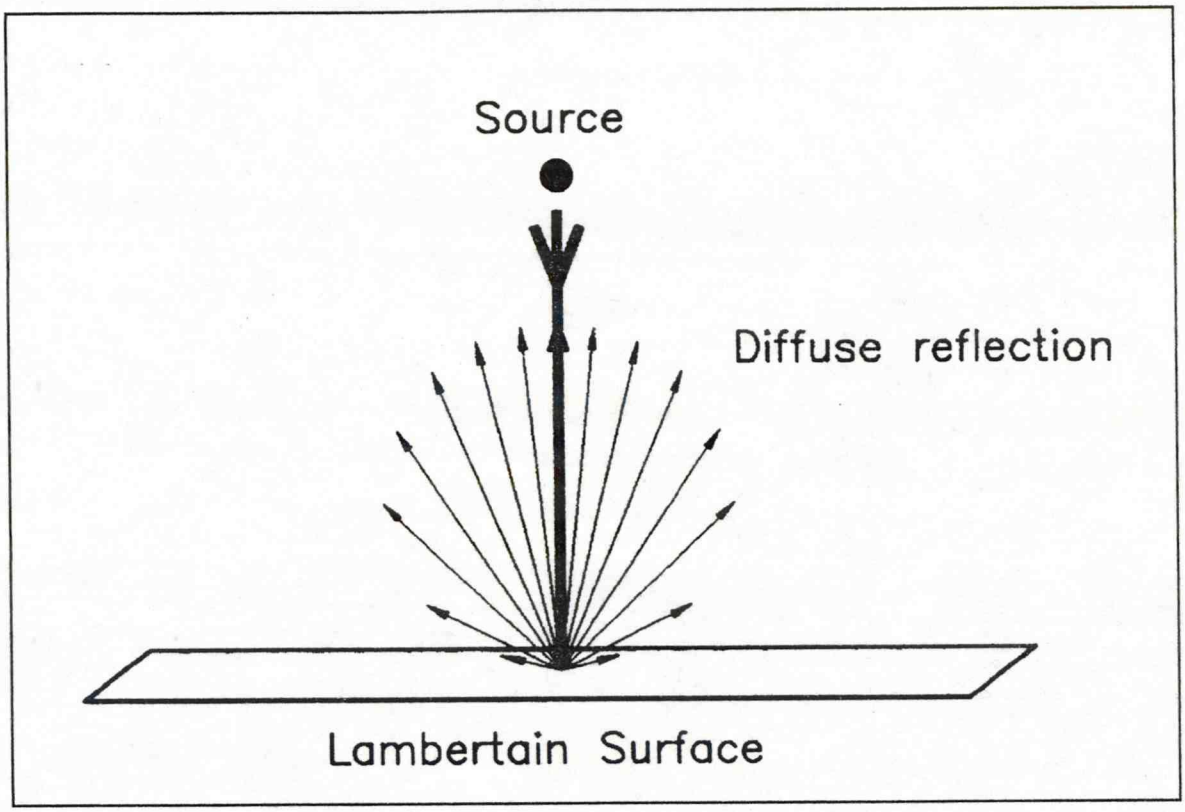

FIGURE 5 - Lambertain reflection. When a radiant source is incident upon a diffuse (Lambertain) surface, light is reflected in all directions from the microscopic surfaces that make up the outside layer. The intensity is highest directly above the incident point and reduces with the apparent surface area, when viewed from an angle.

Most surfaces will display all of these properties to some degree. Three examples which demonstrate the extremes are:

(i) A common mirror which will reflect 80% of light specularly and give 10% Lambertain reflection whilst the remaining 10% is absorbed.

(ii) A piece of white matt paper will give a dominant diffuse Lambertain reflection of 95% and will absorb the remaining 5%.

(iii) Brushed aluminium will give both specular and Lambertain reflection levels of 20% whilst it absorbs the remaining 60%.

Lambertain reflection was the most suitable quantity to measure as it was less dependent on target orientation, although it did vary according to the different surface properties.

Two methods of achieving an output position function that is independent of surface type have been proposed. The first by Okada and Rembold[39] was a mechanical solution, where a position was found on a spinning disc, such that the correct geometric relationship between a spiral slot and a light source existed, so that radiated light passing through it struck the target surface directly normal to the receiver. The angular position of the disc determined the distance of the target object from the receiver (see Figure 6). A second method proposed by Paul Regtien[40] had no moving parts but used two receivers, one closer to the target than the other. Whilst different surfaces give different reflected light intensities, he demonstrated that the ratio of one measured signal to the other determined a characteristic function with distance for any diffuse surface. Unfortunately this was a non-linear relationship which would require calibration for each geometric possibility. Regtien recommended that the division of the two signals was best done digitally with a microprocessor system.

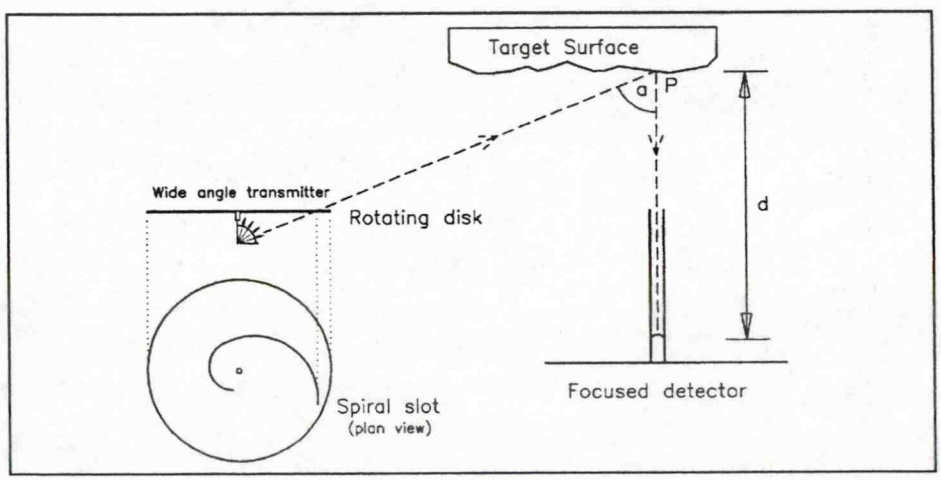

FIGURE 6 - Okada's linear solution, at distance "d" from the sensor. The target surface at point "p" forms a unique angle "a" with the transmitter source. There is only one position of the disc where light can pass uninterupted through the slot. The angular position of the disc directly represents the distance between the target surface and the focused detector.

Whilst the two systems demonstrate two possible ways of designing a proximity sensor with a linear output, they cannot directly be applied to the measurement of reed valves. The disc system would have to rotate once for every data point. So in order to obtain one degree interval data, when the engine was running at 10000 rev/min, it would have necessitated an impractical speed of 3600000 rev/min. Therefore such a system would only be useful for the detection of slow moving objects where the position information required was to define where an object *is*, rather than continually sense *how* it is moving.

Paul Regtien's proposal of two receiving elements which needed to be placed apart, would not be convenient for measuring reed valve position nor would the independence of object colour be essential since the reed valve would have a defined colour and surface texture.

2.3 THE POSITION SENSOR

It was felt that infra-red (I.R.) light emitting diodes and silicon photodiode receivers similar to those commonly used in T.V. remote controls, were an ideal source of cheap front end optical hardware. The simplicity of the infra-red LED and photodiode had the following advantages:

(i) Their small size and mass made them easy to attach to a complicated structure.

(ii) As the sensor could be attached directly to a structure, common mode signals affecting components under observation within the structure, such as vibration, would be significantly reduced.

(iii) These sensors had a high bandwidth.

If I.R. is transmitted toward an object, the intensity of the light reflected would be a function of its size, its reflectivity (both colour and shape) and its distance from the source. Unfortunately the relationship with distance is non-linear. The function relating distance with reflected light contains terms that are inversely proportional to the fourth power of the distance between sensor and target.

To generate a linear and calibrated signal from this non-linear relationship would require extremely complex data processing hardware. However, it was felt that if the signal was digitised it could be easily processed using a computer. Consequently, it was thought that by coupling the flexibility of a simple front end with the data processing ability of an existing small computer, it should be possible to develop a system that was both powerful and cheap. When measuring the position of reed valves there is only one degree of freedom and only a single object with consistent optical characteristics under observation at any time. Consequently, some of the general problems associated with the sensor's non-linear behaviour would not apply in this application.

As a result the magnitude of the output from the sensor would be a direct function of the distance between the sensor and the object. To linearise the sensor, a look-up table was used. The data required for this array was predetermined from a static calibration procedure. This procedure needed to be repeated for any change in the variables, but it was neither complicated nor time consuming.

2.4 POSITION SENSOR DESIGN AND DEVELOPMENT

A prototype circuit for the sensor was constructed which consisted of four sub-units: the optics, the null stage, the amplifier and the filter. The design and circuit description along with the circuit diagrams can be found in Appendix 1. Having developed a prototype, its performance was evaluated and some time spent considering ways to improve it before the experimental program commenced.

One of the aims during development was to maximize the signal to noise ratio, since this would improve the resolution of the instrument. Two ways of achieving this were tried:

(i) Increasing the magnitude of the optical signal being measured.

(ii) Reducing the amount of noise entering or generated in the system.

2.4.1 INCREASING THE OPTICAL SIGNAL

Three modifications were made to improve the signal strength:

(i) Originally the reed was painted with unreflective black paint, with a small reflective spot painted as shown in Figure 7a. This provided a highly reflective but diffuse surface necessary to provide immunity to signal changes resulting from any slight angular variations in the target orientation. A much larger reflective area was used to indicate the position of the reed, so the whole of the reed tip was painted white resulting in an increase in signal strength that was proportional to the increase in surface area (by a factor of 5). This gain in signal was achieved without any increase in the background noise.

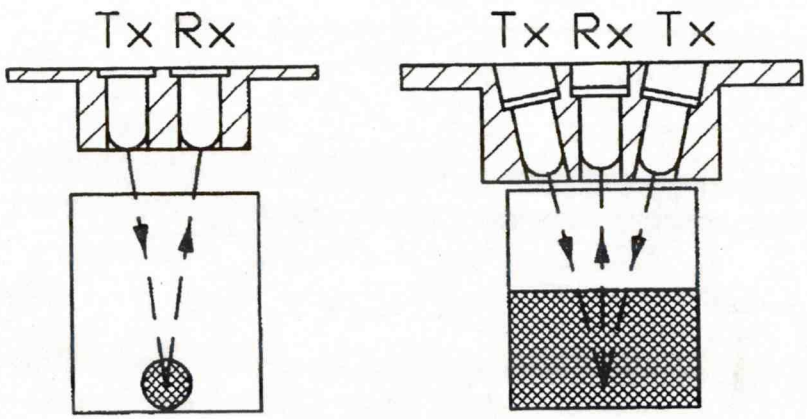

a b

FIGURE 7 - The original optical arrangement (a) showing the single spot painted on the reed tip and the final arrangement (b) with the whole of the reed tip painted.

(ii) By pointing the optics (LEDs) to a place on the closed reed, instead of mounting them parallel to each other, the linearity of the sensor was improved. This resulted from the light going out of focus as the target approaches, attenuating the signal. This modified the distance to signal-strength function to oppose some of the non-linearity from the fundamental distance/signal-strength relationship.

(iii) The original infra-red source was picked because it was suitable and commercially available. In preliminary trials the transmitter was operated at a conservative power level of 100mW. Any increase in transmitted power increased the noise performance by the same margin. The original transmitter was replaced by a high power, high efficiency variant and two were used instead of one (doubling the output). The output power per device was increased to 200mW (the maximum specified limit).

Together these changes increased the amount of received I.R. by a factor of 20 making a significant improvement in the performance. The design was rebuilt using surface mounted components, reducing its size and enabling it to be housed in a small machined assembly (see Plate 1 below).

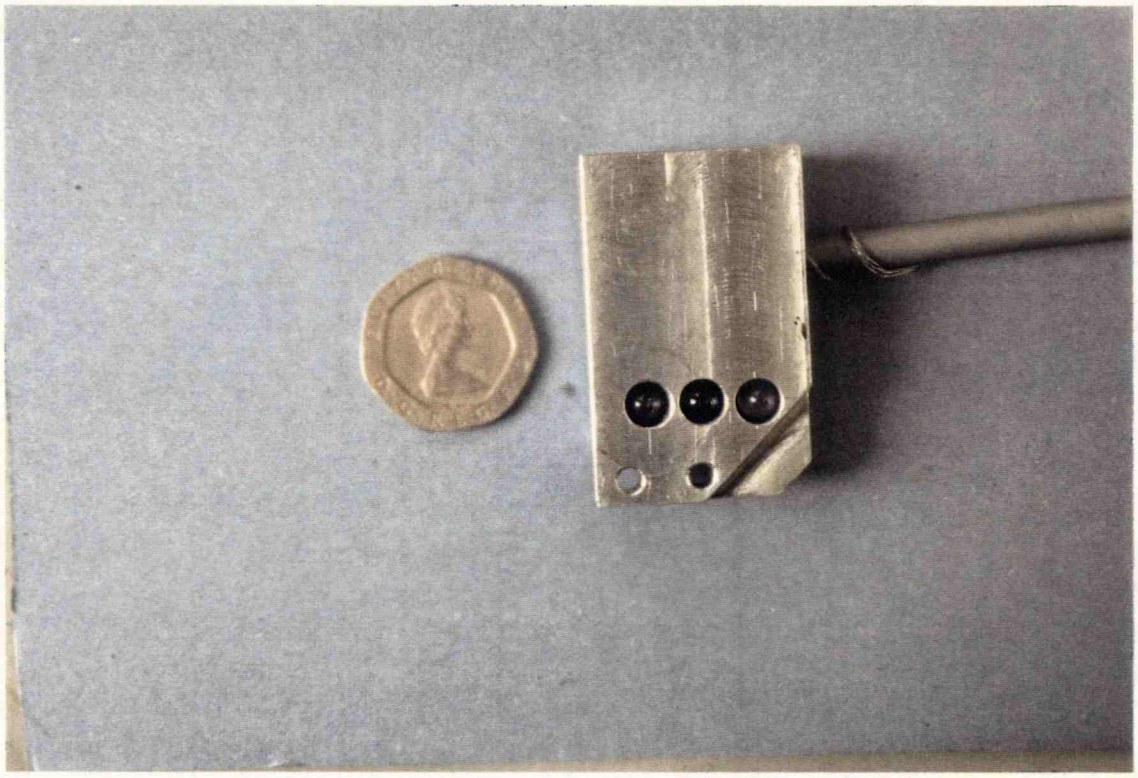

PLATE 1 - The new position sensor showing a central receiver photodiode between two focused transmitters.

2.4.2 REDUCTION OF NOISE

Noise occurred from three sources, electrical, optical interference and differential vibration. These needed to be quantified and any possible improvements incorporated. Electrical noise occurred from both internal and external sources. The system was dc-coupled and damped by the low pass filter stage, consequently, the internal noise generated was less than 1mV

which after calibration equated to a position uncertainty of 0.002mm.

External noise was generated in three different ways, by line noise and both capacitive and magnetic coupling. Line noise was limited by careful connection of the ground lines and optimisation of the sensor signal paths. Coupled noise was caused by changes in the electric or magnetic fields surrounding the sensor. In the engine environment the worst source of such field changes was the ignition system, since this generated the highest rates of change in voltage and current. To limit this interference the ignition was enclosed and blanketed in conductive material to restrict the radiation, and the sensor was shielded to reduce penetration. Differential vibration (movement between the sensor mountings and the target under observation) was determined by obscuring the moving target with a fixed target. Any differential vibration would have been recognised as change in distance from the fixed target to the sensor. To quantify this, the reed stop was replaced with one lacking an aperture and the differential vibration was found to generate the equivalent to 0.005mm of error signal. This amount of differential vibration would not contribute significantly to measured error.

Two main sources of optical noise were considered to exist:

(i) Background ambient light from the laboratory.

(ii) Light from the combustion flame, since it could have a reflective path through the boost port.

Each source had the potential to cause a different type of signal corruption. Background light could affect the lift/signal-strength function as this was defined once during calibration consequently data corruption could have been caused during tests from different levels of background lighting. This error was measured by blacking out the sensors and measuring the

signal difference which equated to 0.08mm. The real error levels were not as large as this, as tests were not carried out under such large changes in ambient lighting. Flame-induced signals on the other hand, would have been cyclic and could modify the measured lift profile. This was easy to quantify by running the engine with the transmitters in the sensor switched off. Any cyclic optical signals would have come from the flame source and be evident by its correlation with the boost port being open. In practice this concern was unfounded since there was no evidence of any such noise in the measurements. All background optical noise was reduced with the use of an optical "daylight" filter which excluded all visible light within the receiver device and in the sensor. Painting all surfaces, other than those under observation, matt black also reduced any ambient reflections.

2.5 THE POSITION SENSOR SYSTEM

Having developed the position sensor it was interfaced with other hardware to complete the sensor system, which was subsequently used extensively throughout the experimental work. This consisted of the newly developed sensor, Microlink data acquisition hardware and an IBM Personal Computer (PC). An instrumentation schematic and full details of the instrumentation system are given in Chapter 5.

The sensor provided an analogue signal which was a function of the distance between the optics and any object in their focus. This signal was converted to a digital signal using a 12 Bit Analogue to Digital converter (A/D). The sampling rate could be as high as 100kHz which was controlled by either the internal time-base or an external clock source such as the output from the three degree shaft encoder, attached to the crankshaft of the engine. The digital data

digital data was stored on instruction in the memory of the data acquisition system which was then down-loaded onto the PC using an IEEE protocol. Once resident in the PC, the data could be manipulated and further processed.

2.6 THE APPLICATION OF THE ANALOGUE OUTPUT

The output from the sensor was non-linear with large changes in the signal. However, with very small signals (less than 1mm) changes could be treated as if they were linear (see Figure 8 below). The direct output was analogue and consequently the bandwidth and displacement were not restricted by the sampling rate or quantization error associated with analogue to digital conversion.

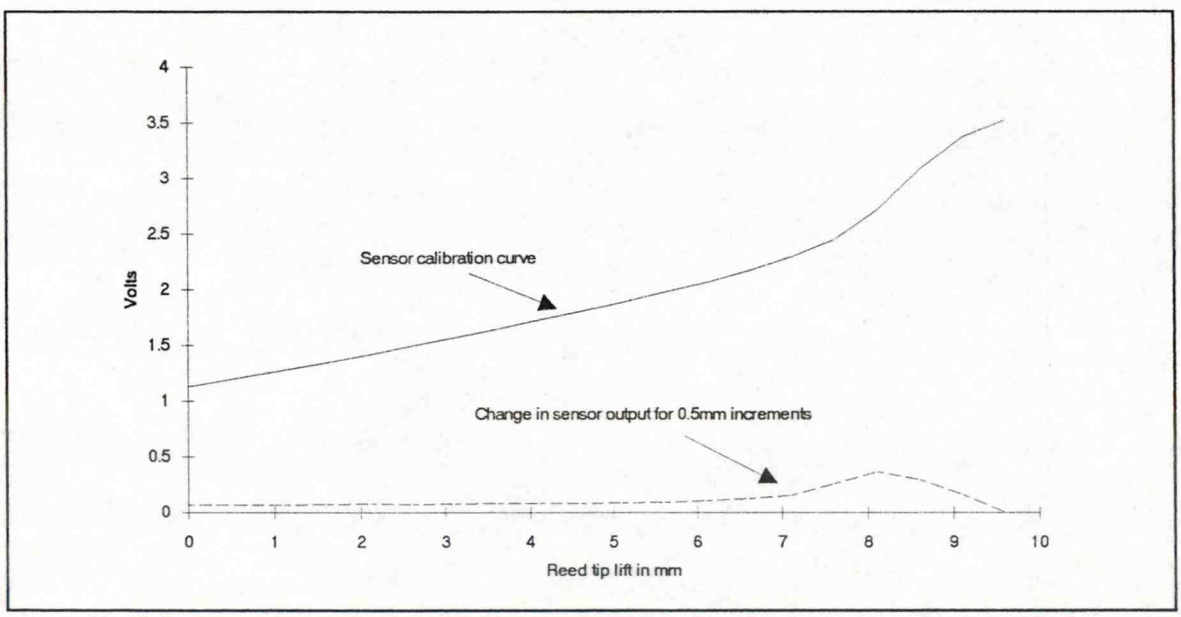

FIGURE 8 - Shows the calibration curve for the sensor. For reed lift of up to 5mm very small changes in position can be considered to give a linear output.

In this program of work, the direct output was used for modal analysis, analysis of the decay of free vibration and also for the measurement of the natural frequency of free vibration ($f_{(n)}$). This was possible since the non-linearity of large signals was irrelevant because the frequency of peak amplitudes was the measured parameter. The time domain data was linear and this method of determining $f_{(n)}$ was an easier empirical alternative to the theoretical calculation of $f_{(n)}$ from density, size and Young's modulus. It also allowed Young's modulus to be calculated for an unknown material, purely from size and mass.

2.7 LINEARISATION AND CALIBRATION

For general application the output had to be linear. The most practical way to linearise the output was to generate a function or look-up table for the displacement output relationship and to use this to operate on all test data. This was not attempted in real-time because of the limitation of the maximum data processing speed. Instead, the data was stored electronically using high speed data acquisition hardware, and when required each data file was processed using the linearisation algorithm. The incorporation of this linearisation routine into the preliminary data manipulation programs was a convenient solution.

2.7.1 PROCEDURE FOR SET-UP

Before the system was calibrated it was advantageous to set it up for maximum resolution. The reed was moved into the closed position. The gain control was set to a maximum and the null adjustment set to give an output that represented zero signal on the analogue to digital converter (either 0 or -5 volts). The reed was moved to the fully open position and the gain adjusted so that the output was equal to the maximum voltage of +5 volts. All dynamic

positions of the target during the test generated outputs that fell between these limits, which maximized the resolution of the analogue to digital (A/D) converter. The A/D converter was a 12 Bit device which gave 4096 discrete position possibilities through the sensors working range.

2.7.2 PROCEDURE FOR CALIBRATION

As the system was dc-coupled, static positions of the reed gave the same output as the same position during dynamic operation. Consequently, calibration was possible by multiple static measurements. In practice, a static data set was taken with 20 points representing the likely full scale deflection. The reed block was supported in a Perspex manifold, to which the position sensor was mounted and a special reed stop was machined with an aperture through which the sensor had optical access to the reed tip (see Figure 9 below).

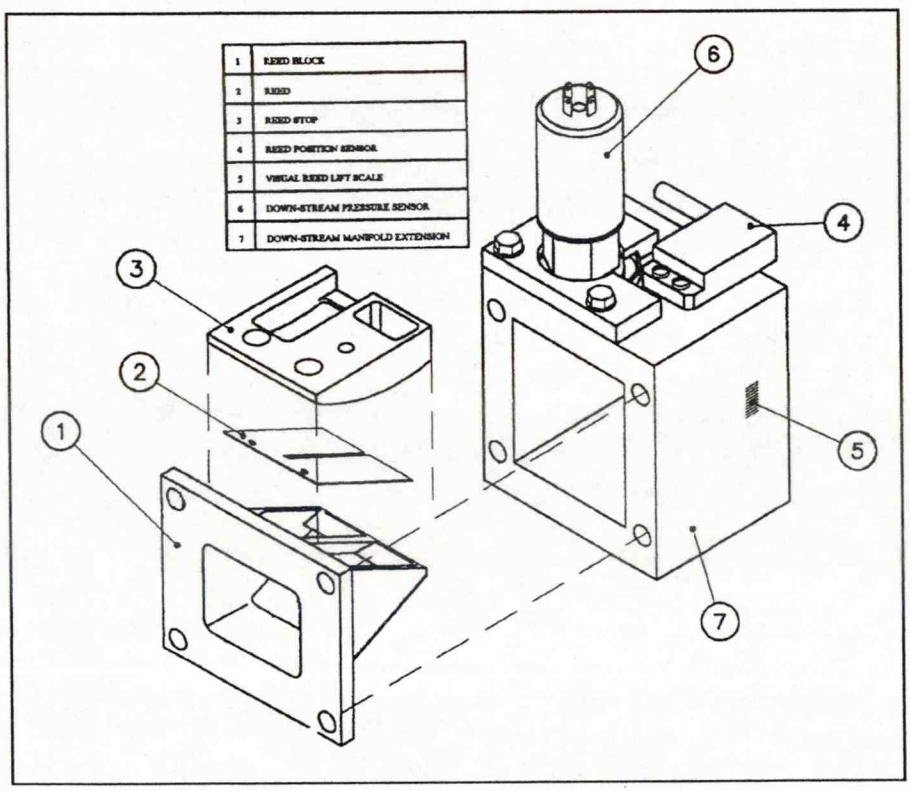

FIGURE 9 - Exploded assembly of the transparent reed manifold and the associated component parts of the reed valve and sensor.

The reed was displaced using a Vernier height gauge ensuring accuracy to within 0.01mm. This non-linear data would then be loaded into an array and a numerical software routine used to interpolate between this data to find the required linear values. With this procedure, calibration could be achieved in 5 minutes.

2.8 VALIDATION OF THE SENSOR SYSTEM

To validate the new position sensor's performance, a comparison between its output and photographic data was essential. An experiment was set up to measure the dynamic position of a reed valve under stable operating conditions using a technique similar to the recognised stroboscopic video used by both Fleck *et al.*,[35] and Hata *et al.*,[18] and the new infra-red sensor.

To achieve this, the engine test rig was run at a stable operating point, both in terms of reed motion and engine speed. The transparent manifold had a scale graduated in 1mm intervals secured to it and placed in such a way, that during play back, tip lift could be read directly from it (see Plates 2 and 3 overleaf). A beat frequency of about 2Hz was chosen as this provided 50 video frames per engine cycle. This was done by adjusting the strobe until such pseudo-motion existed. At this beat frequency there was a good balance between the resolution in the cycle and the number of cycles included in the averaged data. Once the engine and strobe were stable, the Microlink data acquisition system was triggered and this was marked on the video by the illumination of a red light emitting diode (LED) in the corner of the frame. In this way the two data sets could be associated. To optimise the contrast of the video, the test bay was blacked out so that the only light illuminating the reed was from the stroboscope.

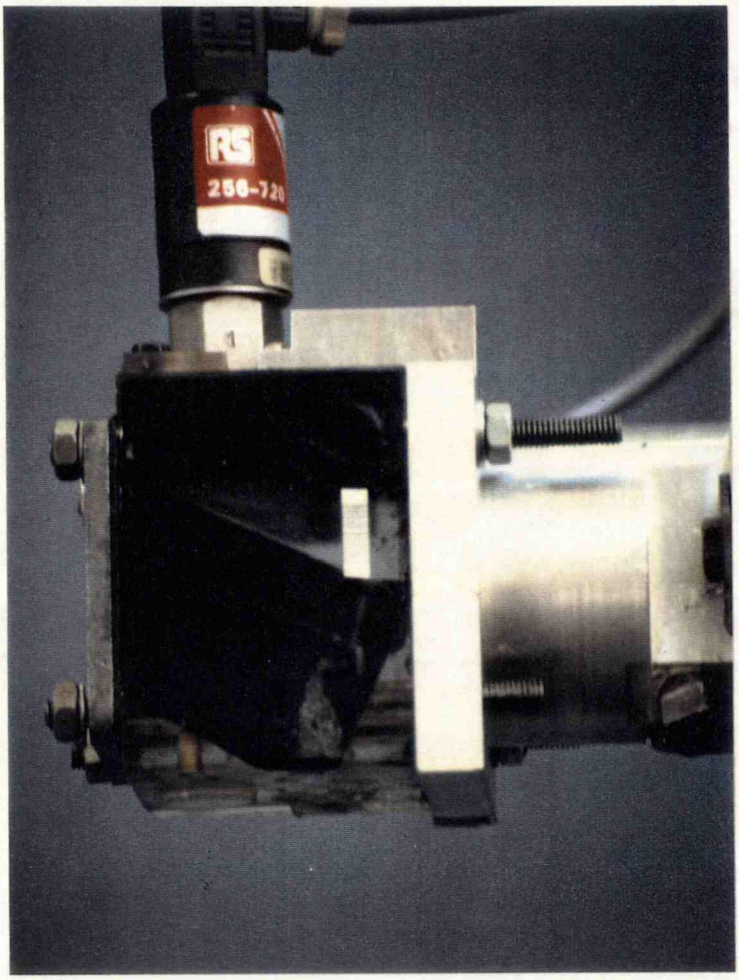

PLATE 2 (left) - A view of the Perspex manifold with scale for stroboscopic videoing of the reed position with the position sensor (and pressure sensor) mounted above to enable real-time measurement.

PLATE 3 (below) - Shows the experimental set-up, with the video camera and stroboscope positioned prior to use.

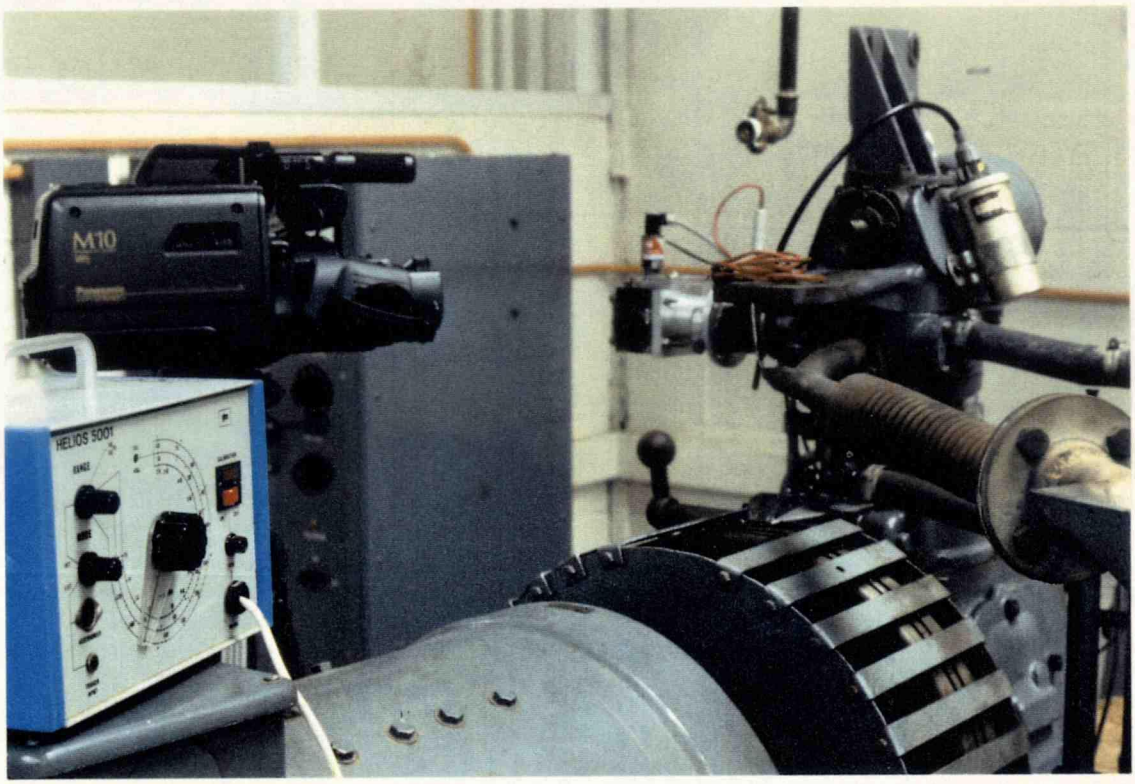

To be valid, these data sets had to be stable. To check this, the number of frames were counted in several successive cycles. When these contained the same number of frames it was considered likely that the data was stable during each cycle. Five photographic cycles were taken and then averaged at each data point and the same was done for the digitally acquired data but for 25 cycles (instead of 5). The data acquisition was initiated by a real-time clock, since the video recorded frames at equal time intervals rather than in positional increments. This was different from the other experimental work performed on the engine, where acquisition occurred at regular angular intervals to avoid errors from any modulation in the angular speed inherent in the crank of a firing engine. These data sets were then compared, not only to provide validation of their mutual calibration, but also to provide an insight into any differences between the two systems. The magnitude of the errors between the data sets lay within the resolution of the video technique, which at best can resolve to 0.5mm as can be seen in Figure 10.

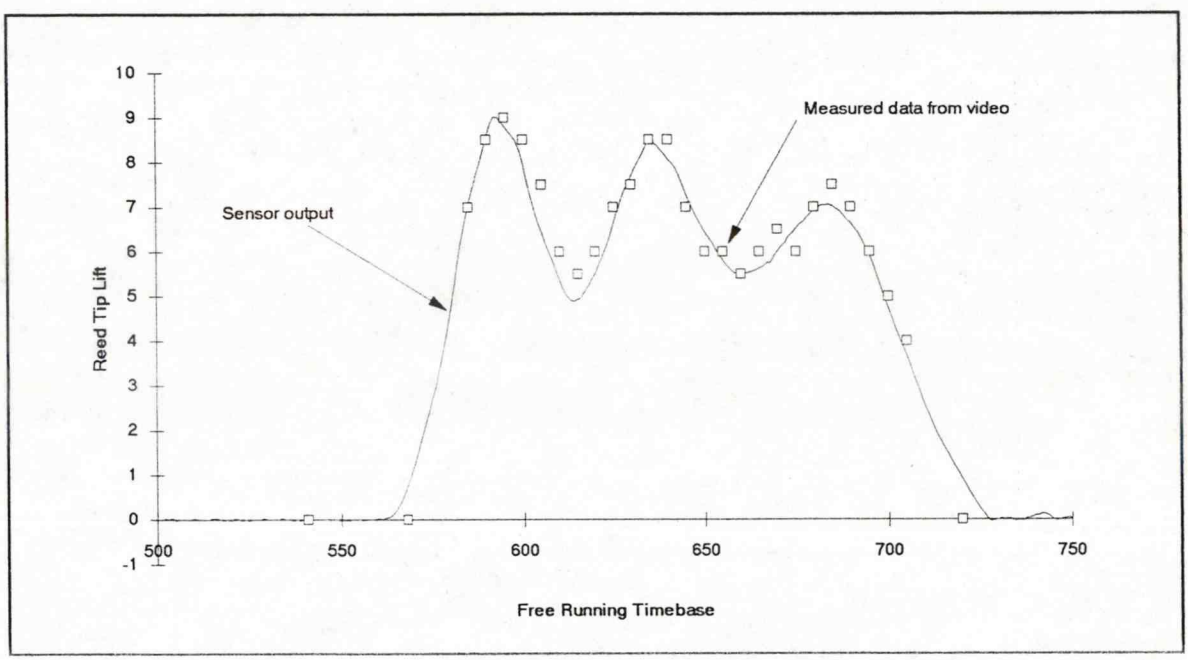

Figure 10 - Comparison between real-time sensor output and video stroboscopic data.

CHAPTER 3 - THEORY

3.1 GENERAL

To fully understand reed behaviour it was necessary to consider the theory relating to reed displacement. As a reed was previously considered to behave as a cantilever,[32,33,35] beam theory was applied in order to understand it's dynamic behaviour. Before the dynamic displacement of the reed could be determined it was first necessary to establish:

(i) The natural frequency of transverse vibration.

(ii) The characteristic function and it's corresponding mode shapes.

(iii) The damping coefficients.

These dynamic aspects are considered first before reed displacement.

3.2 THE NATURAL FREQUENCY OF TRANSVERSE VIBRATION

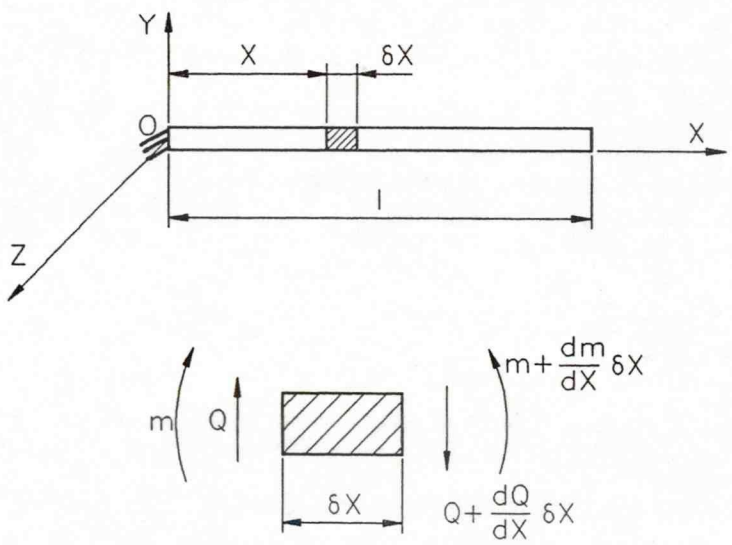

FIGURE 11 - A transverse beam showing the forces and moments that act on an elemental length of the beam at distance x from the pinned end redrawn from Gorman.[41]

The theory of transverse vibration of prismatic beams is laid out in theoretical texts such as Gorman[41] and also in other earlier published work,[32] the key aspects of which are repeated here.

The moments and systems of forces applied to an element of length δx located at x are as shown in Figure 11 (prevoius page), where:

$$m - (m + \frac{dm}{dx}\delta x) + (Q + \frac{dQ}{dx}\delta x)\delta x + \rho g A \delta x \frac{\delta x}{2} = 0$$

as δ tends to zero, components containing the product $\delta.\delta$ can be ignored, this reduces the above so that:

$$Q = \frac{dm}{dx} \qquad EQU\ 1$$

The vertical force on this element is:

$$Q - (Q + \frac{dQ}{dx}\delta x) = -\frac{dQ}{dx}\delta x$$

and applying Newton's second law gives:

$$-\frac{\partial Q}{\partial x}\delta x = \frac{\partial}{\partial t}(\rho A \delta x \frac{\partial y}{\partial t})$$

this can be rewritten as:

$$-\frac{\partial Q}{\partial x} = \rho A \frac{\partial^2 y}{\partial t^2} \qquad EQU\ 2$$

Differentiating equation 1 with respect to x and substituting in equation 2 produces:

$$-\frac{\partial^2 m}{\partial x^2} = \rho A \frac{\partial^2 y}{\partial t^2} \qquad EQU\ 3$$

From the theory of the bending of uniform beams:

$$EI\frac{d^2y}{dx^2} = m$$

E is the modulus of elasticity and I is the second moment of area of the beam where:

$$I = \frac{bd^3}{12} \qquad EQU\ 4$$

Double differentiating this with respect to x and substituting into equation 3 gives:

$$EI\frac{\partial^4 y}{\partial x^4} + \rho A\frac{\partial^2 y}{\partial t^2} = 0 \qquad EQU\ 5$$

This has a solution:

$$y = \phi(x)e^{i\omega t}$$

substituting this into equation 5 gives:

$$\frac{d^4\phi(x)}{dx^4} - \lambda^4\phi(x) = 0 \qquad EQU\ 6$$

where:

$$\lambda^4 = \frac{\rho A\omega^2}{EI} \qquad EQU\ 7$$

and $\phi(x)$ is a function of the coordinate x. Equation 6 has a general solution:

$$\phi(x) = a'\cos\lambda x + b'\sin\lambda x + c'\cosh\lambda x + d'\sinh\lambda x \qquad EQU\ 8$$

The constants a', b', c' and d' are determined by the boundary conditions, where at the clamped end of the beam:

$$x=0 \quad \phi(x) = \frac{d\phi(x)}{dx}=0$$

i.e. the deflection is zero, and at the free end where:

$$x=L \quad \frac{d^2\phi(x)}{dx^2} = \frac{d^3\phi(x)}{dx^3} = 0$$

i.e. the beam has zero bending moment and shear force.

Substituting the first set of conditions into equation 8 gives its first derivative as:

$$a'+c' = 0 \qquad EQU\ 9$$

and:

$$b'+d' = 0 \qquad EQU\ 10$$

When substituted into the second and third derivative, the second set of conditions give the following:

$$a'(-\cos\lambda l-\cosh\lambda l)+b'(-\sinh\lambda l-\sinh\lambda l) = 0 \qquad EQU\ 11$$

and:

$$a'(\sin\lambda l-\sinh\lambda l)+b'(-\cos\lambda l-\cosh\lambda l) = 0 \qquad EQU\ 12$$

consequently:

$$b' = a'.\frac{\sin\lambda l - \sinh\lambda l}{\cos\lambda l - \cosh\lambda l} \qquad EQU\ 13$$

Substituting in equation 11 and simplifying, gives the frequency equation:

$$1 + \cos\lambda l \cosh\lambda l = 0$$

The first three roots of which can be found by plotting cosh λl against sec λl, these are:

$1 = 1.875$

$2 = 4.694$

$3 = 7.855$

Equation 7 can be rearranged to give:

$$\omega_i^2 = \frac{EI(\lambda_i l)^4}{\rho A l^4}$$

(i.e.)

$$\omega_i = (\lambda_i l)^2 \sqrt{\frac{EI}{\rho A l^4}}$$

substituting equation 4 for the second moment of area I and simplifying, gives:

$$\omega_i = (\lambda_i l)^2 \sqrt{\frac{Ed^2}{12\rho l^4}}$$

The frequency of natural vibration in mode (i) is given by:

$$f_i = \frac{\omega_i}{2\pi} = \frac{(\lambda_i l)^2}{2\pi}\sqrt{\frac{Ed^2}{12\rho l^4}}$$

3.3 THE CHARACTERISTIC FUNCTION

For each mode shape the characteristic function is found by substituting the values of the coefficients a', d' and b' from equation 9 and 10 into equation 13. This simplifies to:

$$\phi_i(x) = c'[\cosh \lambda_i x - \cos \lambda_i x - \sigma_i(\sinh \lambda_i x - \sin \lambda_i x)] \qquad EQU\ \ 14$$

where c' is a suitable constant and:

$$\sigma_i = \frac{\sinh \lambda_i l - \sin \lambda_i l}{\cosh \lambda_i l + \cos \lambda_i l}$$

3.4 THE DAMPING COEFFICIENTS

Three methods of analysing the damping of the reed were explored. Two of which were modal techniques and the third was from the analysis of the exponential decay associated with free vibration. Both modal analysis methods shared the same assumption that, in the vicinity of resonance the total response was dominated by the mode whose natural frequency was closest.[42] Each of these methods are considered in turn.

3.4.1 THE FIRST MODAL METHOD

If a system has reasonably separated modes, plotting the Frequency Response Function in a Nyquist format will describe part of a circle. From this information two important parameters can be extracted. The derivation for these will not be included here but are presented elsewhere.[42] These derivations come from the rate at which the locus sweeps around the circular arc, known as the sweep rate. This sweep rate reaches a maximum value at the natural frequency of oscillation for each mode and gives an estimate of the damping. To determine the structural damping (η), required an empirical technique. Points were displayed on a Nyquist plane to which a curve was best fitted by eye. This curve was extrapolated to complete a circle from which the modal information was then extracted.

3.4.2 THE SECOND MODAL METHOD

The exact expression for all levels of viscous damping (ζ) can be developed by considering two specific points on the circle:

(i) At a frequency ω_a above the natural frequency of mode *i*.

(ii) At ω_b below as depicted in Figure 12 below.

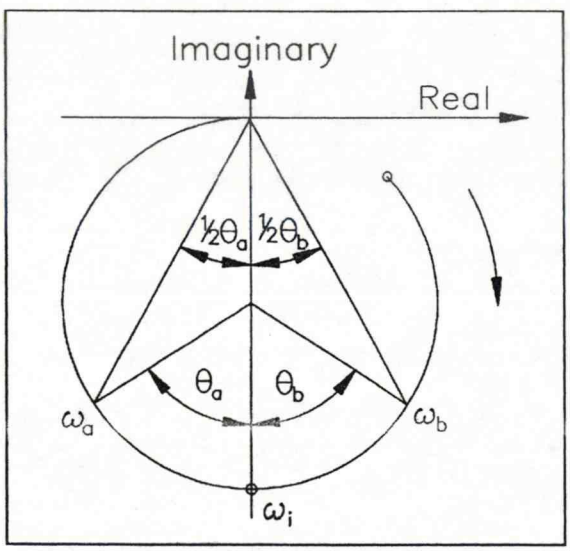

FIGURE 12 - Nyquist representation of the modal circle.

The properties of the modal circle are such that:

$$\tan\left(\frac{\theta_b}{2}\right) = \frac{\left(1-\left(\frac{\omega_b}{\omega_i}\right)^2\right)}{2\zeta\frac{\omega_b}{\omega_i}}$$

and:

$$\tan\left(\frac{\theta_a}{2}\right) = \frac{\left(\left(\frac{\omega_a}{\omega_i}\right)^2-1\right)}{2\zeta\frac{\omega_a}{\omega_i}}$$

An expression for the viscous damping (ζ) for each mode (i) can then be obtained:

$$\zeta_i = \frac{\omega_a^2-\omega_b^2}{2\omega_i\left(\omega_a\tan\left(\frac{\theta_a}{2}\right)+\left(\omega_b\tan\left(\frac{\theta_b}{2}\right)\right)\right)}$$

With light damping, the above expression can be simplified to give :

$$\zeta_i \approx \frac{(\omega_a-\omega_b)}{\omega_i\left(\tan\left(\frac{\theta_a}{2}\right)+\left(\tan\left(\frac{\theta_b}{2}\right)\right)\right)}$$

If the two points θ_a and θ_b equal 90 degrees then (ζ) can be obtained from:

$$\zeta_i = \frac{(\omega_2-\omega_1)}{2\omega_i}$$

Similar treatment of the receptance derives a similar expression from which the structural damping (η) can be obtained:

$$\eta_i = \frac{(\omega_2 - \omega_1)}{\omega_0}$$

3.4.3 THE PEAK AMPLITUDE METHOD

The simplest method for determining ζ for the fundamental mode is the peak amplitude method. ζ can be calculated from the exponential decay of the peak amplitude in free vibration. Since the displacement is dominated by the first mode, so too, will the damping losses.[42] The decay envelope is described by equation 15 below:

$$\alpha e^{-\zeta \omega_0 t} \qquad EQU\ 15$$

α is the starting peak amplitude.

The damped frequency is related to the natural frequency by:

$$\omega_0 = \omega_n \sqrt{1-\zeta^2}$$

and successive displacement peaks related by the equation:

$$\log_e \frac{\alpha_n}{\alpha_{n+1}} = 2\pi\zeta \frac{\omega_n}{\omega_0} \qquad EQU\ 16$$

For lightly damped systems where:

$$\omega_0 \approx \omega_n$$

the damping ratio can be approximated to:

$$\zeta = \frac{\log_e \frac{\alpha_n}{\alpha_{n+1}}}{2\pi}$$

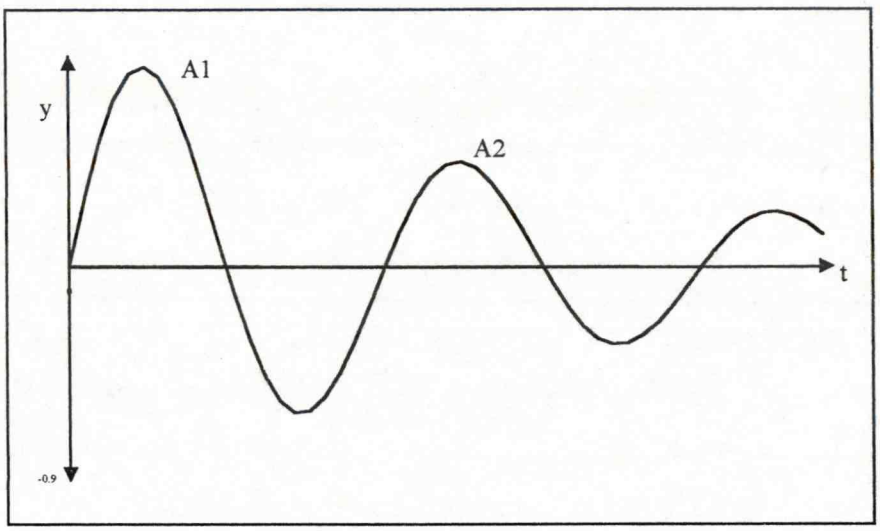

FIGURE 13 - This is a typical damped oscillation where the first and second peak amplitudes (A1 and A2) are related by the general equation EQU 16.

3.5 CALCULATION OF THE DISPLACEMENT OF A REED CANTILEVER

If the reed is considered as a cantilever, then beam theory can be used to determine displacement. As a second order system, a cantilever obeys the following equation of motion:

$$M\ddot{\chi} + C\dot{\chi} + K\chi = 0$$

The three terms generate forces resulting from acceleration, velocity and position, which must equate to zero. M,C and K are the mass, the damping and the spring constants respectively. For all second order systems the following can be defined:

$$\frac{K}{M} = \omega_n^2$$

where ω_n is the natural frequency of oscillation and:

$$\frac{C\omega_n}{2K} = \zeta$$

the damping ratio.

Dividing through by the damping constant (K) gives:

$$\frac{M\ddot{\chi}}{K} + \frac{C\dot{\chi}}{K} + \chi = 0$$

so:

$$\frac{C}{K} = \frac{2\zeta}{\omega_n}$$

substituting for ω_n gives:

$$\frac{\ddot{\chi}}{\omega_n^2} + \frac{2\zeta\dot{\chi}}{\omega_n} + \chi = 0$$

and multiplying by ω_n^2 gives:

$$\ddot{\chi} + 2\zeta\omega_n\dot{\chi} + \omega_n^2\chi = 0 \qquad EQU\ 17$$

For equation 17 to apply to a uniformly loaded cantilever χ must be uncoupled from the modal matrix and replaced with the principal coordinate (z):

$$\ddot{z} + 2\zeta\omega_n\dot{z} + \omega_n^2 z = 0$$

The principal coordinate will be different for each mode i and therefore must be calculated for each mode separately.

If external forces apply then:

$$\ddot{z}_i + 2\zeta\omega_i\dot{z}_i + \omega_i^2 z_i = \frac{F_i}{M_i} \qquad EQU \quad 18$$

where z, is a generalized displacement scalar for which the equations of motion have neither inertial nor elastic coupling[43]. The principal coordinate is not unique for any system but has an infinite number of values. By solving equation 18 for z at each new forcing condition (i.e., each time interval) and multiplying with the result of the characteristic function (equation 14) for points x_i along the reed, the deflection y_i at x_i in each mode i can be calculated:

$$y_i(x,t) = z_i(t).\phi_i(x)$$

The total deflection is considered to be the modulation of all the harmonic modes onto the fundamental modes:

$$y(x,t) = \sum_{i=0}^{\infty} y_i(x,t) = \sum_{i=0}^{\infty} z_i(t).\phi_i(x)$$

This is referred to as the superposition theorem. In practice only the first three values of z are used since the other modes contribute less than 0.5% to the total. The damping factor ζ and the natural frequency of vibration for mode i (ω_i) are required for each mode and the forcing function $F_{(i)}$ and the effective mass $F_{(i)}$ are required for each iterative step.

CHAPTER 4

THE THEORETICAL MODEL FOR PREDICTING THE DYNAMIC BEHAVIOUR OF REEDS

4.1 GENERAL

In the past reed valve models have been developed without the benefit of real-time data and as such, have only been evaluated under extremely stable operating conditions with minimal cyclic instability. One of the objectives of this research was to advance the development of reed valve modelling by considering conditions with unstable reed behaviour. Under such conditions reed behaviour has the most detrimental effect on engine performance and yet is least understood. The availability of real-time data made it possible to study such unstable conditions. During this work a model was developed using current assumptions. Some aspects, such as where real-time reed position data revealed error between the predicted and actual lift position, were then investigated.

The computational model used in this investigation was based on the simple cantilever approach described in the previous chapter. It generally followed the published work of Hinds and Fleck[32,35] carried out at QUB, but where real-time data errors revealed errors between predicted and measured lift, the model was modified to account for these discrepancies. The load on the reed and hence the forcing function was calculated from the differential pressure across the reed and it's surface area. It was assumed that the pressure distribution was constant along the reed which generated a uniform load. The differential pressure used was the difference between the manifold pressures up- and downstream of the reed.

Prediction of the forcing function had been the subject of investigation by Hinds,[32] who considered the reed surface to be divided into elemental strips and calculated the pressure

acting on each strip by its position with respect to the boundary pressures. However, Fleck *et al.*,[35] later found that equally good results could be achieved by using the simpler method of considering the pressure that acted on the reed area to be the difference between the up- and downstream pressures multiplied by a fractional constant.

4.2 THE SOFTWARE MODEL

A program was written using the *Initval* Unit from the Borland Turbo-Pascal Numeric Tool Box, as the central software algorithm to solve the second order differential equation of motion (see equation 18 in the previous chapter), which was an initial value problem (see Appendix 2 for code detail). This found z, the principle coordinate, which described the motion of a cantilever beam. The solution was found using the fourth order, two-variable Runge-Kutta formula. The reed was split into segments along its length. At each time step the position of each segment was found for each of the first three modes. The tip lift was the summation of all the incremental deflections along the reed, from all the relevant modes. Calculating the three modes separately and then summing them (effectively modulating them onto one another), is referred to as superposition. This nodal lift data was then written into an output data file for subsequent use. This whole process was then repeated for the next time step which was at an interval of 1.5 degrees of engine rotation. The solution of the displacement of the reed tip for one engine cycle is a numerically intensive exercise and even with a 50MHz 32 Bit processor it took several minutes.

In order to solve these equations, data was required about the physical parameters, the geometry of the reed and reed stop, the density and Young's modulus of the reed material as

well as the data to generate the forcing function, the pressure up- and downstream of the reed and the time interval between each value.

The data was arranged by using two files, one for the parametric data and one for the input pressure data. Once the parametric data was determined this then remained the same for a series of predicted dynamic behaviours. For every new time step, a new force was defined by the forcing function, and the final position of all nodes in the last time step formed the initial conditions for the next time step. The free length i.e., the length of reed not in contact with the reed stop, was re-calculated as the contact point changed with reed lift. This necessitated the natural frequency of vibration to be re-calculated for each new free length.

The motion of the reed is dominated by the fundamental mode, with the first and second harmonics contributing very little. The model from QUB used the first three only. Originally in this model, the first four modes were calculated, but the results supported the practice of using only the first three modes, since the fourth contributed less than 0.5%. Consequently only the first three were included in this model. In the QUB model, the damping coefficients were picked empirically to give the best correlation between the predicted and actual lift. To gain a further insight into reed damping an experimental investigation of the damping coefficients was undertaken, however, as will be explained later, it was still necessary to alter the damping coefficient to optimise the model. The actual reed lift at all nodes along the reed was limited by a pair of boundary conditions. The maximum lift was controlled by the reed stop and the minimum allowable value of lift was forced to be zero (the shut position). This constrained the model to operate in a defined envelope of lift positions. The model was

initially tested using simple mathematical functions as data sets. The reed was subjected to pressure steps and ramps known from previous published work and earlier set-up tests to be of typical magnitude. The model then predicted lift profiles which were not unreasonable (see Figure 14 below).

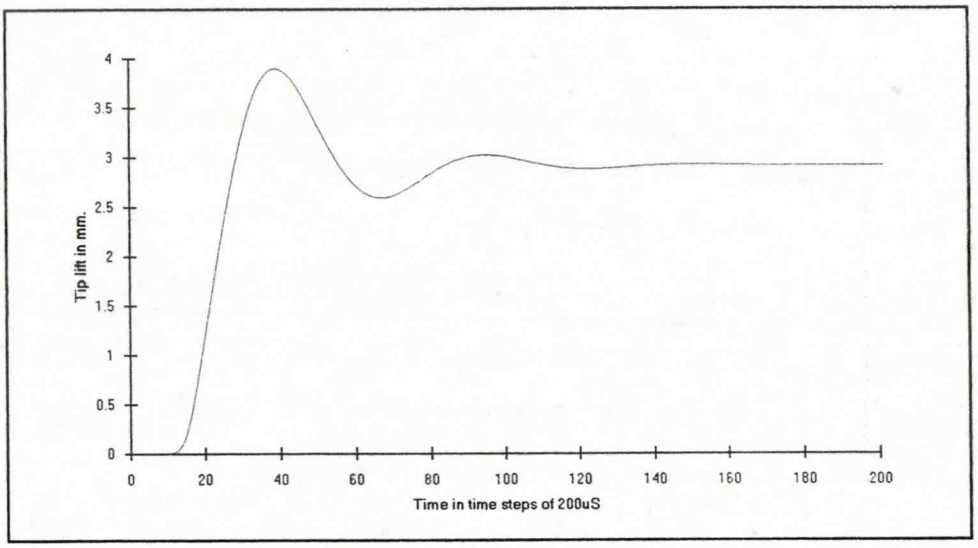

FIGURE 14 - Response of the model to a step pressure difference of 30mBar.

When tested against data taken from other published work,[35] it was found that the model over-predicted the reported reed lift and showed little correlation with the modulated detail. Consequently, it was felt that an investigation of the model should be undertaken with particular reference to the forcing function and damping coefficients. To enable this to be carried out, reliable pressure and lift data was required from a reed operating in a pulsed flow. To achieve this, the reed assembly was placed in the inlet manifold of a motored Ricardo E6 engine, which offered the following advantages over attempts to obtain good low noise data in a firing two-stroke.

(i) With no carburettor, only one pressure measurement needed to be taken since the reed valve could open directly to the atmosphere.

(ii) Being of a larger swept volume (approximately 500cc) than the engine for

which the reed was intended, the Ricardo produced good reed lift across a wide range of throttle positions and speeds, which generated significantly different lift profiles.

(iii) Phase errors between the pressure on the reed and the measured pressure were minimized not only by operating at lower speeds, but also because it was possible to locate the pressure sensor close to the reed valve.

(iv) Of most benefit was the ease with which the reed could be made to resonate. This provided the complicated real-time pressure and lift data required to check the accuracy of model's dynamic performance.

All the tests used the same standard Yamaha RD250 reed block and reed style. The reed stop with its specially machined apertures was also used allowing optical access to the reed tip from above the reed block and pressure measurements to be taken close to the reed as shown in Plate 2 from Chapter 2 and Figure 15 overleaf. The reed block was located in a Perspex manifold on which the optical position sensor was also mounted. This allowed for non-intrusive access. Flexible mountings were used to isolate the pressure transducers from any engine vibration.

The motoring Ricardo produced good low noise pressure and reed lift data. From this it was possible to draw fundamental conclusions about the model's performance for the first time.

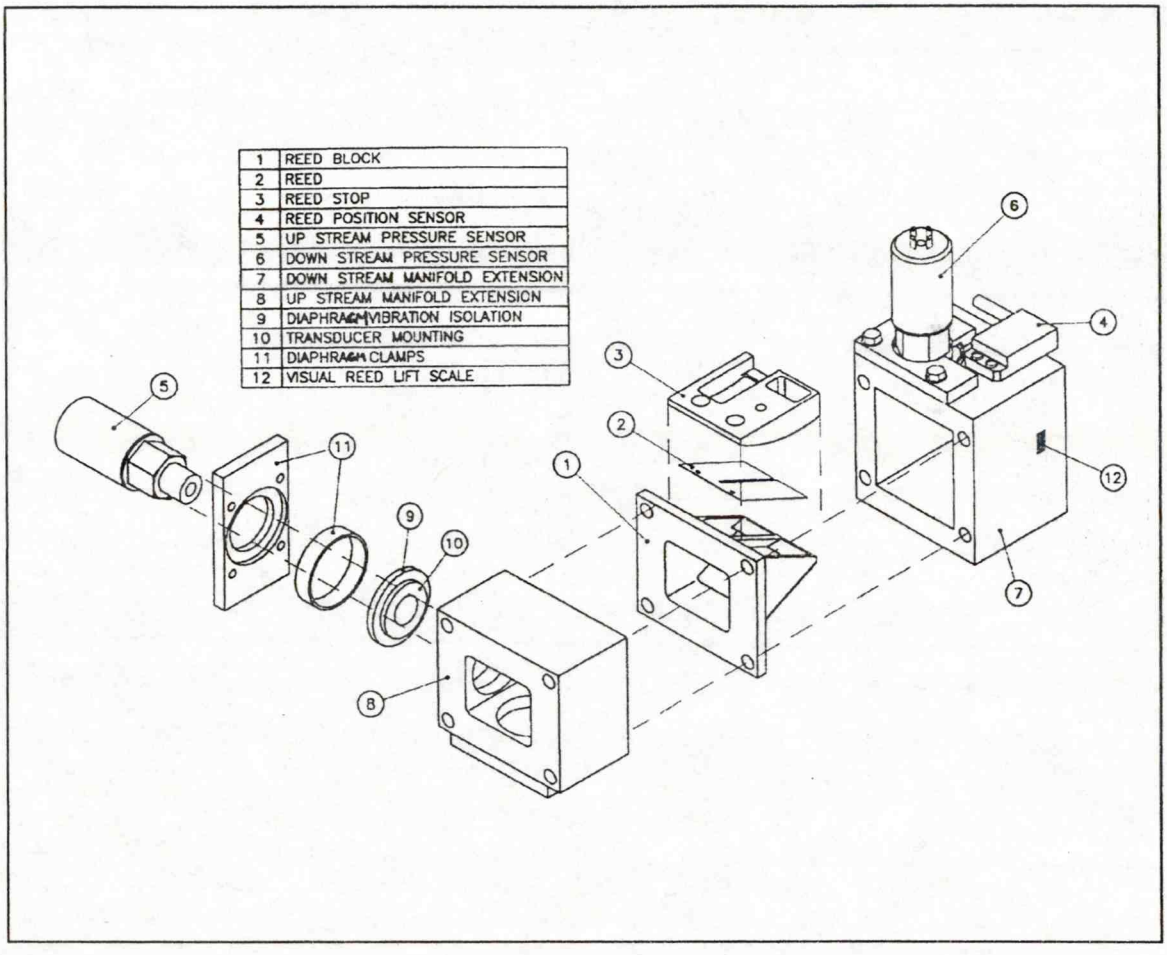

FIGURE 15 - Exploded assembly of manifold extensions showing the position of the sensors and the detail of the flexible mountings.

The model exhibited two fundamental flaws; it over-predicted the magnitude of the lift and demonstrated an over-damped response when compared to the measured lift profile. This is illustrated in Figure 16 (overleaf).

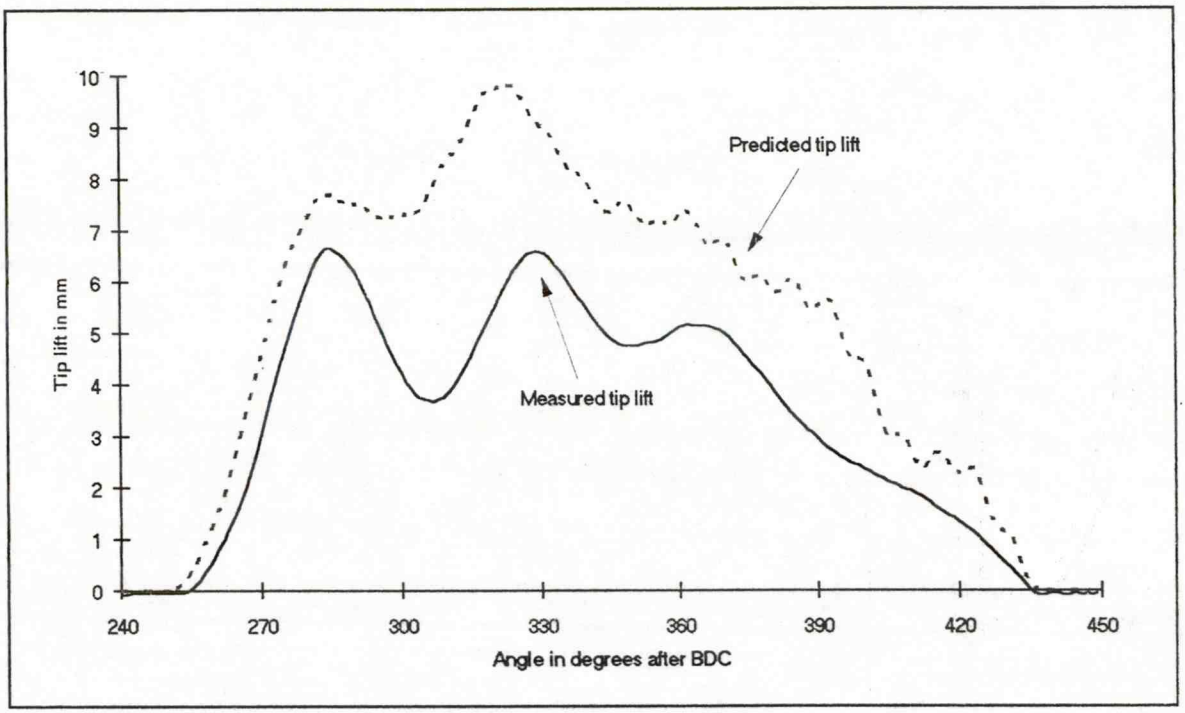

FIGURE 16 - Predicted and measured reed lift from the model using the simple forcing function.

It was considered that the model could be improved upon, consequently aspects of its performance were investigated and modifications implemented.

4.3 DEVELOPMENT OF THE FORCING FUNCTION AND DAMPING TERMS

Data from the real-time sensor suggested that the assumptions in the original model were the probable cause of only a basic correlation between measured and predicted lift. When the reed was closed it was assumed that little variation in pressure distribution existed, this justified the assumption of a uniform load and the associated differential equations. At all other times when there was flow through the valve, some distribution of pressure inevitably occurred. This was apparent when the up- and downstream pressures were considered to be connected by a nozzle which was formed by the open reed valve. As it was necessary to derive the forcing function from the up- and downstream pressures alone, a detailed

understanding of the pressure distribution across the open reed at all lift positions was necessary. This was difficult to obtain, so an empirical strategy was adopted to improve the performance of the model.The variance demonstrated by the model resulted in the following two proposals:

(i) To use an attenuator on the forcing function.

(ii) To investigate the damping parameters.

Initially a simple fractional attenuator was used to reduce the predicted magnitude. By iterative trial and modifying, it was possible to make the peak magnitude the same as the measured, but it also produced under-prediction at low levels of reed lift as can be seen in Figure 17 overleaf. On reflection, it was felt that this under-prediction came from the assumptions made in obtaining the forcing function. The forcing function format was the same whether the reed was closed or fully open. This assumption was too crude to give a good correlation in highly resonant conditions, and was consequently amended.

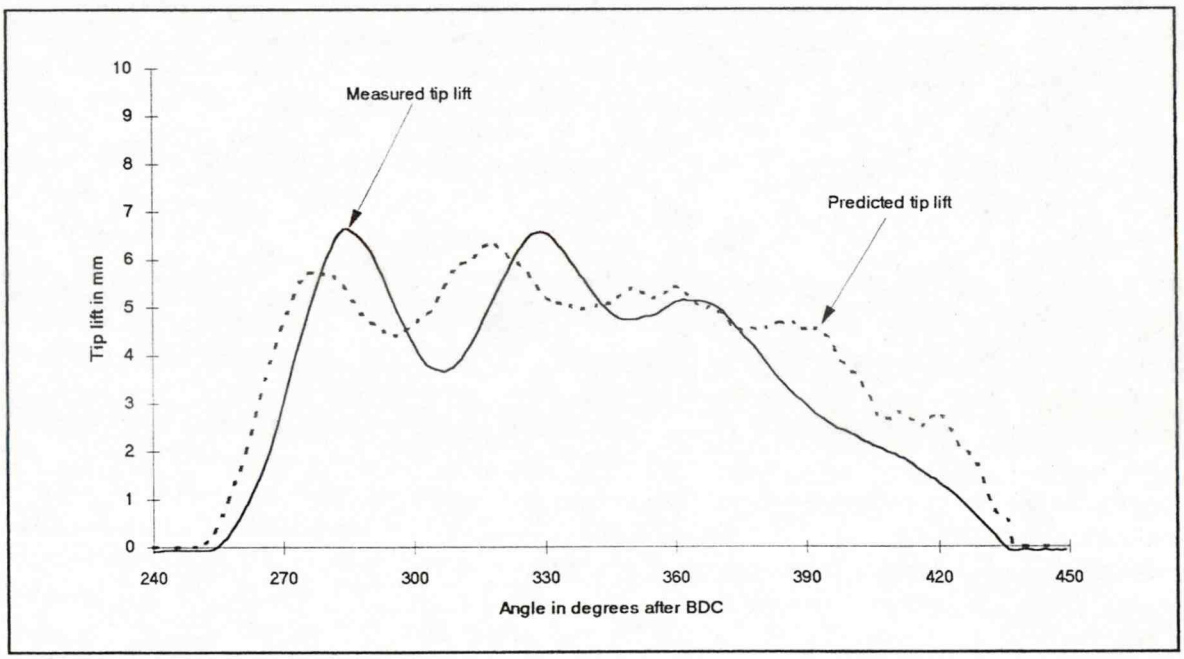

FIGURE 17 - Measured and predicted lift with model forcing function modified with a scalar to give similar peak lifts.

When the reed was closed, the force on the reed was defined by the pressure difference between the measured up- and downstream pressures multiplied by the area of the reed. With no flow, the pressure distribution would be sufficiently constant to make this initial assumption useful. With the reed fully open, the two pressure measurements would have had a pressure gradient associated with them which passes through the throat of the reed valve. There was a significant pressure distribution across the reed and the forcing function could not be defined from the pressure difference alone. It was decided to attenuate the full pressure difference by an amount to be empirically determined. Instead of the fixed attenuator, the forcing function was adjusted so that the degree of attenuation was proportional to the reed lift. This took the form of:

$$\frac{j - lift_{mm}}{k}$$

where j and k controlled the rate and extent of attenuation with lift. This modification improved the model so that it was optimised for one data set (see Figure 18 below).

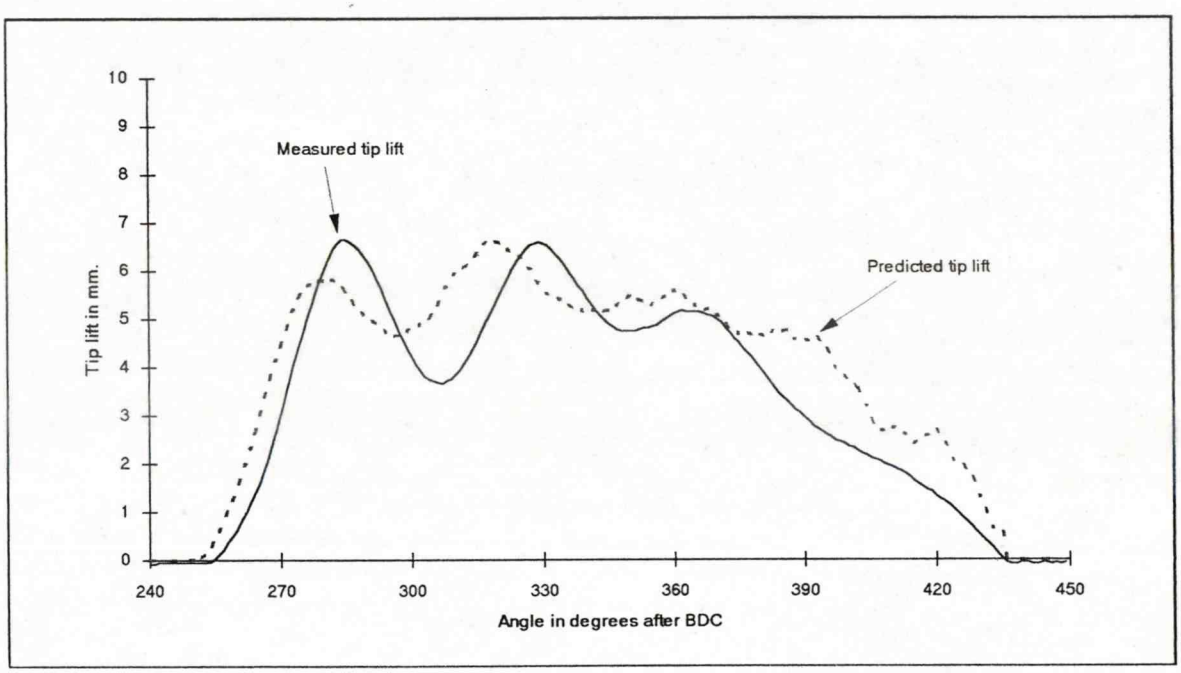

FIGURE 18 - Measured and predicted lift with forcing function modified to include a lift dependent term.

The final forcing function used was:

$$(P_{up} - P_{down} - P_{off}) \times \left(\frac{15 - tip\ \ lift}{15}\right) \times Reed\ \ effective\ \ \ area$$

This assumption was based on the premise that with no, or very small openings, the low flow velocity induced negligible static pressure drop along the length of the reed and that any pressure drop occurred in turbulence and eddying through the small openings. Consequently the upstream pressure acted over almost all of the reed's surface. In contrast when the reed is wide open there are high flow velocities through the valve and a corresponding high static pressure drop along and across the reed. Under these conditions the pressure difference was multiplied by a fractional scalar, consistent with previous work from QUB.[35] It was assumed that the scalar varied in some way between these two limits, the simplest of which was in a linear fashion, where it was at a maximum when fully open (highest velocity) and unity when closed. Iterative trial and testing gave best results when the maximum attenuation was set to 1/3 at a peak tip lift of 10mm.

It was still evident that the model had fundamental problems, since the opening ramp exhibited variance from the measured lift. From close inspection of the opening point, it was apparent that although highly sensitive to small forcing pressures, the measured lift profile displayed a lag in its opening point and therefore in its subsequent opening ramp. This was found to be caused by a pre-load on the reed which meant that some forcing pressure was required to offset this before lift occurred. To get the model to simulate this, an offset was

added to the data set to balance this pre-load which was determined by inspection of the measured pressure and lift data. With yet more adjustment of the forcing function, a good correlation on the opening ramp was achieved (see Figure 19 below).

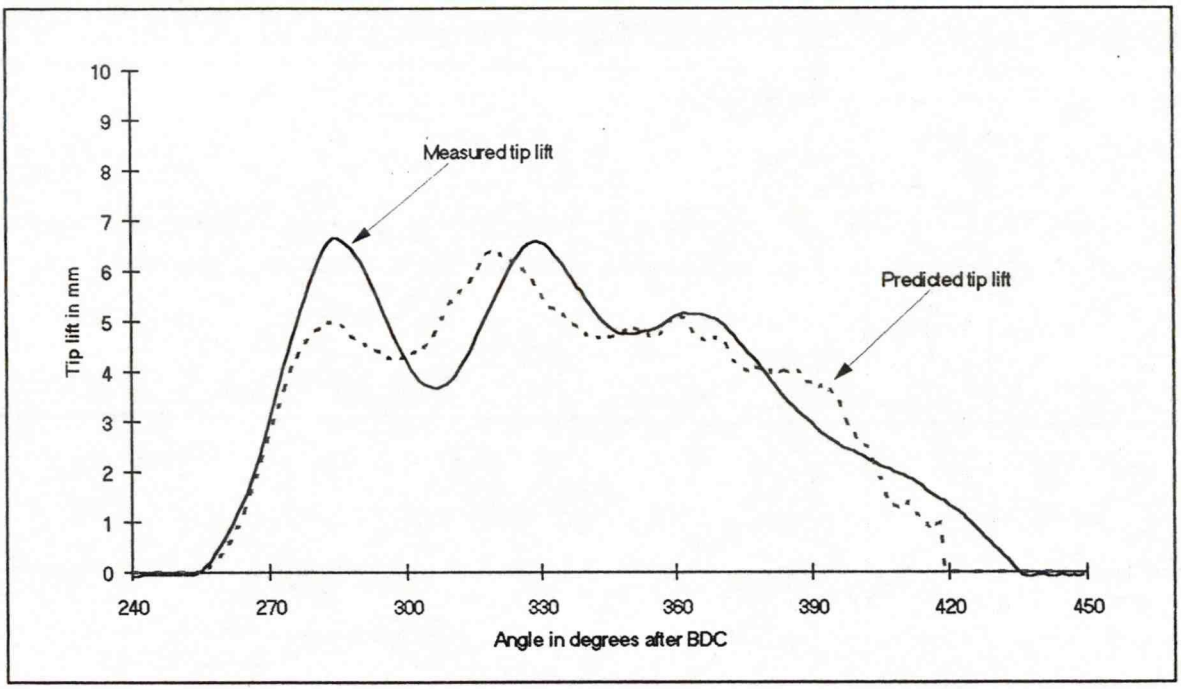

FIGURE 19 - Measured and predicted lift using forcing function with lift term included and pre-load offset error correction.

The remaining anomaly was the characteristic over-damping displayed by the model. The damping coefficients originally used were those used by Hinds[32] who had chosen them by inspection. As a result of bench top tests it was decided that some adjustment was required. The model was extremely sensitive to the damping coefficient and this became more apparent since the lift profile being modelled showed significant resonant behaviour during the open period. The damping factor of 0.5 used by QUB was considered too high and a change in value to 0.35 allowed the model to function in a satisfactory manner as seen in Figure 20 overleaf.

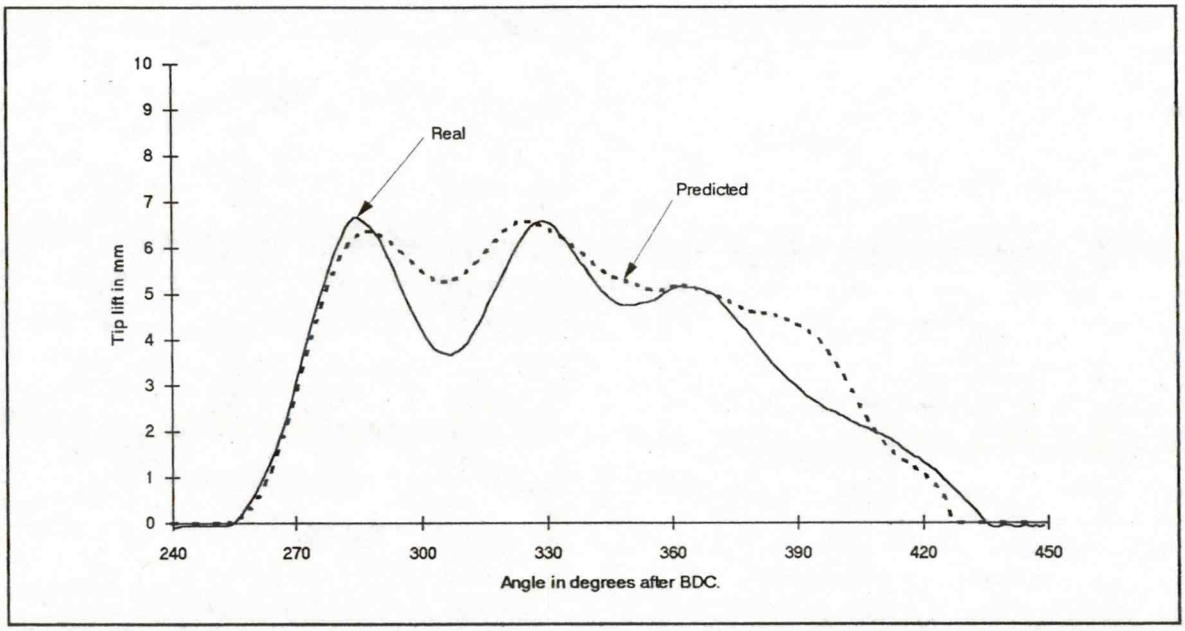

FIGURE 20 - Measured and predicted lift with forcing function modified to include lift dependent term, pre-load offset error correction and a suitable damping factor.

4.4 MODEL EVALUATION

The reed model was developed and optimised using one standard data set which exhibited several characteristics of interest. Since the modelled lift profile was compared with that measured by the new position sensor, an opportunity to make fine adjustments to the model and to gain an insight into the way in which changes in the input parameters affected it's behaviour, was possible. To check the model's general performance with different data sets, experiments were carried out to evaluate it's optimisation. The engine was motored under various throttle and load conditions which were designed to stimulate a wide range of dynamic behaviours from the reed. The reed tip lift was measured in real-time along with the pressure across the reed. The pressure data was used to predict the dynamic behaviour of the reed, and this was compared to the actual lift data to assess the performance of the model.

4.4.1 DATA SET I. 1200 REV/MIN FULL THROTTLE

This data set was the development data set. Its peak lift was 6.5mm, so the tip lift was only constrained by the fluid-dynamic balance between the flow through the reed and its own spring stiffness (ideal for comparative purposes). The profile showed dynamic behaviour resulting from the effect of manifold resonance on the lift. Accuracy was important since this was the first time that real-time data of this quality was available to compare actual and modelled lift. The results of the comparison between the measured and predicted data showed excellent correlation with the opening ramp, peak lift and the valve open interval. The valve closing point was within 10 degrees and the model tracked the closing ramp, although it showed a tendency to oscillate about it (see Figure 21 below and overleaf). A phase error existed between the real and predicted lift which was investigated extensively.

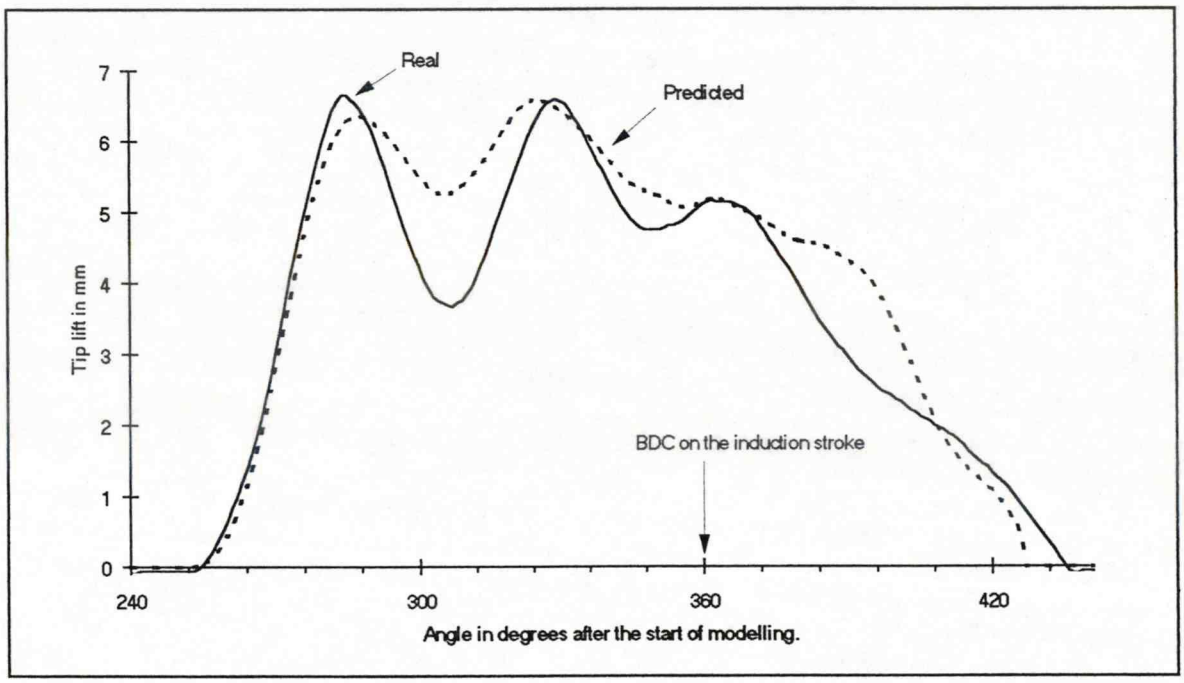

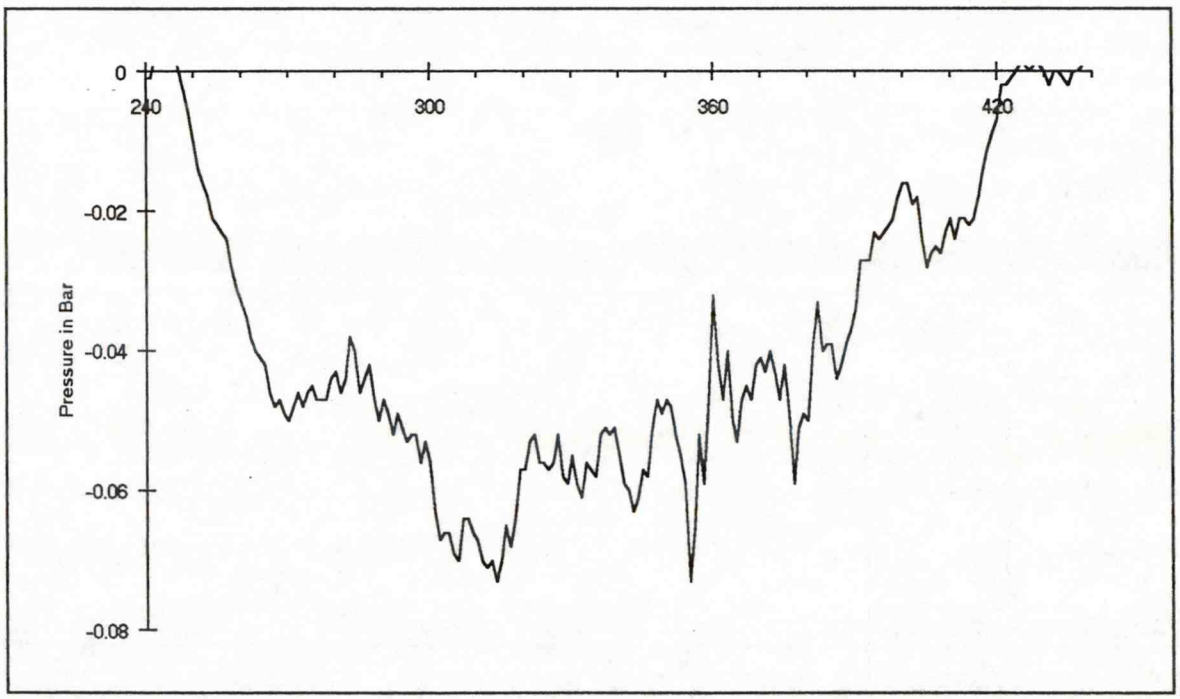

FIGURE 21 - Data set I. 1200 rev/min and full throttle. Measured and predicted lift (previous page) and forcing pressure (above).

It was not possible to correct this error by modification to either the time errors in the data set between actual and measured, the damping factor, the physical properties of the reed valve, or the effects of the reed stop. It was probable that this was caused by the general assumptions in the model. Having achieved this otherwise encouraging correlation between measured and predicted profiles, a series of different data sets were modelled without any changes being made to the software itself.

4.4.2 DATA SET II. 1400 REV/MIN 1/4 THROTTLE

This set of data showed an opening point error of about 5 degrees, an overshoot on peak lift of some 0.6mm and an error in closing point of 10 degrees. It predicted the number of peaks, but as the model included no algorithm to take account of rebound, it did not predict the reed bounce against the stop whilst settling. It did not overshoot all of the peaks in the profile,

under-predicting the first and the fourth peaks by approx 1mm in each case. It appeared that the forcing function would have worked better if it had attenuated low lift to a lesser amount and medium lift more (see Figure 22 below).

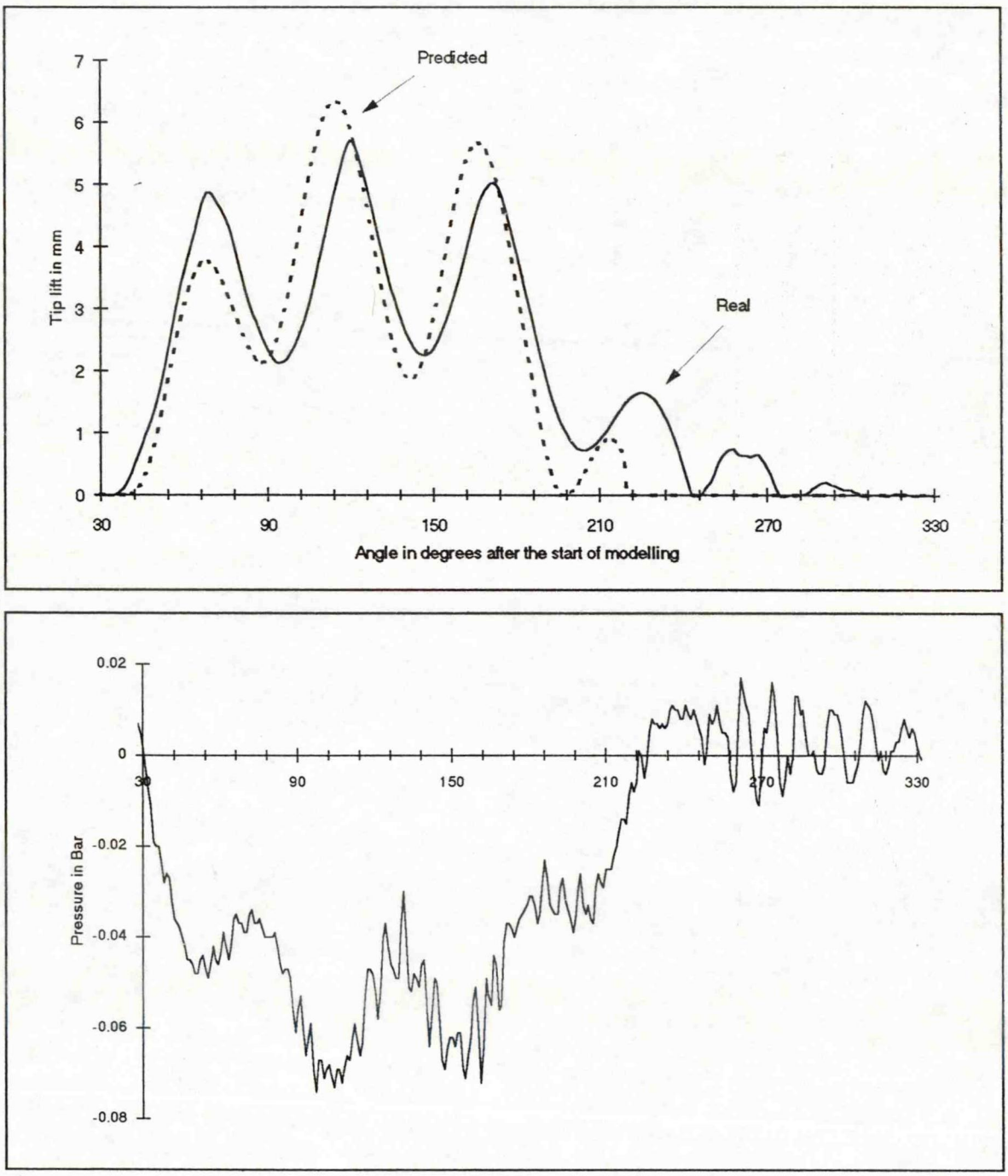

FIGURE 22 - Data set II. 1400 rev/min and 1/4 throttle. Measured and predicted lift and forcing pressure.

4.4.3 DATA SET III. 1300 REV/MIN FULL THROTTLE

This set predicted the general lift envelope particularly well. The opening ramp showed extremely close correlation and the closing ramp tracked without oscillation, although it did exhibit phase advance of about 5 degrees (see Figure 23 below).

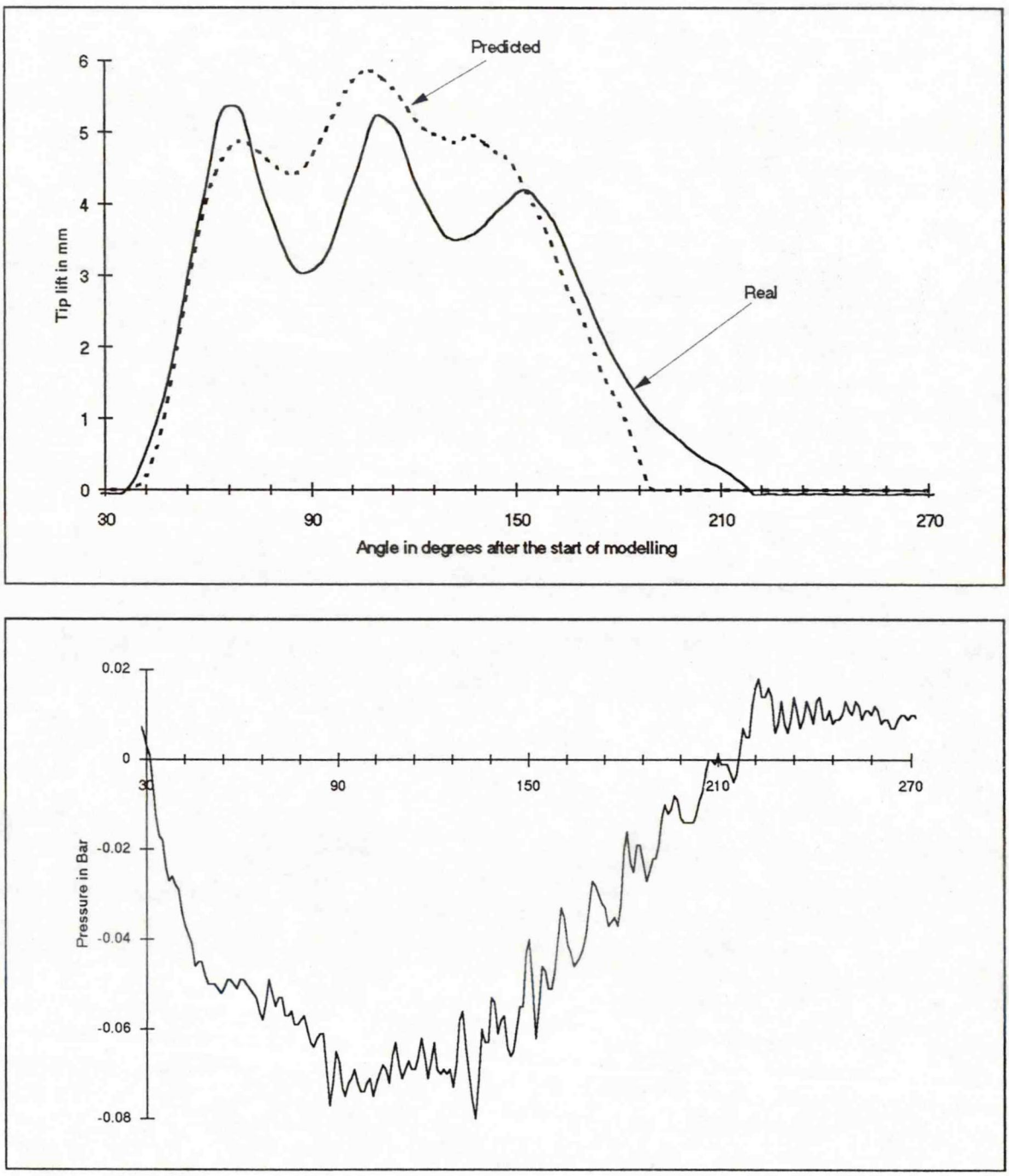

FIGURE 23 - Data set III. 1300 rev/min full throttle. Measured and predicted lift and forcing pressure.

The closing point showed an error of some 25 degrees, most of which occurred when the lift was under 1mm. The measured lift was shown to just close as the rising pressure bisects the axis. Although 3 peaks were clearly predicted, the peak to trough amplitude was clearly under-predicted; interestingly, the pressure trace did not show the excursions that would normally be associated with such resonance (as in data set v).

4.4.4 DATA SET IV. 1300 REV/MIN 1/2 THROTTLE

This set also showed good general correlation but exhibited errors similar to earlier modelled profiles. Both the opening and closing ramps were closely matched until 1mm from closing, when the predicted lift departed from the real path and closed 22 degrees early. The three peaks were predicted but the first was under-predicted and the other two over-predicted by about 1mm. The persistent error in the phase shift during the resonant portion of the profile was still evident (see Figure 24 below and overleaf).

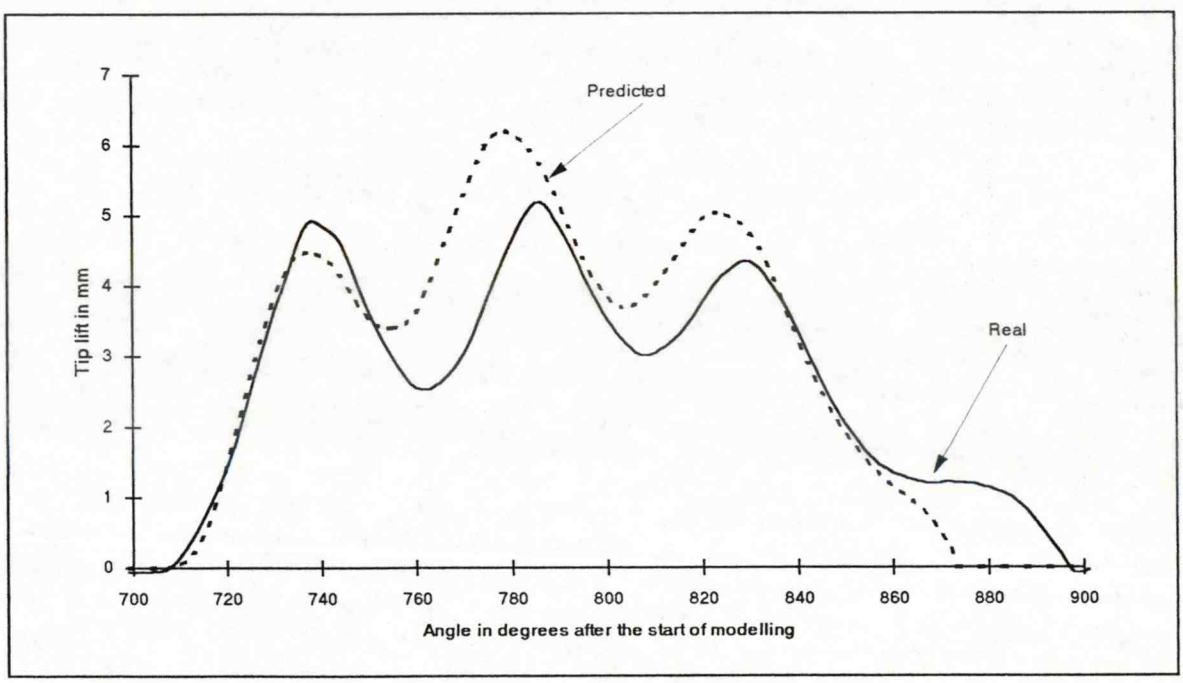

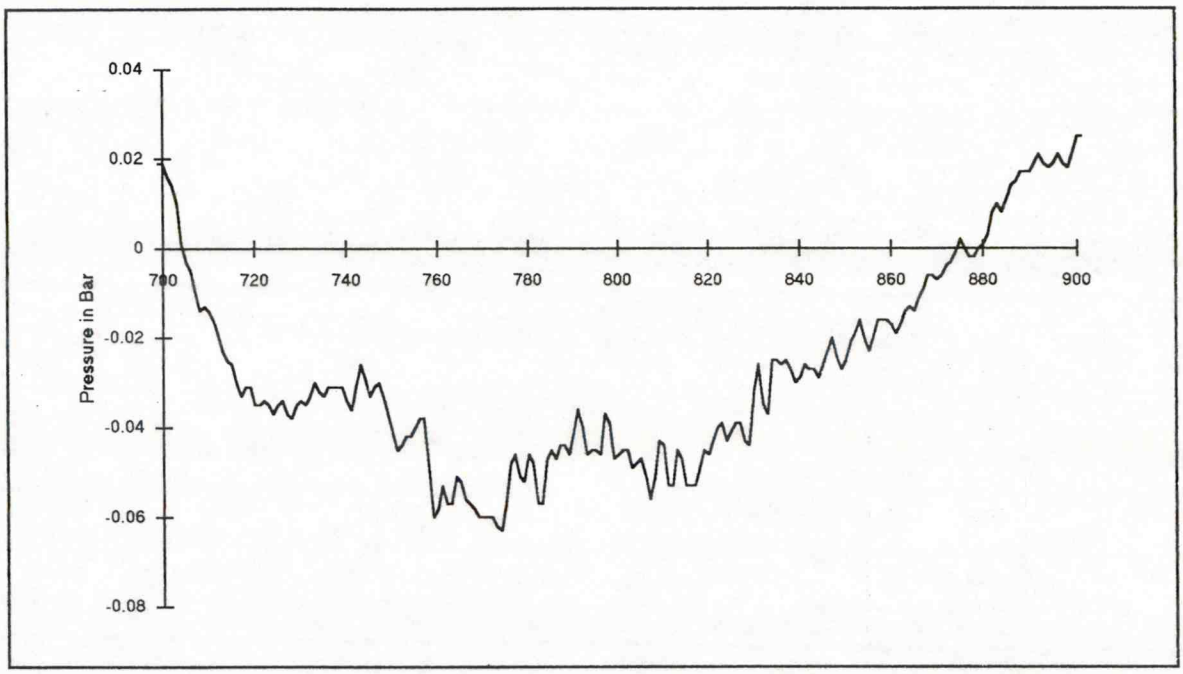

FIGURE 24- Data set IV. 1300 rev/min at 1/2 throttle. Measured and predicted lift (previous page) and forcing pressure (above).

4.4.5 DATA SET V. 1300 REV/MIN 1/4 THROTTLE

With a long period of gentle induction, the inlet manifold and the reed resonated strongly producing a significantly different looking lift profile. The model generated a close prediction of the lift profile. Four resonant peaks were predicted with maximum lift occurring on the third peak with an error of 0.1mm. The opening ramp showed excellent correlation but overshot by 0.6mm, and the closing ramp tracked well, but with a phase lead of 15 degrees characteristic of the model. Again, the absence of a rebound model meant that the model data implied a closed valve, but the measured lift clearly showed that there were three bounces on the stop. The first rebound being strong enough to cause the reed to lift by almost 2mm (see Figure 25 overleaf).

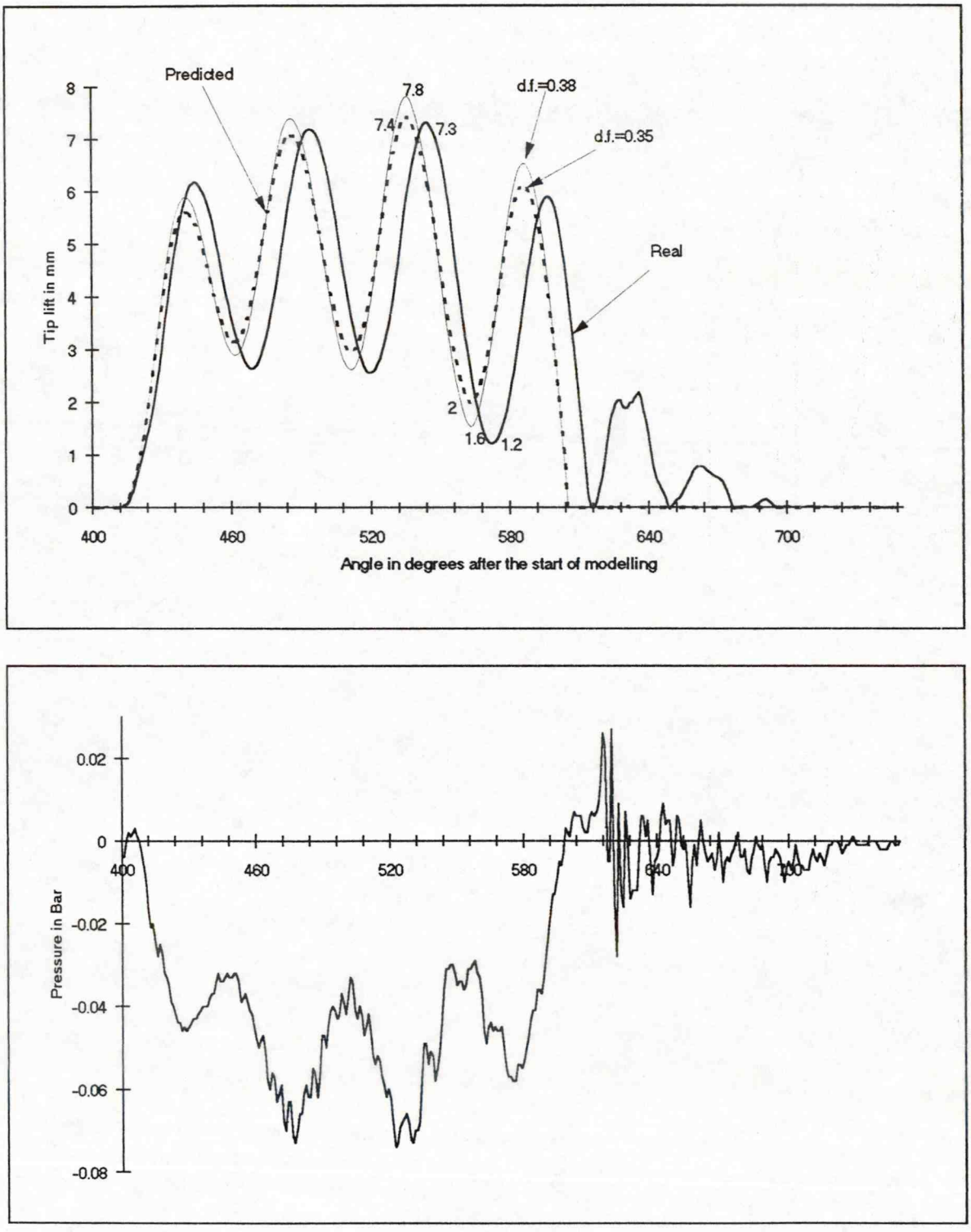

FIGURE 25 - Data set V. 1300 rev/min at 1/4 throttle. Measured and predicted lift showing the effects of various damping factors, and forcing pressure.

This modelled profile showed a way for future development as the two errors evident manifested themselves at the same time. It appeared that the under-prediction of the first peak caused an early downturn in the modelled lift and the phase shift, which remained constant throughout the rest of the data. It was likely that this would be a key area for future consideration.

CHAPTER 5

TEST FACILITIES AND SUMMARY OF EXPERIMENTS

5.1 GENERAL

To allow the experimental set-up to remain undisturbed, several standard items of laboratory equipment were replaced with dedicated equipment designed and built during this program of work. These included two power supplies and a two-channel strain gauge amplifier for use with the silicon bridge pressure transducers. Details of these designs and their circuit diagrams can be found in Appendix 3.

The experiments other than those to develop the model were categorized into two groups, those which concentrated on the physical properties of the reeds and were defined as 'bench top' experiments and those that studied the behaviour of the reeds in the firing engine.

5.2 TEST FACILITIES FOR THE BENCH TOP TESTS

When supported as cantilevers, reeds have natural frequencies of oscillation at which they can be stimulated to resonate. Using the real-time sensor, it was possible to measure both the resonant frequency and the frequency response to input stimuli. Under these experimental conditions the sensor could resolve displacement to less than 0.01mm. The samples were stimulated by a swept frequency, generated and amplified by a Environmental Equipment signal source (type 1531) and converted into a mechanical input by an Environmental Equipment shaker (type 1501). The actual mechanical input was measured by an accelerometer and the reed motion was measured by the position sensor. These two signals were input into an Ono-Sokki CF350 Fourier Function Transformer (FFT) which was able to determine the frequency response of the system.

Damping data was obtained using three modal techniques, one of which did not require specialized hardware. This third technique analysed the damping through the decay of free vibration. The reed was clamped as a cantilever and released from a deflected position. As the reed oscillated the magnitude of successive cycles described an envelope of exponential decay. The position of the reed was measured by the new sensor and this data was recorded by the data acquisition system. The reed motion was characterised by both the damping ratio and the natural frequency of oscillation. The rate of decay was a function of the damping and was calculated from the decay between successive peaks. The direct measurement of the fundamental frequencies of free vibration was also possible and was more accurate than calculation from shape, density and Young's modulus.

To determine Young's modulus a reed sample was prepared and a strain gauge attached to it. The sample was loaded and the strain and elongation measured. This was repeated for several loads, and from this data, Young's modulus was calculated.

5.3 TEST FACILITIES FOR THE ENGINE TEST BED

The experiments on reed valves under firing conditions in real-time were carried out on a hybrid Yamaha RD250 engine with the standard Yamaha RD250 reed block using several different reed styles. A special reed stop was machined with apertures cut in it which allowed optical access to the reed tip from above the reed block and also allowed pressure measurements to be taken close to the reed. These can be seen in Figure 26 overleaf.

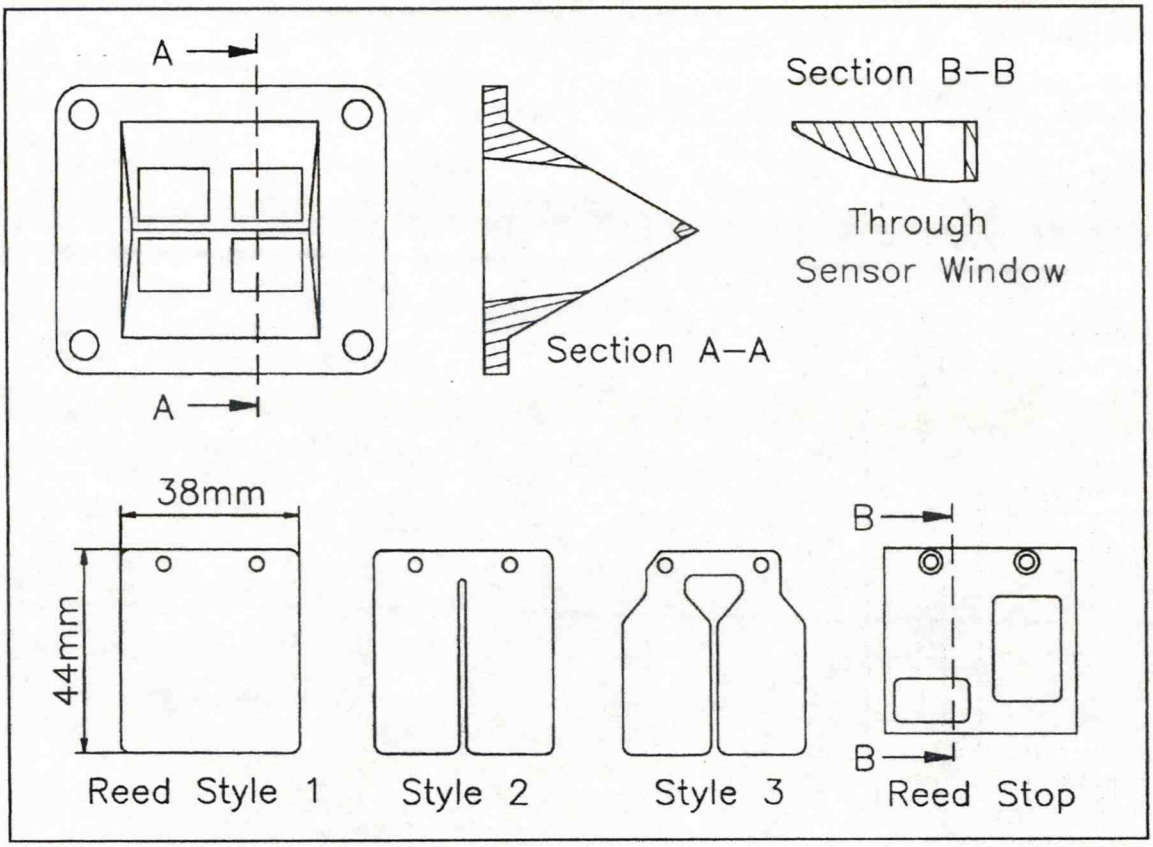

FIGURE 26 - Reed block, machined reed stop and 3 reed styles.

The engine was of RD250E origin, but was modified by removing one of the piston/conrod assemblies. This was replaced with a bob-weight which allowed it to be converted into a single cylinder 125cc engine. This minimized the complexity of the firing engine and reduced fuel consumption, exhaust gases, heat release and noise. The original air cooled barrels were replaced for convenience with a more modern water cooled variant from a RD250LC, which allowed the use of a water circuit for pre-heating before, and cooling during, the tests. The last major modification included the use of the Perspex reed valve housing as described earlier. Whilst it was recognised that this housing altered the characteristics of the engine, it simplified the test set-up by making the reed block easily accessible without requiring any modification to the cylinder barrels.

This was further justified since the program of work was primarily interested in the function of the reeds, rather than the specific performance and characteristics of the engine being used. The engine was run on a pre-mixed fuel of four-star petrol and mineral lubricant at a 32:1 ratio. The engine was connected via its conventional chain output drive to a Heenan & Froude DPX2 150 hp water brake, with a total loss cooling system. Other instrumentation connected to the engine included a Gaebridge shaft encoder (Type 120m/60/23/5-n/10-27), the newly developed position sensor, plus two silicon bridge pressure transducers (Radio Spares Type 256-720). The shaft encoder provided two outputs, one at 3 degree intervals and one every revolution; these were used indirectly to trigger and clock the Microlink A/D. The shaft encoder was joined to the crank by anti-backlash coupling. The position sensor was mounted onto the manifold directly above the reeds and focused on the right hand reed tip. The pressure sensors were placed upstream and downstream of the reed valve.

To record data from these sensors, the Microlink high speed data acquisition system was connected to, and controlled by an IBM PC micro computer. The Microlink had two Analogue/Digital (A/D) inputs and could run at conversion speeds of up to 100KHz. Data was converted into a 12 Bit digital format giving a maximum resolution of 1/4096 of full scale deflection. To store data during testing, the Microlink had 64K of RAM. Conversion started after an internal or external trigger and continued with subsequent internal or external clocking. These clock signals were generated by the position encoder. The captured data was held resident in the Microlink and was then transferred using an IEEE protocol via the serial port to the memory in the PC, where it was stored in ASCII format.

To fully integrate all the instrumentation, dedicated equipment including an Instrumentation Enhancement Unit (IEU), amplifiers and power supplies were designed and constructed.

Other non-dedicated equipment used included a Farnell DTS12P digital storage oscilloscope for on-line signal monitoring, a Nippon Seiki tachometer, a Farnell LFP1 signal generator for fixed period clocking of the Microlink, a Helios 5001 stroboscope and Panasonic M10 video camera for pseudo-real-time position recording. A test bed schematic is shown in Figure 27 below.

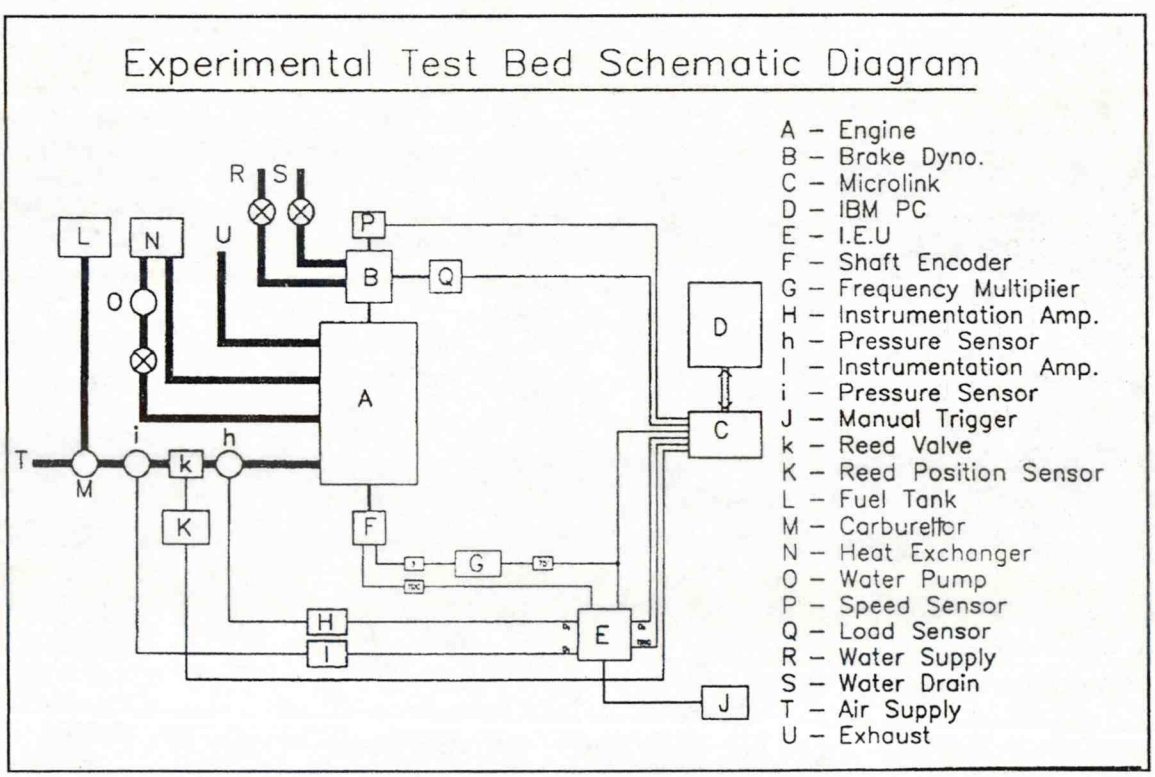

FIGURE 27 - Test bed and instrumentation schematic.

5.3.1 INSTRUMENTATION ENHANCEMENT UNIT (IEU)

The various instruments had performance parameters that did not allow optimal system compatibility. For example, the maximum clock speed that the Microlink could run at was 100kHz, yet the shaft encoder could only generate a maximum frequency of 20kHz at 10000 rev/min. The IEU was a dedicated design intended to manipulate and enhance the various specifications to produce optimised system performance.

There were three main design objectives:

(i) To increase data resolution using a phase locked frequency multiplier to speed up the sampling time without losing synchronization to the crank position.

(ii) To increase the sample frequency to allow multiplexing through a single data input.

(iii) To use the Top Dead Centre (TDC) pulse to trigger and sequence data acquisition.

Using the shaft encoder to directly control the data acquisition limited the sample frequency to 20kHz. To make use of the higher speed capability of the A/D, and thereby increase the data resolution, the fundamental frequency was multiplied using a phase locked loop with a divide by 4 counter in the feedback path. Being a dynamic frequency multiplier it was able to track the shift in frequency as the speed of the engine changed. This design provided data sampling at 3/4 degree intervals. A full circuit diagram can be seen in Appendix 3.

A limitation of the Microlink data acquisition system was that it only had two high speed data inputs. It was desirable to measure reed tip position and both the upstream and downstream pressures simultaneously. This was achieved by the inclusion of a two-channel multiplexer in the IEU, enabling the reed tip position to be measured every 3/4 degree whilst the pressures were sampled alternately. Each pressure was sampled every 1.5 degrees. This did not compromise the data resolution as analysis of the pressure data sampled at 0.75 degrees did not reveal any information that interpolation of the slower data speed could not provide. This was not a surprise since the sample speed was 240 times that of the fundamental pumping frequency (the speed of the engine) and was therefore fast enough to measure even the fastest reflections and transients.

The third function of the IEU was to provide a manual trigger for the acquisition system and to ensure that the two multiplexed signals were sampled in the same order after triggering. This was essential since the data manipulation software required a consistent file format to the data array. The hardware in the IEU reset the system prior to triggering, and forced the multiplexed channel (a) to be present at the data port during the first sample. The clock pulses that enabled the first and subsequent samples then toggled the multiplexed input between the two channels after a delay of 10^{-5}s. A full circuit diagram can again be found in Appendix 3.

5.4 EXPERIMENTAL SOFTWARE PROCEDURES

Several software routines were written and used to manipulate and process the sampled data as well as proprietary applications. Their purpose and function is described here.

5.4.1 DE-MULTIPLEXING SOFTWARE

Each raw data file from the Microlink was stored as a single column array. The first and every other location contained reed lift data and intermediate locations contained the pressure data. The pressure data was multiplexed between the upstream and downstream pressures. Data was captured in parallel so the data existed in pairs with respect to time. The primary function of this software was to de-multiplex and sort the data into its component data sets. The data was imported in a block of 960 rows which represented 360 degrees of engine rotation, sampled every 3/4 degree on two channels. This file contained data whose magnitude was expressed as a decimal number between 0 and 4096, where 0 and 4096 represented signals between -5V and +5V respectively.

5.4.2 LINEARISATION AND CALIBRATION OF REED TIP POSITION DATA

This software operated on sorted data and generated an output file which held the data in terms of the relevant measurement units. The reed lift data had to be linearised and scaled before being stored in mm. This was achieved through interpolation between data points from a look-up table which was obtained through the experimental calibration procedure described earlier in Chapter 2. The interpolation routine used was standard Pascal code from the Borland Numeric Tool Box. The block of data was written into an output file and subsequently used by the subroutines for any of the desired analyses. The pressure data was operated on by a simple scalar to convert the data into mBar units.

Other digital processing that improved the data and avoided noise from corrupting subsequent data, was spike removal. This was achieved by setting a maximum allowable slope in the signal which, if exceeded, was replaced with interpolated information.

5.4.3 PRESSURE DIFFERENCES

This subroutine subtracted the upstream pressure from the downstream pressure and wrote this pressure difference, reed lift and crank angle into a data file. This was of interest as it was the pressure difference that generated the force on the reed.

5.4.4 ON-LINE GRAPHICS

It was an advantage to be able to ensure that as each data set was taken, the captured data had not been corrupted in any way. It was easy to repeat tests during a test phase and maintain the same operating conditions, but not easy to repeat on another occasion. The previous subroutines were drawn together into a program with graphical output, so that each data set could be quickly inspected during the test phase. As the output data sets were being saved, they were displayed on screen, a block at a time, in a magnitude against crank angle format.

5.5 SUMMARY OF EXPERIMENTS

5.5.1 BENCH TOP EXPERIMENTS

Bench top tests were undertaken to provide empirical data for comparison with that which was calculated in the model. These included the following:

(i) Determination of the natural frequency for four reed samples at their fundamental and first harmonic frequencies.

(ii) An investigation of damping using a modal technique.

(iii) An investigation of damping by analysis of the damped decay of free vibration.

(iv) Experimental determination of Young's modulus for the standard steel reed.

5.5.2 REED TESTS IN THE FIRING ENGINE

Tests on the firing engine were undertaken to both demonstrate the versatility of the new sensor and to compare the performance of different reeds. The reeds used were a proprietary tapered and a standard steel reed, a proprietary composite and a laminated fibreglass reed.

The tests were conducted at the same speed and load or at the same speed and throttle settings. Each test was repeated at a series of different speeds to obtain a range of different data sets for each reed type. In each test, the lift profile was measured so that observations and comparisons could be made.

These experiments were split into four groups, designed to study reed behaviour under the following conditions.

(i) Performance investigation of four different reed types at low speed.

(ii) Comparison between the performance of the 'best' and 'worst' reeds at medium speed and at medium power.

(iii) A study of the cyclic variation of a composite reed, first at part throttle and then at peak power.

(iv) Comparison of the best steel and the best composite reeds at peak power.

CHAPTER 6 - RESULTS AND DISCUSSION OF EXPERIMENTAL DATA

6.1 PHYSICAL PROPERTIES OF REEDS

Bench top tests were carried out to obtain parametric data about the reeds used in the experimental work. All the reed types were investigated to obtain natural frequency of vibration data, which was then used to compare with their subsequent performance in the firing engine. The standard steel reed was also investigated for its damping ratio for comparison with that used in the model.

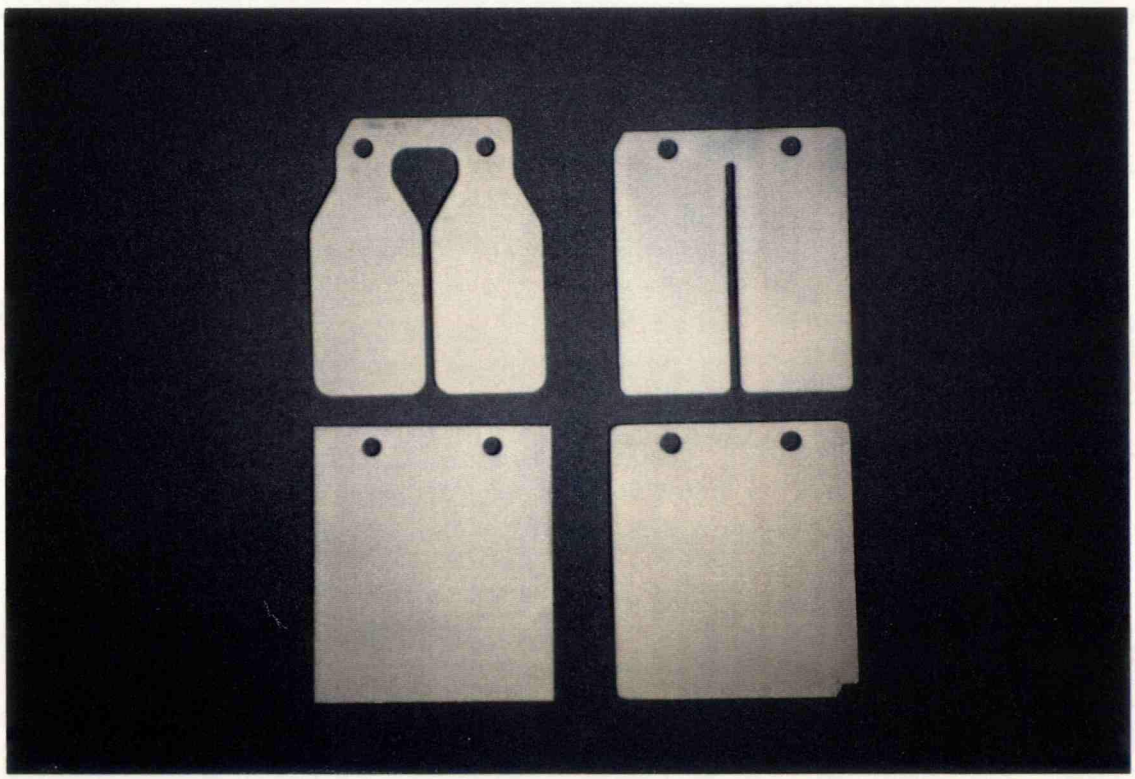

PLATE 4 - Four reed types: tapered steel (top left); standard steel (top right); fibreglass (bottom left) and proprietary composite (bottom right).

6.1.1 NATURAL FREQUENCY OF FREE VIBRATION OF FOUR REED SAMPLES

The position sensor developed during this study was coupled to a Fourier Function Transformer and used to investigate the frequency response function of four different reed

types. The frequency response for the standard steel reed is displayed graphically in Figure 28 below and the data for the other reed types is illustrated in Appendix 4. Table 1 summarises the parametric data for all the reed types. This data was subsequently used to determine the natural frequency of vibration for the first and second modes for each reed.

TABLE 1. First and second mode frequencies of four reed types.

REED TYPE	MODE 1	MODE 2	MASS (g)
Standard Steel	120 Hz	742 Hz	2.7
Tapered Steel	138 Hz	885 Hz	3.1
Prop. Composite.	154 Hz	960 Hz	1.7
Fibreglass	183Hz	1140 Hz	2.1

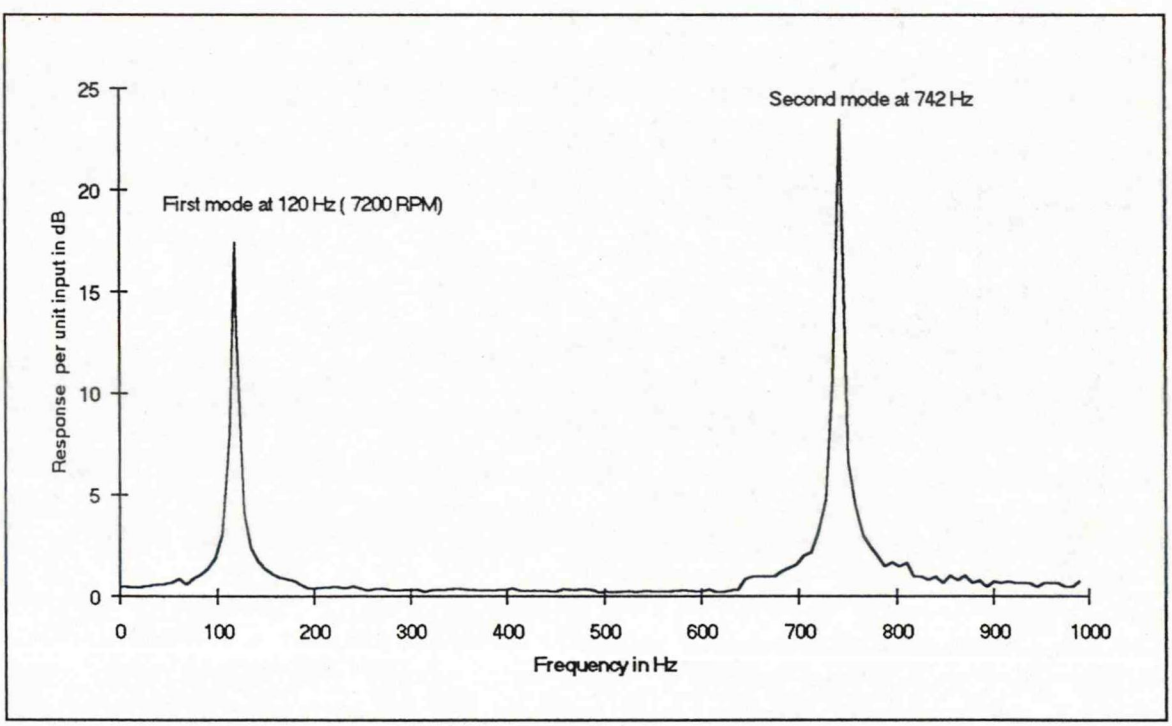

FIGURE 28 - Frequency response of the standard steel reed.

6.1.2 MODAL DAMPING OF THE STANDARD STEEL REED

With further dedicated processing of the standard steel reed data (using ICATS software), it was possible to determine the structural damping for the first resonant mode. The theory for this modal analysis is presented in Chapter 3. ICATS is an interactive program which required the user to select the points in the complex plane, through which a curve was then best fitted. An indication of the accuracy was provided by considering two check parameters; these were the variation in the radius and the damping plane. The good signal to noise performance of the position sensor allowed radial variation to be less than 2.5% and damping variation to be better than 5%. For the standard steel reed, the structural damping ratio was calculated to be 0.8759%. This data can be seen in Figure 29 below.

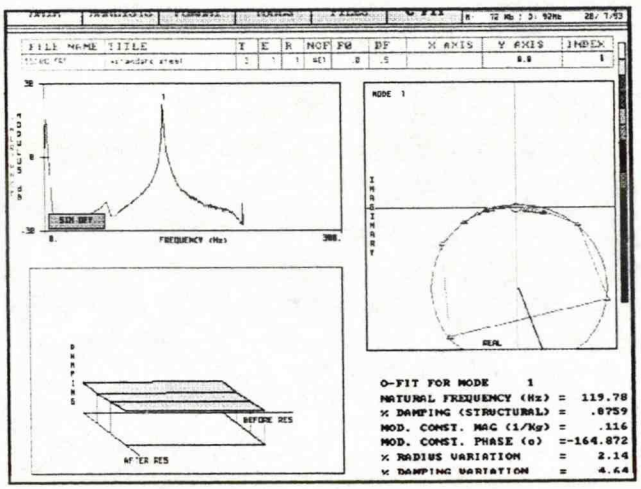

FIGURE 29 - Screen capture from ICATS software showing a fitted curve to the modal analysis data and the associated values for structural damping and variances.

6.1.3 VISCOUS DAMPING DURING FREE VIBRATION

The shape of the decay envelope of a cantilever during free vibration is exponential and the rate of decay is controlled by the amount of damping. In this case, the total damping is considered to be dominated by the viscous damping. To increase the accuracy of the experiment, the decay between subsequent cycles was determined by the average of 95 successive cycles.

The following data shows the decay envelope from which the damping was determined (Figure 30 below). From this data the viscous damping ratio in still air was calculated as 0.386%.

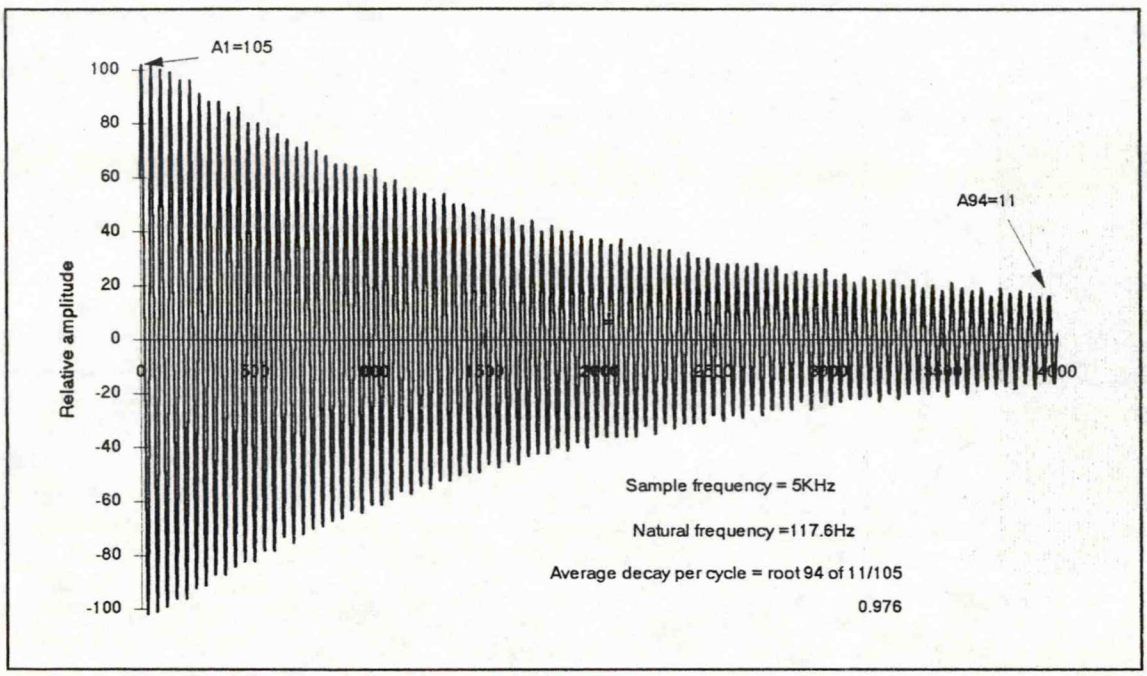

FIGURE 30 - Damped free vibration of the standard steel reed.

6.1.4 DETERMINATION OF YOUNG'S MODULUS FOR THE STANDARD STEEL REED

The purpose of determining Young's modulus for the standard steel reed by experimentation, was to provide an accurate value to use in the reed model. A sample of the material was cut to the required dimensions and then prepared for testing by bonding a strain gauge to it (see Plate 5 overleaf). The sample was progressively loaded and the strain measured. Young's modulus was found to be 226 GNM^{-2}.

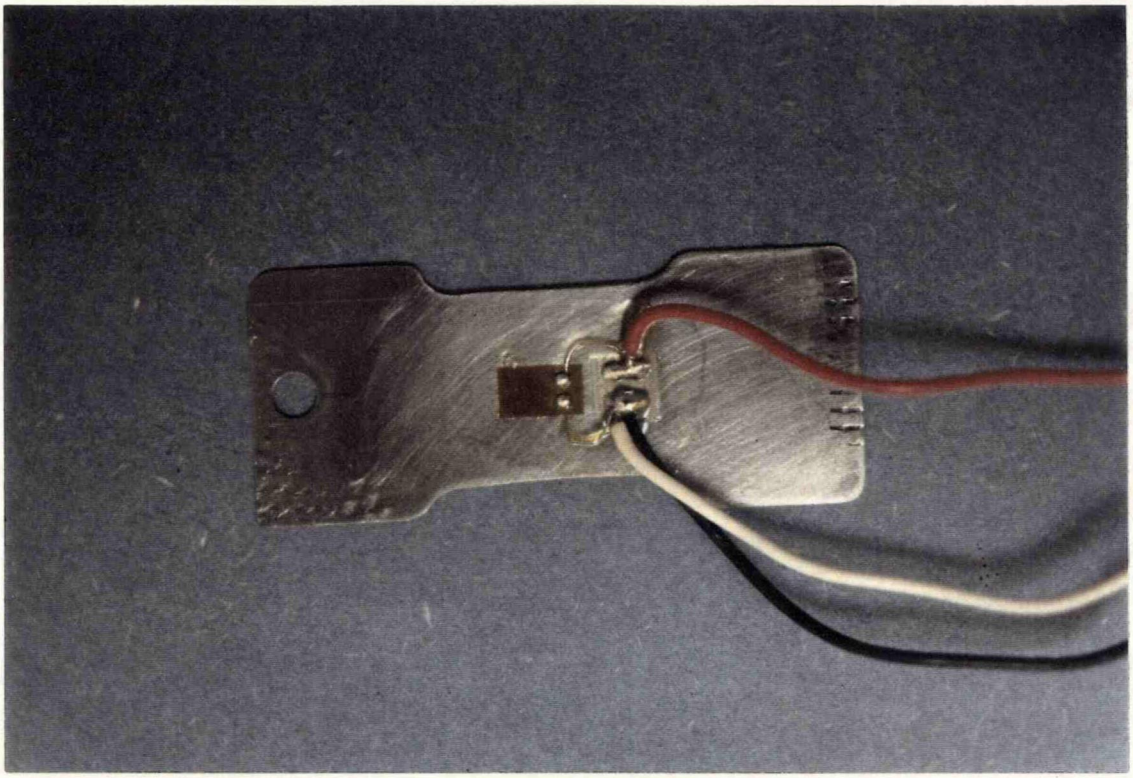

PLATE 5 - Strain gauge bonded to a sample of standard steel reed valve material.

6.2 EXPERIMENTAL COMPARISONS OF FOUR DIFFERENT REED TYPES IN A FIRING ENGINE

The tests compared the dynamic behaviour of the different reeds subjected to the same operating conditions in a firing engine. These experiments were repeated using a range of stable and unstable conditions with both high and low load. In each test, the lift profile was measured so that observations and comparisons could be made. These experiments were split into four groups designed to study reed behaviour under the following conditions:

(i) Group I - four reed types at 5000 rev/min with full load (tests 1-4).

(ii) Group II - standard steel and proprietary composite reeds at 6000 and 7000 rev/min (tests 5-8).

(iii) Group III - cyclic stability at 9000 rev/min (tests 9 and 10).

(iv) Group IV -proprietary composite and tapered steel reeds at 9000 rev/min (tests 11 and 12).

6.2.1 GROUP I - FOUR REED TYPES AT 5000 REV/MIN WITH FULL LOAD (TESTS 1-4).

For this set of tests the engine was run at full throttle on the hydraulic dynanometer. Tests were run consecutively, with the reed type being changed between tests. For these four reeds the brake power varied from 5.2-6.7 kW. Although similar, the lift profiles reflected these differences. The poorest performance was given by the standard steel reed (test 1; Figure 31). It had the lowest natural frequency and was one of the heaviest of all the reeds, consequently it was sluggish to open (93 degrees Before Top Dead Centre {BTDC}) and close (80 degrees After Top Dead Centre {ATDC}). Although this reed attained reasonable lift of 7.1mm, this was achieved late in the cycle at 12 degrees ATDC and there may have been significant inflow. The slow closure shown, allowed the possibility of reverse flow and it was not surprising that the performance of this reed could be improved.

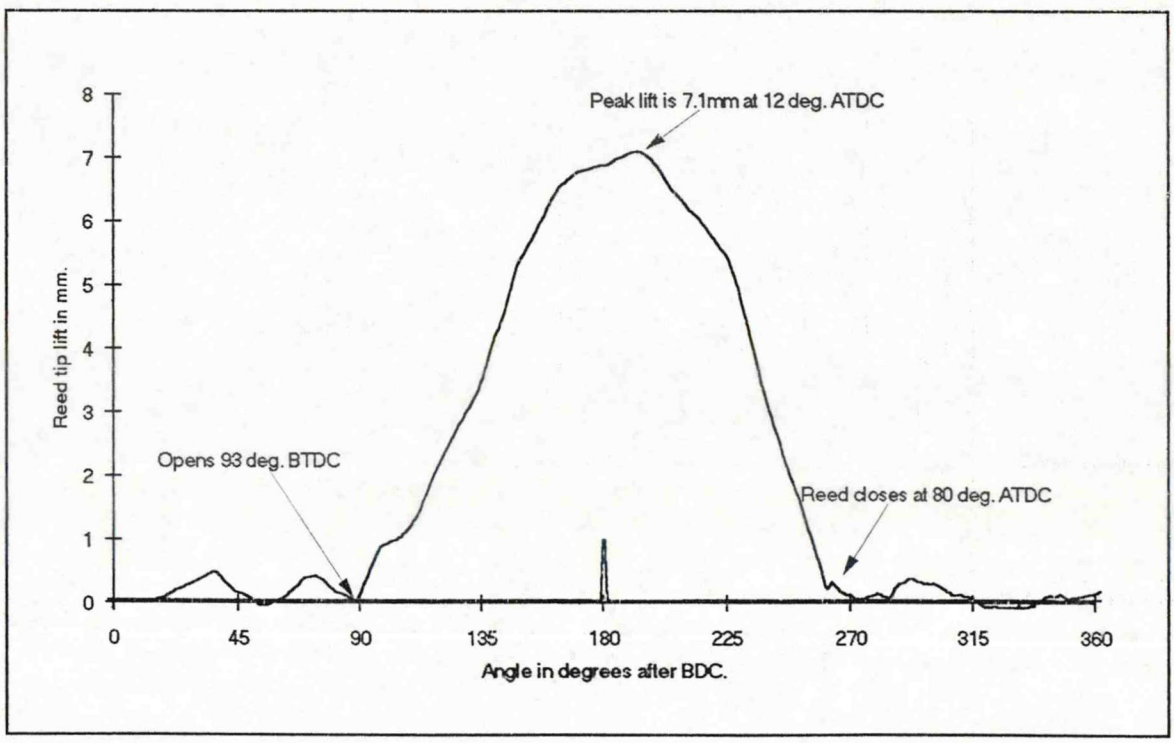

FIGURE 31 - (Test 1) Standard steel reed at 5100 rev/min, 5.2kW load and full throttle.

The tests involving the tapered steel and fibreglass reeds (tests 2 and 3) were interesting to compare, not only to each other but also with the other reed types, since they both generated the same performance but in different ways. The reed used in test 2 was the tapered steel reed design, which allowed a 'rising rate' spring stiffness with lift. This gave an early opening point at 128 degrees BTDC and a characteristic triangulated lift profile which peaked at 7.0mm, at 16 degrees BTDC. It closed at 60 degrees ATDC, with some evidence of secondary opening. In contrast, the same performance was achieved by the conventional fibreglass reed in the third test which performed better than the reed in test 1, since both opening and closing occurred 10 degrees earlier and tip lift peaked at 6.3mm and 6 degrees BTDC (see Figures 32 below and 33 overleaf).

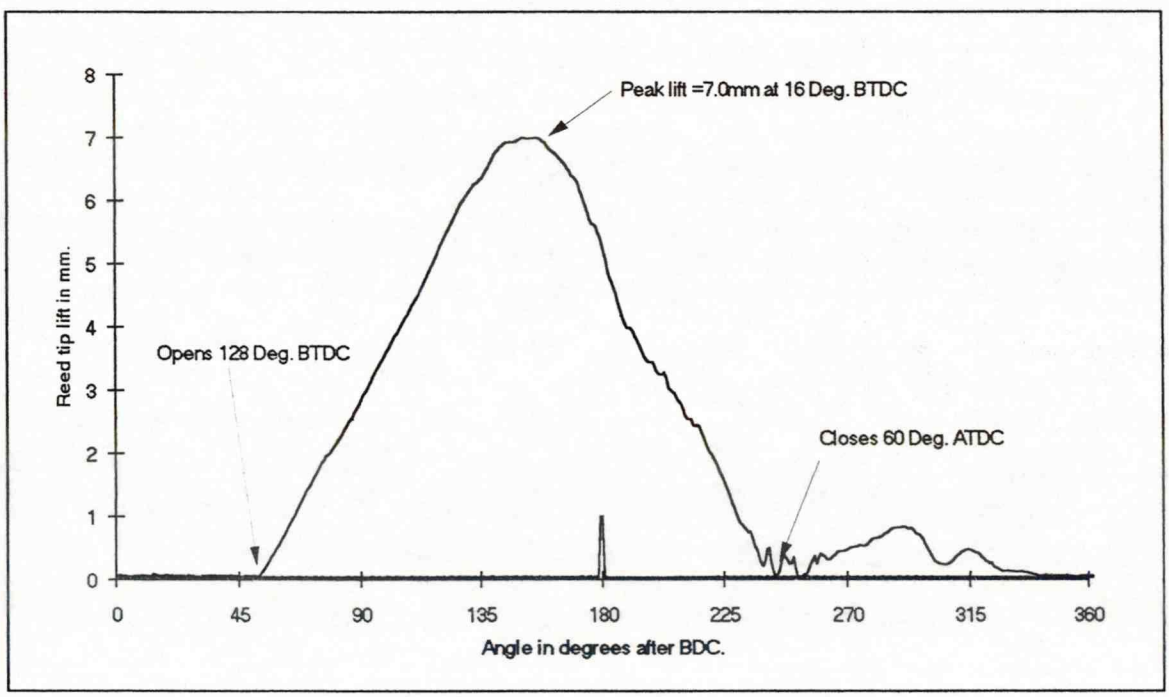

FIGURE 32 - (Test 2) Tapered steel reed at 5000 rev/min, 5.8kW load and full throttle.

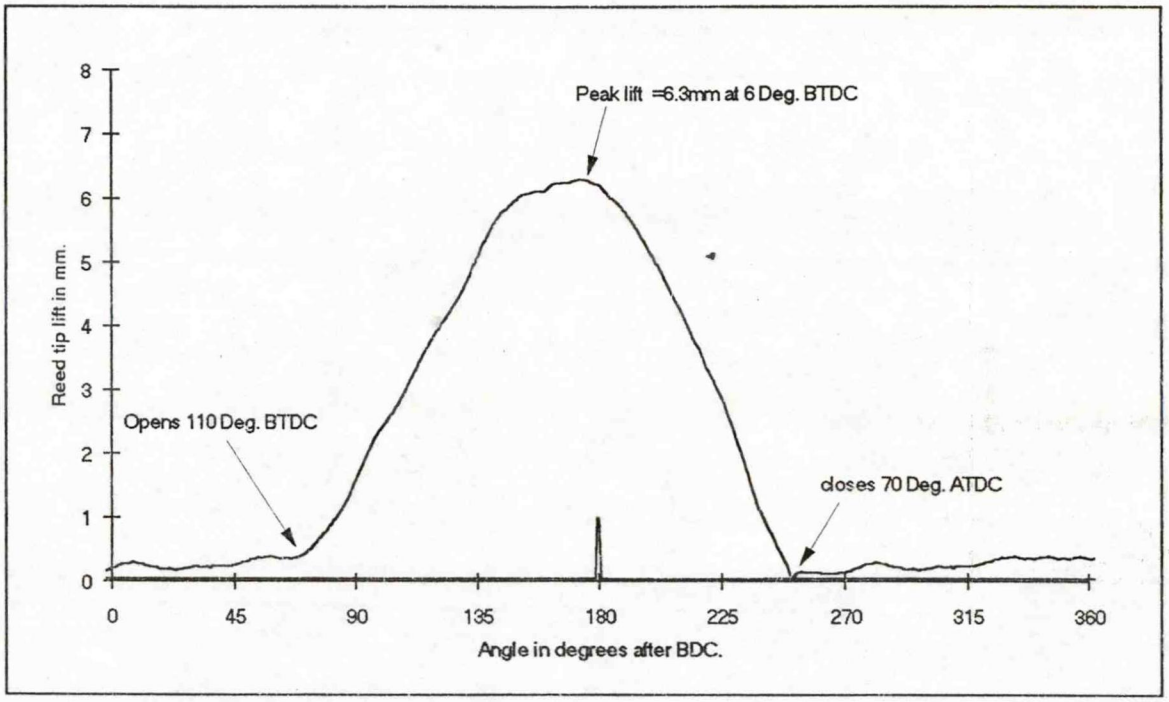

FIGURE 33 - (Test 3) Fibreglass reed at 5000 rev/min, 5.8kW load and full throttle.

Test 4 used a proprietary composite reed which performed well, giving early opening and the highest peak lift of 7.3mm, at 3 degrees ATDC. The closing point which, although late at 82 degrees ATDC, had the steepest closing rate exhibited by any of the four samples. This reed allowed the engine to generate 6.7 kW.

Information provided by the lift sensor in all of the tests supported the belief that lighter composite reeds with higher stiffness to weight ratios generally had dynamic behaviour which could out perform conventional spring steel reeds. It was interesting to observe that the change in physical shape of the reed to include tapering at its root, also had an advantage, showing how both materials and design can improve performance (Figure 34 overleaf).

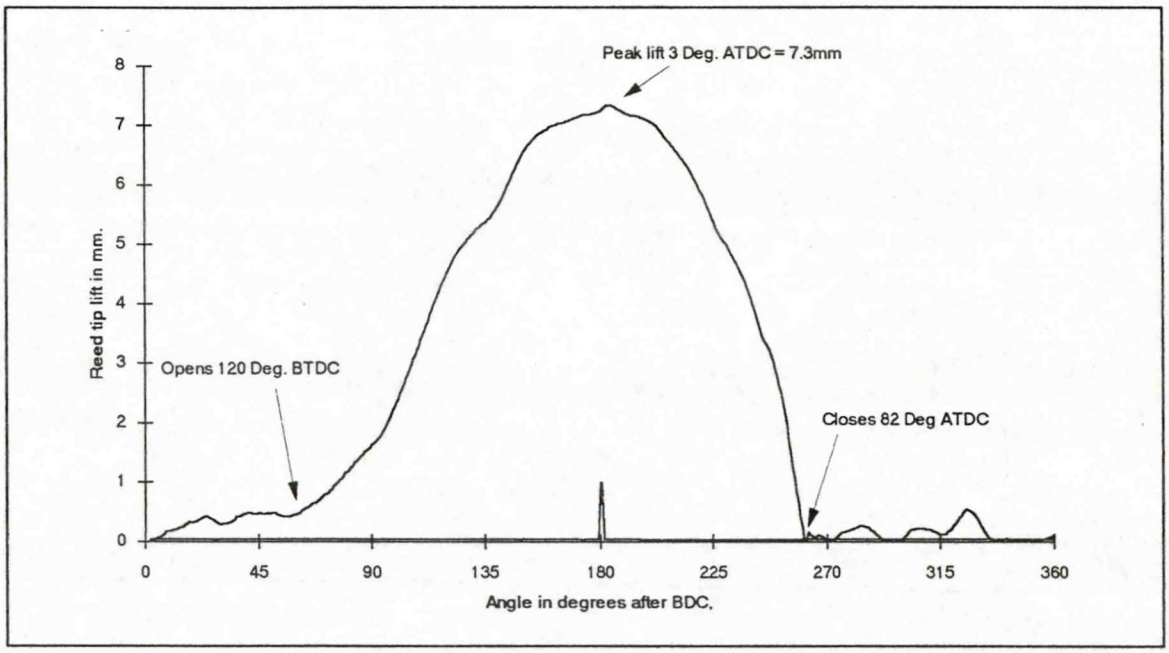

FIGURE 34 - (Test 4) Proprietary composite reed at 5000 rev/min, 6.7kW load and full throttle

.

6.2.2 GROUP II - STANDARD STEEL AND PROPRIETARY COMPOSITE REEDS AT 6000 AND 7000 REV/MIN (TESTS 5-8).

The best and worst performing reeds (the proprietary composite and standard steel reed respectively) were used in the next tests and were run at a similar speed and load, with the throttle adjusted accordingly. Tests were carried out at 9 kW brake power and at 6000 and 7000 rev/min. Tests 5 and 6 clearly showed the causes for the difference in performance between the two reeds. The composite reed produced 11% more power but with less lift and a reduced opening period. The most significant difference was the delay in closing. Here the superior mass to stiffness ratio (higher frequency of natural vibration) allowed the composite reed to close 19 degrees before the standard reed. It was probable that this resulted in less reverse flow, and consequently, less throttle was necessary. Such conditions resulted in the reed opening point being later by 5 degrees and the peak tip lift being marginally less by

0.5mm. In other respects the lift profiles were similar, both opening ramps followed the same general shape with similar rates of change (see Figures 35 and 36 below).

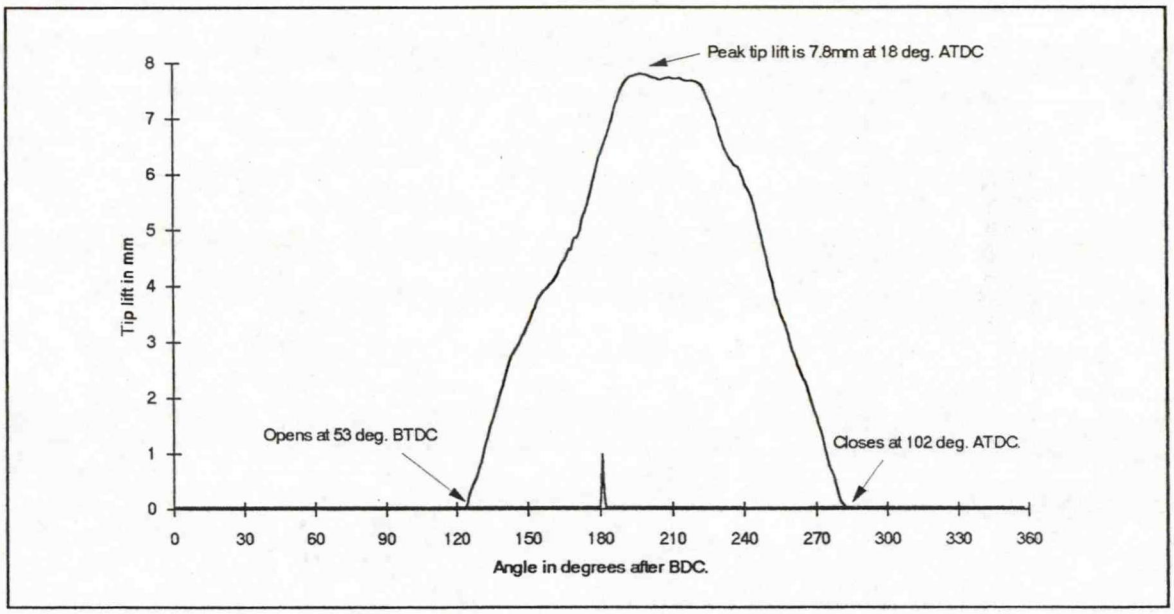

FIGURE 35 - (Test 5) Standard steel reed at 6000 rev/min, 9kW load and part throttle.

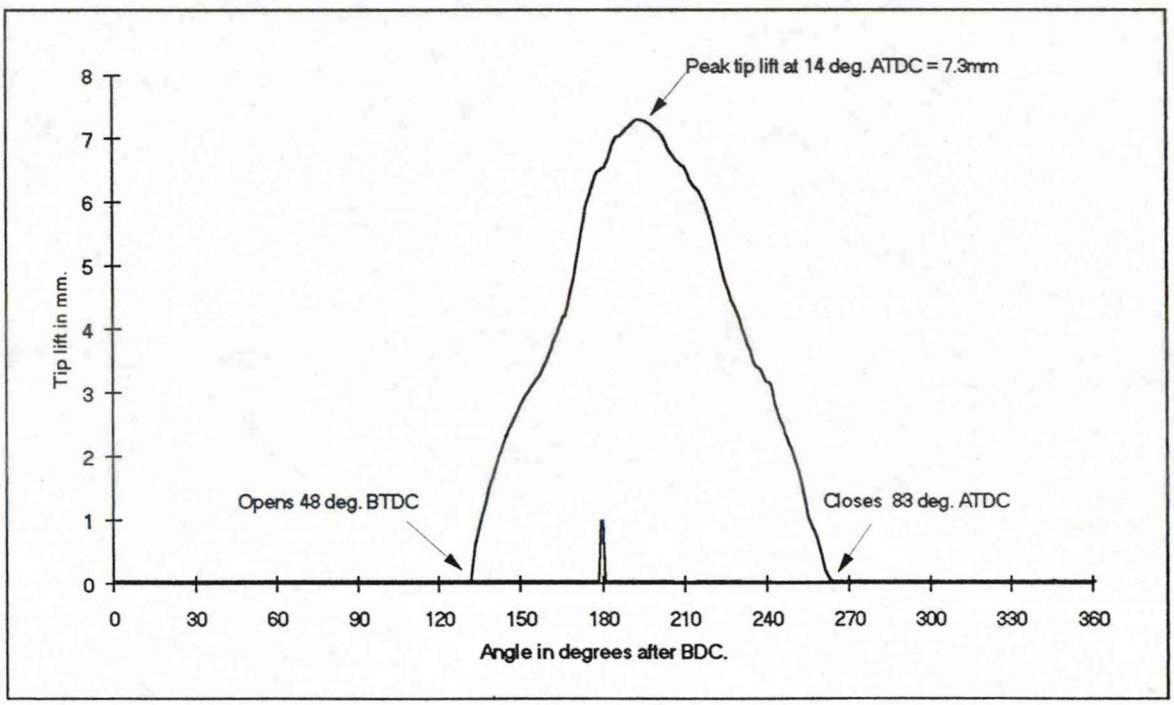

FIGURE 36 - (Test 6) Proprietary composite reed at 6000 rev/min, 10.0kW load and part throttle.

Tests 7 & 8 used the same reeds and conditions as used in tests 5 & 6, but at 1000 rev/min faster. The throttle settings were lower than in the previous tests, since the engine began to approach its power band and it was not possible to compare these tests directly, but it was interesting to note that although the composite reed allowed more power to be developed, both reeds opened at approximately the same time. The composite reed closed earlier by 13 degrees from a peak lift 0.4mm higher. The composite reed opened faster and achieved peak lift 18 degrees earlier than the steel reed. It is possible that this could be attributed to slightly more throttle, but the faster response of the composite reed was likely to have been the dominant factor (see Figures 37 below and 38 overleaf). All the part throttle data sets exhibit less stable and more ragged lift profiles than those at full throttle. Two-stroke engines are notoriously unstable at speeds approaching the power band, where there is a high degree of cyclic instability. This was shown clearly in these data sets by the high degree of modulation evident on the lift profiles. This was investigated further in tests 9 and 10.

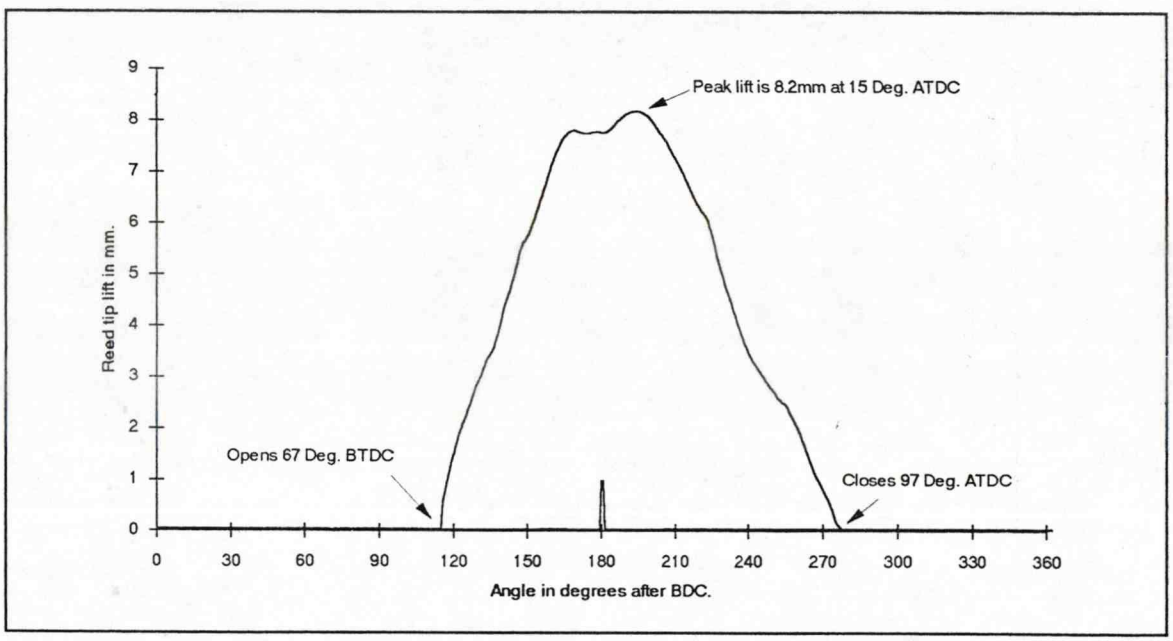

FIGURE 37 - (Test 7) Proprietary composite reed at 7000 rev/min, 10.6kW load and part throttle.

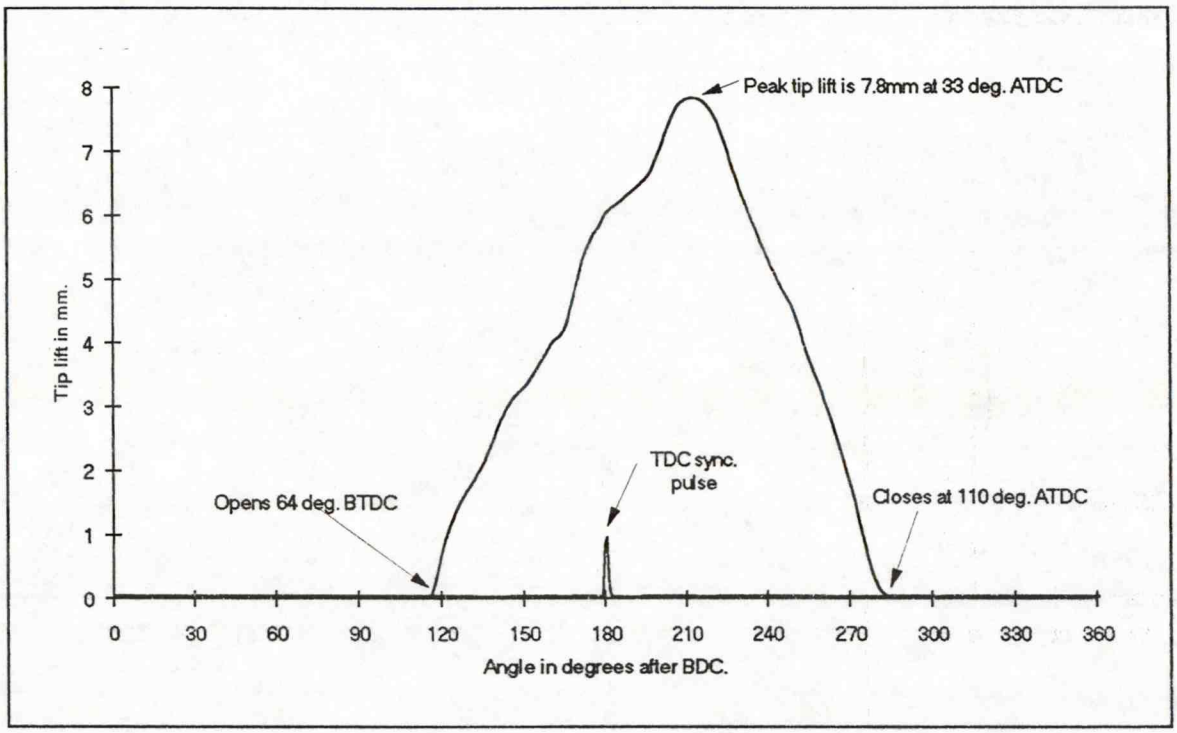

FIGURE 38 - (Test 8) Standard steel reed at 7000 rev/min, 9.4 kW load and part throttle.

6.2.3 GROUP III - CYCLIC STABILITY AT 9000 REV/MIN (TESTS 9 AND 10)

Real-time data is invaluable for studies of cyclic variation, and the development of the position sensor made this particular study possible. Only a small amount of work has been published to date about the cyclic variations of reed valve motion in two-stroke engines or reed motion during unstable operating conditions. Tests 9 and 10 demonstrated the power of the sensor by providing real-time data sets whilst the engine ran at part throttle at the start of its power band, also whilst the engine ran at 3/4 throttle at peak power. This reflected a small change in engine speed but resulted in a change from an unstable to a stable engine regime with an associated power increase of 70%. Test 9 (Figures 39, 40 and 41) displayed data from seven consecutive cycles which showed a high degree of cyclic stability. From the test, the peak lift was shown to change by only 0.3 mm (Figure 39 overleaf), and where the

first five full cycles were superimposed, the opening point was seen to change from limit to limit by only 12 degrees and the closing point by approximately 8 degrees (Figure 40 below).

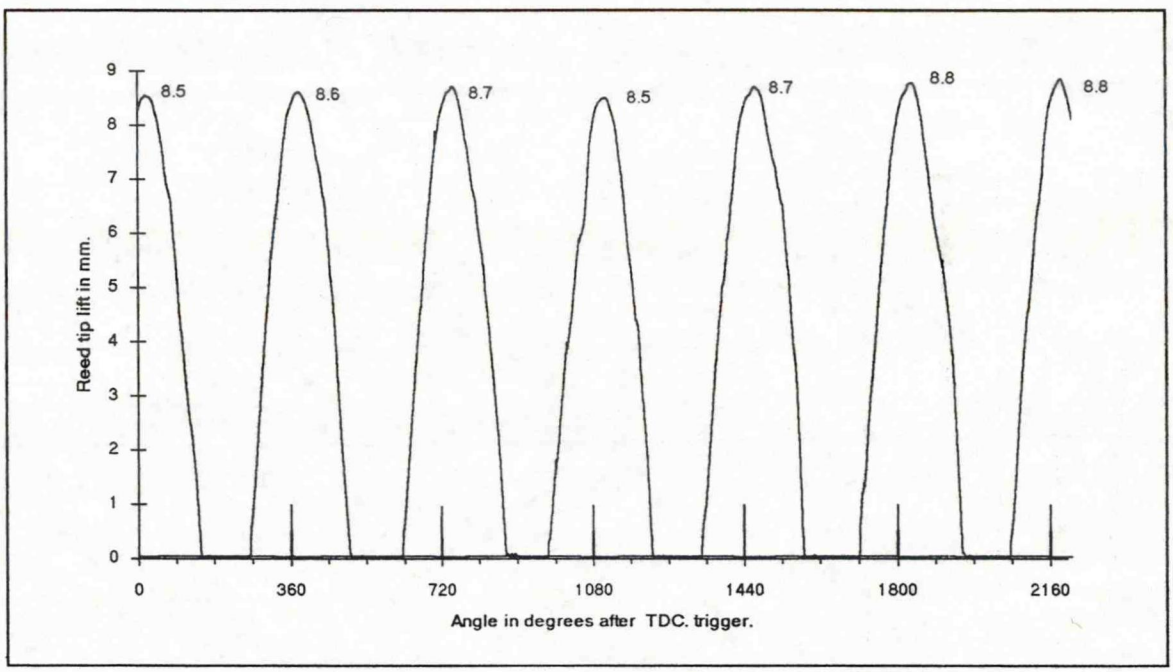

FIGURE 39 - (Test 9) Five consecutive cycles at 9000 rev/min and 19.6 kW load.

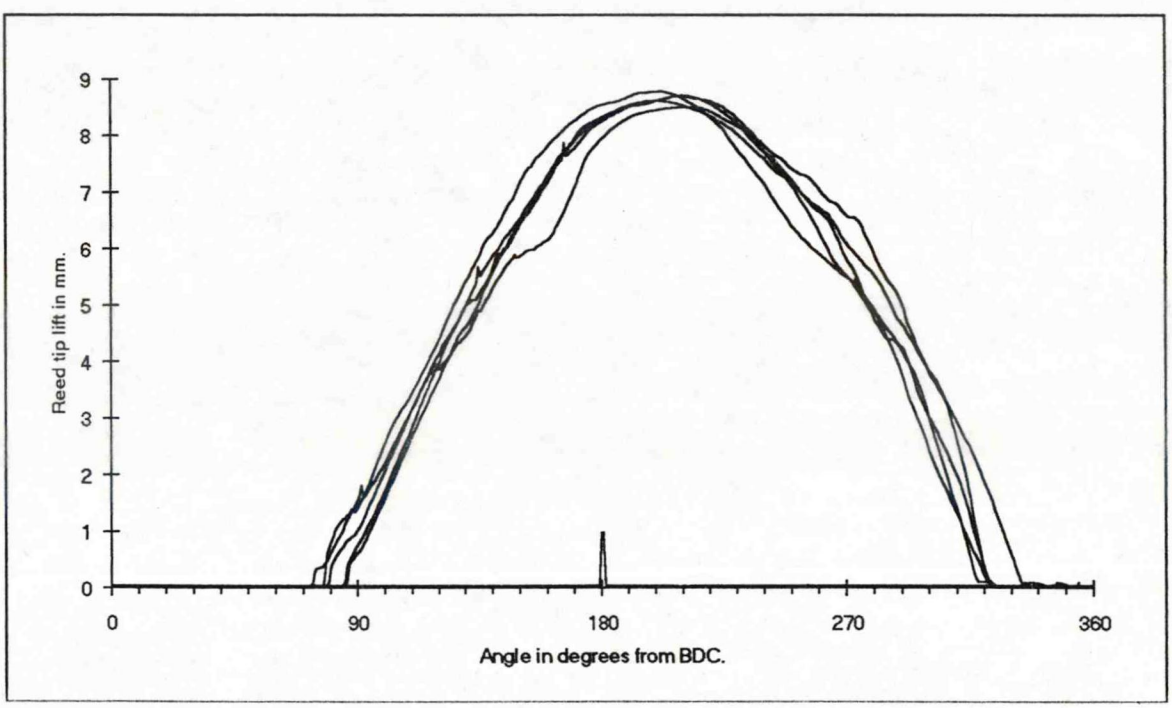

FIGURE 40 - (Test 9) Five superimposed cycles.

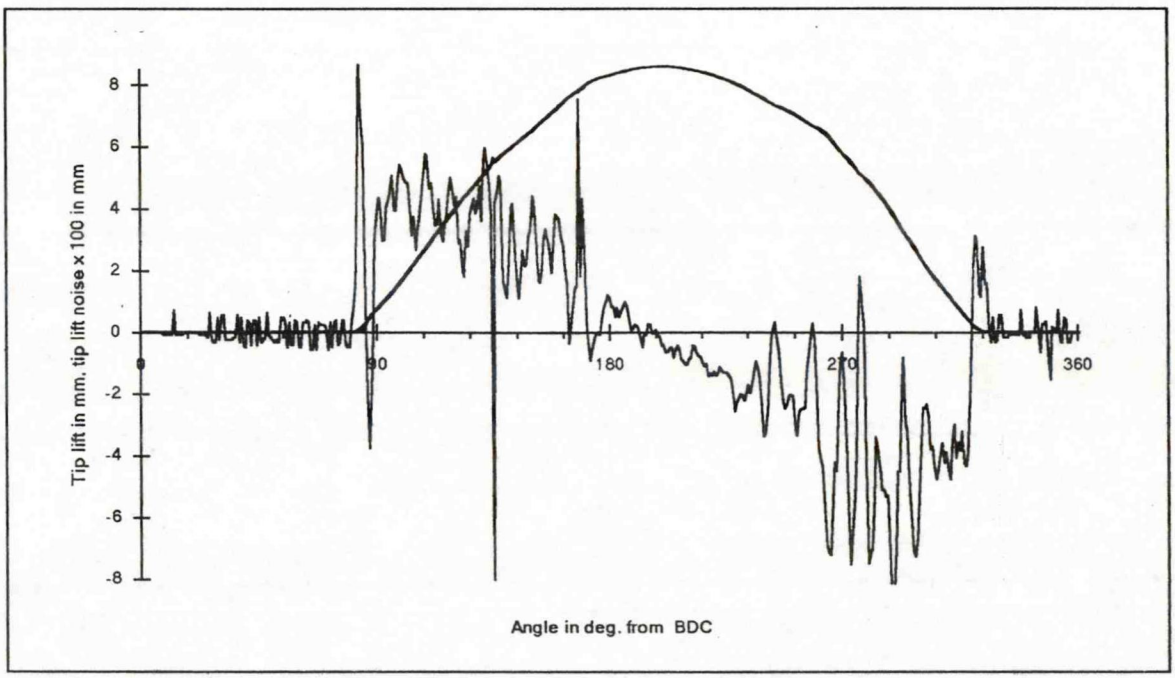

FIGURE 41 - (Test 9) Noise investigation showing actual and filtered reed lift, together with the difference signal.

In contrast, test 10 (Figure 42 overleaf) demonstrated a high degree of cyclic variation with the tip lift changing by 1.5mm, causing very different tip lift profiles. A similar deviation in opening and closing points was also evident, with the opening point showing a 50% change in the worst instances.

The tip lift profile around peak lift can be seen to be ragged, this was likely to have resulted from the optical noise created by the excess fuel spray that exist and arose from poor carburation during these operating conditions.

Having considered the differences between tests 9 and 10 it was useful to return to the test 9 data set and consider the data in terms of the performance of the sensor, since it provided an empirical indication of data confidence.

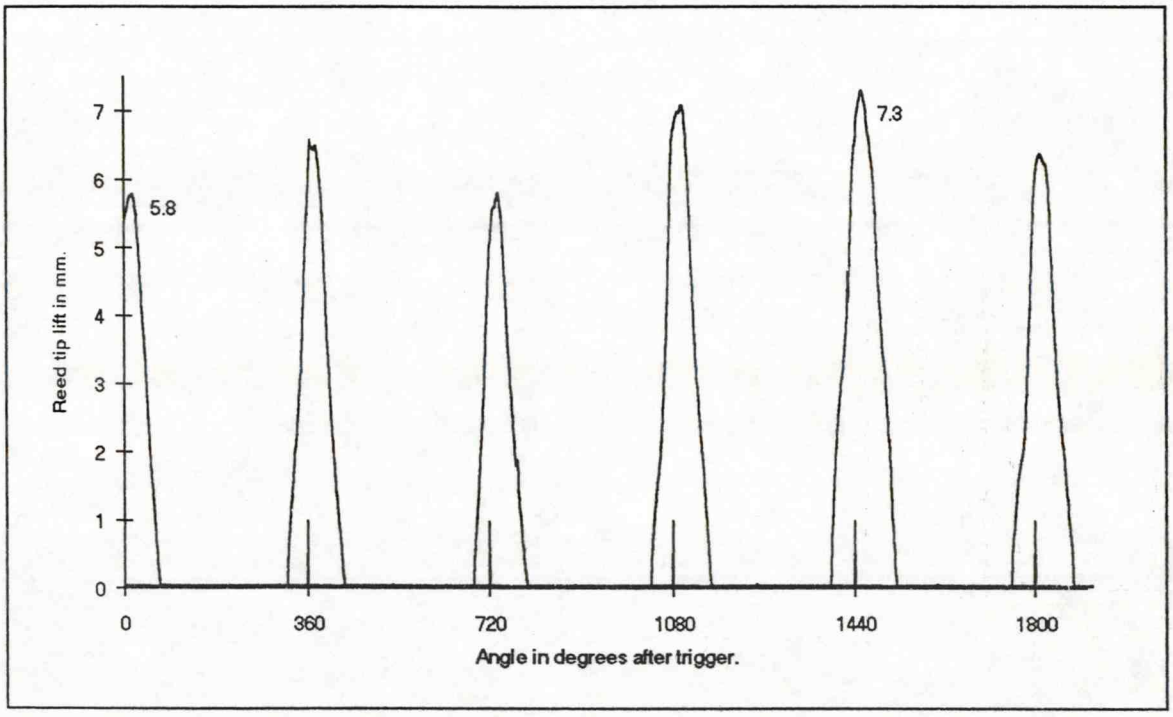

FIGURE 42 - (Test 10) Six consecutive cycles of the proprietary composite reed at 7000 rev/min and 11.7 kW at part throttle.

The five cycles in test 9 (Figure 40) showed three things clearly. Firstly, that there were five distinctly different tip excursions which have several very similar general features - (the opening and closing point, the opening and closing ramp and the path near peak lift). Secondly, that all the traces had some noise modulated on them, and thirdly that there was one trace that exhibited data corruption between 140 and 170 degrees from BDC.

Test 9 (Figure 41) evaluated the noise by plotting the raw data from a single cycle alongside data which had been processed by a ten point floating average. This was a method of defining a path in terms of a simple position time algorithm, which considered every point in the context of its past and future known positions, as well as its current measured position. A reed valve with known inertia and subjected to maximum known forces, could only

deviate from its current position by a finite amount. We could define the extent of the noise by the deviation of the data from this theoretical profile. The raw data and best fit, formed two almost indistinguishable traces in Figure 41, but the third trace displayed the noise in terms of the difference between the two. The peak difference was 0.08mm with the majority existing inside the 0.05mm limits. This suggested that confidence in the data integrity to be within 0.1mm.

Data integrity could be lost through corruption as well as through noise. Test 9 (Figure 40) shows one cycle where just such a corruption occurred. The profile shows a 'bite' taken out of it, with the path deviating for approximately 30 degrees before returning to the uncorrupted path. The sensor required the optical medium to remain constant (as explained in the chapter on sensor design). In a firing engine this required a homogenous fuel/air mixture. It was possible that in this case a fuel droplet was responsible for such a corruption. As such corruption was apparent these data sets could be studied further, ignored or 'repaired' with subsequent data processing.

6.2.4 GROUP IV - PROPRIETARY COMPOSITE AND TAPERED STEEL REEDS AT 9000 REV/MIN (TESTS 11 AND 12)

Tests 11 and 12 (Figures 43 and 44 respectively) were data sets taken at full power and at almost the same speed (2% power difference). In many respects the key features of the lift profiles were identical, the peak lift and closing point were exactly the same whilst the opening point of the tapered steel reed was 10 degrees later than that of the composite reed. The feature of interest was the phasing of the profiles. The composite reed showed an almost

symmetrical profile about TDC, whilst the steel reed retained some asymmetry. At the limit of it's performance a reed valve's asymmetric timing collapses as it begins to follow the symmetrical nature of the piston port behind which it is situated.

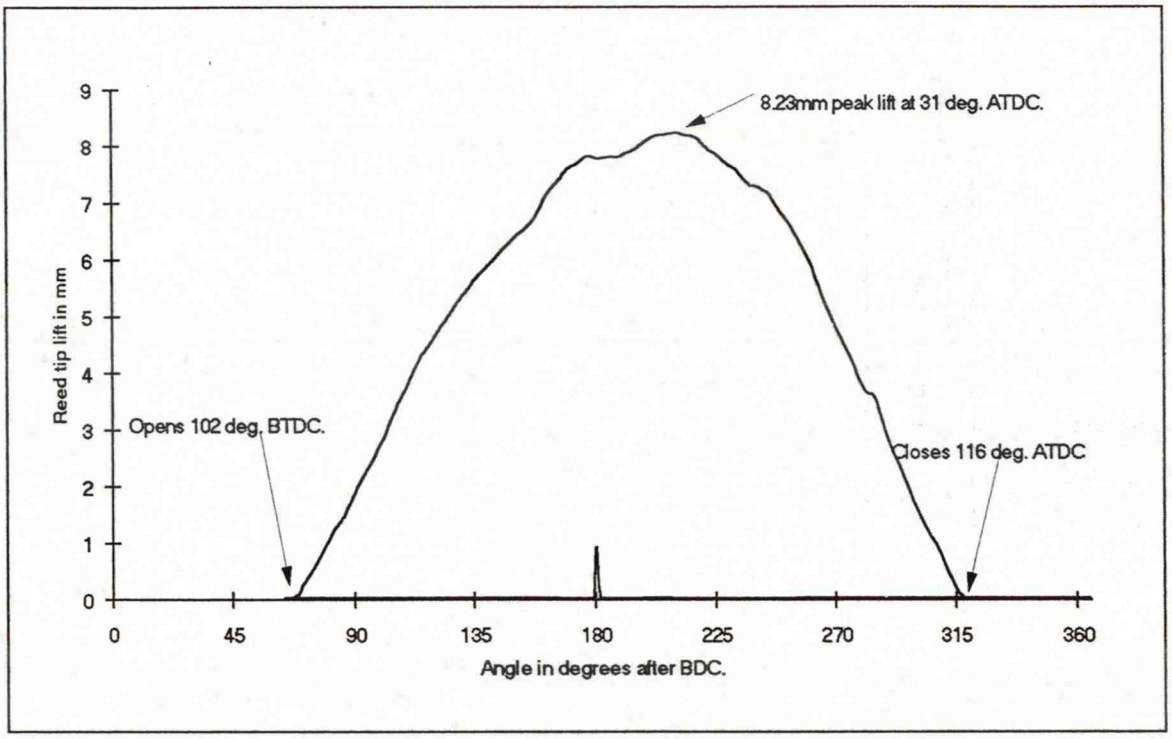

FIGURE 43 - (Test 11) Tapered steel reed at 8400 rev/min with 23.6kW load.

Test 12 (Figure 44 overleaf) suggests that this was happening in the composite reed, whilst the tapered steel reed could probably operate at a higher speeds. Both lift profiles show signs of tip flutter at peak lift.

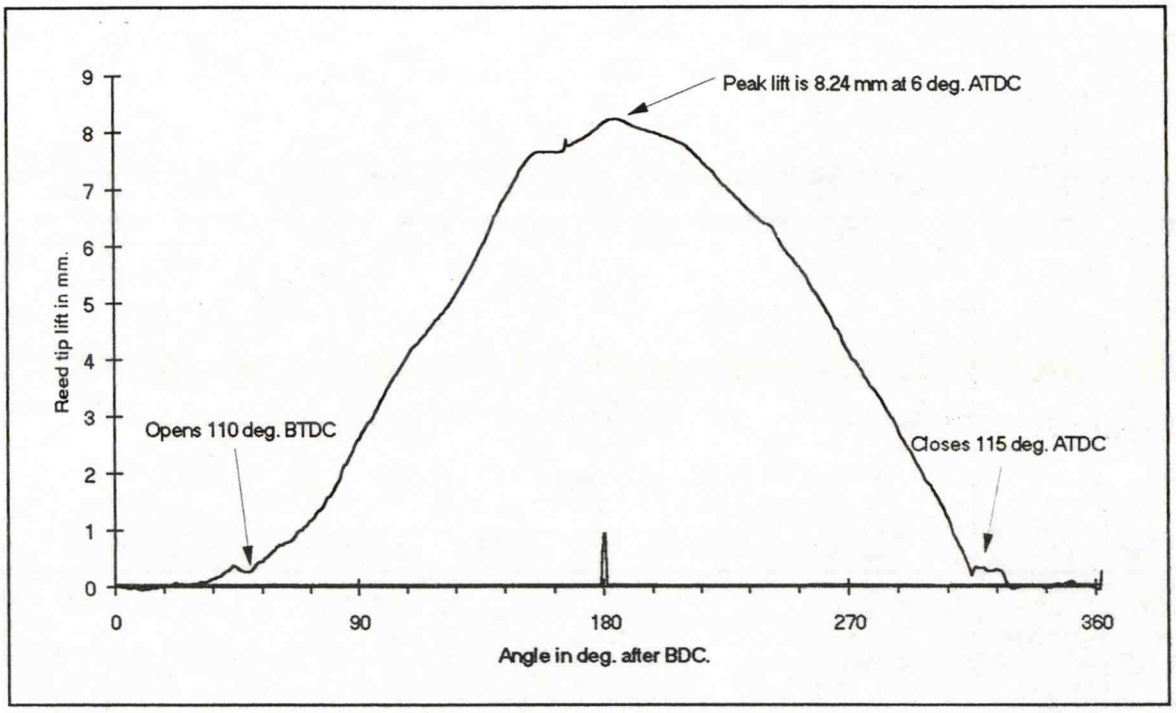

FIGURE 44 - (Test 12) Proprietary composite reed at 8500 rev/min with 24.3kW load.

CHAPTER 7 CONCLUSION AND FUTURE WORK

7.1 CONCLUSION

The sensor development successfully produced a cheap high resolution device with a bandwidth of 25kHz able to resolve reed displacement to 0.01 of a millimetre. The sensor could have a production cost of less than £10. Evaluation showed that this sensor provided real-time data which would allow studies of the unstable aspects of reed behaviour to be investigated in detail for the first time. The new sensor enabled basic performance comparisons to be made under various operating conditions and with different reed designs.

Four different reed samples were analysed and their dynamic behaviour correlated to their design or composition. The results confirmed that reeds with higher natural frequencies work better at high speed and that lighter composite reeds perform better than the spring steel type, whilst a tapered design with its natural rising rate stiffness, performed better than the conventional parallel design. The improvements resulted from better reed response allowing more flow into the engine and/or reducing outflow. The data also demonstrated that at the limit of high speed performance, the reed dynamics followed the symmetrical nature of the piston port and revealed the errors in stroboscopic reconstruction data showing 'jitter' in the dynamic behaviour. In contrast, the real-time data measured the continuous response which occurred in this low frequency inertial system.

The validation of this data gave a high degree of confidence in the analysis of the noise and cyclic variation. The noise existed as high frequency modulation on the position data whereas in contrast, the cyclic variation was evident as a shift from cycle to cycle with a variation that was an order of magnitude greater than that of the noise. The new sensor allowed for fast

parametric testing of the reeds and was able to provide data from which the resonant frequencies and the associated modal damping factors could be determined. The frequencies had previously been calculated from the reed's dimensions, density and Young's modulus. This was a quick way of empirically confirming the fundamental frequency of a composite design which, because of its construction is more difficult to theoretically predict.

The most useful application of the new position sensor was recognised through its contribution to the improved modelling of reed dynamic behaviour. The high degree of confidence in the data provided by the sensor, allowed changes to the model to be introduced and their beneficial effects easily assessed by the difference between the real and predicted behaviours. It was possible to investigate the subtle aspects of the model by using data sets with highly resonant characteristics, as opposed to the more stable data used by previous researchers. In addition, these complex data sets exaggerated errors in the model which facilitated fine tuning of all the included parameters. The early model was based upon a recognised assumption that the reed could be treated as a cantilever with a uniformly distributed load, derived from the differential pressure across the reed.

It provided a basic correlation between the actual and predicted position but it lacked accuracy in modulated detail. The introduction of a lift dependent term on the forcing function, based upon the premise that the pressure distribution changed with lift, made a quantifiable improvement to the model.

Through the development of the model, an understanding of the effect of the various included parameters was gained. This led to an insight into the possible causes of the remaining inconsistencies.

If it is accepted that there can be pressure distribution along the reed, then using a solution for uniformly distributed load is flawed and the system should be considered as a cantilever with an unevenly distributed load. This would complicate the analysis of the system, since the load and therefore pressure distribution would be required for each new point in time. Also the structural and gas dynamic conditions would need to be re-defined and solved every time the magnitude and distribution of these pressures changed.

The model used a value for the damping coefficient that was much higher than that determined by experiments out of the engine. These experimental results were checked by using two different methods, suggesting that there were either other damping issues involved or that adjusting the damping ratio was a mechanism for correcting some other deficiency in the model.

There was one significant difference, the reed was operating in a high velocity flow. Bodies immersed in a stream of flowing fluid experience drag and lift forces. The magnitude of these forces is proportional to the square of the velocity[44] and they are affected by the flow separation around the body. These forces will influence the damping experienced by a vibrating body in a moving fluid stream and may add to the viscous damping or stimulate further vibration.

The conclusion is clear, the damping ratio should include terms which are a function of the velocity and include contributions from each of the different types of damping: structural, viscous and pressure drag. In still air, the contribution from pressure drag is negligible and the viscous damping dominates. When the reed is in the induced flow, the damping probably becomes dominated by the pressure drag. Unfortunately, the flow velocity is not a function of the reed tip position, nor is it likely that the damping is the same for flow in both directions. A simple assumption is unlikely to make the same improvement that the empirical change made to the forcing function attenuator, which only ranged by a factor of three. In contrast the damping factor would be required to range by approximately one hundred (the difference between that found in still air and that used in the model). It is probable that the phase shift error is associated with the use of a fixed damping ratio.

Other contributing errors include the assumption that the reed is only affected by the pressure forces acting on it. Video photography of the engine shows it to rock and vibrate, this must inject a mechanical stimulus into the root of the reed which would not cause an instantaneous change in the tip position but could have significant effect on the reed at it's natural frequencies. It is possible that some of the noise on the data from the firing engine was in fact, differential vibration of the reed block with respect to the reed tip.

7.2 FUTURE WORK

Since the research proposal for this program of work, where the reed valve was predicted to rise and become the preferred method of induction control, time has shown it to have come about. The amount of published work that exists in the public domain is small compared to the wide-spread use of this device, consequently there are many possibilities for future research. The natural extension of this work lies in two areas, the possible commercial development of the sensor and the improved modelling of reed behaviour.

7.2.1 FURTHER SENSOR DEVELOPMENT

To develop and package a pre-production prototype requires a survey of other applications where the direct output could be used. It would be necessary to establish the availability of A/D cards for desk top computers before a full system could be integrated and evaluated. Fast modal analysis of reed samples allows their performance to be assessed before they are tested in firing engines, the development of these out-of-engine tests would reduce the time required for optimising designs and consequently reduce costs. It is hoped that commercial application of these procedures becomes possible.

7.2.2 FURTHER DEVELOPMENT OF THE MODEL

Through this work it has been recognised that the assumption of a uniformly distributed pressure load is necessary for manageable modelling of reed dynamics. However, before the load distribution is reconsidered, it is felt that future work should focus on aspects such as the effects of gas velocity on the damping factors and the consequence of vibrational stimulation of the reed root. This may improve the accuracy of the model to a point where, for practical purposes such as the inclusion in general engine models, it may not be necessary to review the assumptions in the fundamental modelling strategy.

References

1. Blair GP and Cahoon WL. *A more complete analysis of unsteady gas flow through a high-specific-output two-cycle engine.* SAE paper No. 720156 (1972).

2. Wallace FJ and Nassif MH. *Air flow in a naturally aspirated two-stroke engine.* Proc. I.M.E., Vol 168, PP 515, (1954).

3. Benson RS. *The thermodynamics and gas dynamics of internal combustion engines.* Horlock JH and Winterbone DE, eds. Clarendon Press. Oxford (1982).

4. Blair GP and Ashe MC. *The unsteady gas exchange characteristics of a two-cycle engine.* SAE paper No. 760644 (1976).

5. Blair GP. *Prediction of two-cycle performance characteristics.* SAE paper No. 760645 (1976).

6. Fleck R, Houston RAR and Blair GP. *Predicting the performance characteristics of twin cylinder two-stroke cycle engines for outboard motor applications.* SAE paper No. 881266 (1988).

7. Blair GP. *Alternative method for the prediction of unsteady gas flow through the internal combustion engine.* SAE paper No. 911850 (1991).

8. Sweeney MEG. *A direct assessment of the scavenging efficiency of two-stroke cycle engines.* Doctoral thesis, The Queen's University of Belfast (1986).

9. Uzkan T. *Analytically predicted improvements in the scavenging and trapping efficiency of two-cycle engines.* SAE paper No. 880108 (1988).

10. Sato K and Nakano M. *A method of separating short-circuit gas from exhaust gas in a two-stroke cycle gasoline engine (a good use of exhaust gas).* SAE paper No. 871653 (1987).

11. Blair GP, Hill BW, Miller AJ and Nickell SP. *Reduction of fuel consumption of a spark-ignition two-stroke cycle engine.* SAE paper No. 830093 (1983).

12. Tsuchiya K, Hirano S, Okamura M and Gotoh T. *Emission control of two-stroke motorcycle engines by the butterfly exhaust valve.* SAE paper No. 800973 (1980).

13. Blair GP, Houston RAR, McMullan RK, Steele N and Williamson SJ. *A new piston design for a cross-scavenged cycle engine with improved scavenging and combustion characteristics.* SAE paper No. 841096 (1984).

14. Douglas R and Blair GP. *Fuel injection of a two-stroke cycle spark ignition engine.* SAE paper No. 820952 (1982).

15. Beck NJ, Johnson WP, Barkhimer RL and Patterson SH. *Electronic fuel injection for two-stroke cycle gasoline engines.* SAE paper No. 861242 (1986).

16. Sato T and Nakayama M. *Gasoline direct injection for a loop-scavenged two-stroke cycle engine.* SAE paper No. 871690 (1987).

17. Huang H-H, Peng Y-Y, Jeng M-J and Wang JH. *Study of a small two-stroke engine with low-pressure air-assisted direct-injection system.* SAE paper No. 912350 (1991).

18. Hata N and Iio T. *Improvement of two-stroke engine performance with the Yamaha Power Valve System (YPVS).* SAE paper No. 810922 (1986).

19. Blair GP and Johnston MB. *Unsteady flow effects in exhaust systems of naturally aspirated, crankcase compression two-cycle internal combustion engines.* SAE paper No. 680594 (1968).

20. Desantes JM, Boada F and Corberán JM. *Exhaust pipe design method for the optimization of the scavenging process.* SAE paper No. 850083 (1983).

21. Blair GP and Johnston MB. *Simplified design criteria for expansion chambers for two-stroke gasoline engines.* SAE paper No. 700123 (1970).

22. Blair GP. *Basic design of two-stroke engines* Society of Automotive Engineers (SAE), (1990).

23. Blair GP and Arbuckle JA. *Unsteady flow in the induction system of a reciprtocating internal combustion engine.* SAE paper No.700443 (1970).

24. Hata N, Fujita T and Matsuo N. *Modifications of two-stroke engine intake system for improvements of fuel consumption and performance through the Yamaha Energy Induction System (YEIS).* SAE paper No. 810923 (1981).

25. Sanz MS. *Two-stroke cycle engine with flow induction corrected at the intake and transfer phases.* SAE paper No. 850184 (1985).

26. Tanaka M, Sato T and Watanabe K. *Pulsation effects on the air fuel ratio of carburettor engines.* SAE paper No. 861241 (1986).

27. Groth K and Kania N. *Modifications on the intake ports with the aim to reduce the noise of a two-stroke crankcase-scavenged engine.* SAE paper No. 821069 (1982).

28. Iwamoto J and Deckker BEL. *An experimental study of gas flow through a rotating disc valve.* SAE paper 841092 (1984).

29. Blackwell PH. *Investigation into fitting reed valves into a two-stroke engine.* MSc dissertation, Manchester University (1977).

30. Krieger RB, Booy RR, Myres PS and Uyehara OA. *Simulation of a crankcase scavenged two-stroke S.I. engine and comparison with experimental data.* SAE paper No. 690135 (1969).

31. Wambsganss MW and Cohen R. *Dynamics of reciprocating compressors with automatic reed valves. Theory and simulation.* Proc.XIIth Int. Cong. Refrigeration (1967).

32. Hinds ET. *Intake flow characteristics of a two-cycle engine fitted with reed valves.* Doctoral thesis, The Queen's University of Belfast (1978).

33. Blair GP and Hinds ET. *Predicting the performance characteristics of two-cycle engines fitted with reed induction.* SAE paper No. 790842 (1979).

34. Blair GP and Cahoon R. *A more complete analysis of unsteady gas flow through a high specific output two cycle engine.* SAE paper No. 720156 (1972).

35. Fleck R, Blair GP and Houston RAR. *An improved model for predicting reed valve behaviour in two-stroke cycle engines.* SAE paper No. 871654 (1987).

36. Piccone A and D'Angelo D. *Application of reed valves to a four-cycle spark ignition engine.* International Federation of Engineers, 23rd Congress G01648334, pp 325-331, (1990).

37. Loughin C. *Proximity sensors: close to you.* Sensor Review 8, (4) pp 198-202. IFS Publications, 0260-2288 (1988).

38. Noviski VE. *Black on black sensing methods.* EI Monthly No.EIM9111-060154 (1991).

39. Okada T and Rembold U. *Proximity sensor using a spiral-shaped light emitting mechanism.* IEEE Transactions on Robotics and Automation. Volume 7 No 6, pp 798-805, December 1991.

40. PPL Regtien. *Accurate optical proximity detector.* EI Monthly No.EIM9011-046715 (1990).

41. Gorman DG and Kennedy W. *Applied solid dynamics.* Butterworth (1988).

42. Unins DJ. *Modal testing: theory and practice.* Research Studies Press Ltd. (1986).

43. Timoshenko S, Young DH and Weaver JR. *Vibration problems in engineering.* John Wiley and Sons (1974).

44. Blevins RD. *Flow-induced vibration.* Van Nostrand Reinhold, New York (1977).

Appendix I

Description of the position sensor design, and circuit diagram

1. Optics

The optics consisted of a Gallium Aluminum Arsenide (GaAlAs) solid-state transmitter and a silicon photodiode receiver encapsulated in epoxy lenses. These devices could focus either transmitted or received light.

When a voltage is applied to the reversed biased (non-conducting) receiver, the semi-conducting current is proportional to the incident light and the photodiode can be considered to behave as a light-controlled current source. This current flows through a load resistance, generating a signal voltage proportional to the current and therefore to the amount of incident light. This characteristic was the basis of the sensor.

Infra-red light was generated by passing current (100mA) through the transmitter. This light is focused on the reed and the reflected light returns to the receiver. This reflected light was then converted into the corresponding proportional electrical signal.

2. The null stage

From its rest position, any target can move in one of three ways: away from the sensor and back, towards the sensor and back or back and forth about its rest position.

To maximize sensor sensitivity it was desirable that the full scale deflection of the target is represented by a full scale electrical swing between the chosen output voltages. It was considered essential that the output of the sensor could be adjusted so that the output at rest could either be at a maximum, minimum or some other mid-voltage, that would correspond

to the rest position of the target. This was achieved using the null adjustment, which balanced the amplifier to a reference signal.

In the case of the reed valve, the valve at rest was shut and its rest position was furthest from the sensor. It was desirable to set 'zero lift' to be 0 volts. In this position the sensor was still receiving some background signal. The null adjustment is used to apply a reference voltage equal to this smallest signal level. The amplifier was then presented with only the difference between this null voltage and the input signal and consequently it was possible to amplify the subsequent changes in signal, rather than the absolute magnitude of the signal. This manual null adjustment could have been replaced by an ac- coupled input, but there were several avantages using the dc-coupled inputs:

(i) Static calibration was possible, i.e. the target could be moved from its rest position and held whilst the sensor output was observed. This allowed the sensor to be calibrated or checked.

(ii) The sensor could be adjusted for maximum sensitivity and therefore optimum resolution.

(iii) It facilitated the measurement of very slow moving targets.

3. The amplifier

The gain of the amplifier needed to be sufficient to boost the input signal to the desired output voltage. A gain of 100 was chosen. The bandwidth requirements were determined from the maximum rotational speed of the engine. At 9000 rev/min the fundamental cyclic speed was 150 Hz. It is likely that a bandwidth 100 times this (i.e. 15 KHz) would be

sufficient to measure most other modulated information. The data resolution frequency was in any event limited to half that of the maximum A/D sample frequency. At 9000 rev/min sampling every 0.75 degrees limited this is 36KHz.

4. The filter

Compared to the system noise, the operating reed valve had a very low maximum frequency and slew rate, (typically 15KHz and 10mm/ms). This compared with the high frequency noise which existed beyond 1MHz as background `hiss` and occasional spikes with equivalent slew rates of 200mm/ms. This large signal to noise separation allowed simple single order filter networks to perform an adequate signal conditioning function, a low pass filter with its 3dB point at 40 KHz and a roll-off of 6dB per octave greatly improved the signal integrity.

1				2				3				4			
ISSUE	DATE	CHANGE	APPROVED	ISSUE	DATE	CHANGE	APPROVED	ISSUE	DATE	CHANGE	APPROVED	ISSUE	DATE	CHANGE	APPROVED
1	27.9.92	ORIGINAL													

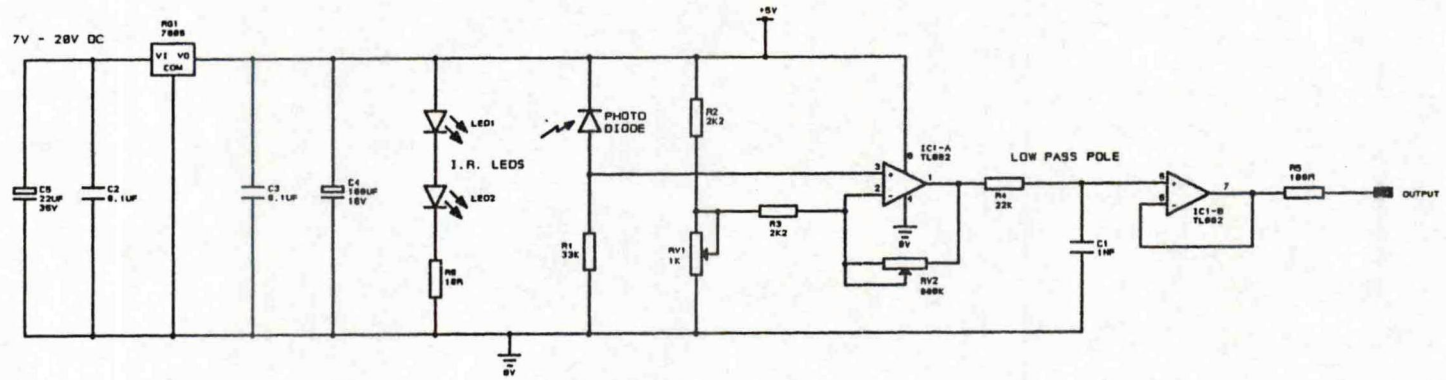

IC TABLE			
IC	DEVICE	POWER	GROUND
1	TL082	8	4

TITLE:
CIRCUIT DIAGRAM FOR :-

INFRA RED POSITION SENSOR

NEXT ASSY		DRAWN	P.COLLINS	TRACED	

DRAWING NUMBER

ASSEMBLY No

Appendix II

Source code for the reed model

```
Program Reed_simulation(infile,infile1,outfile,outfile1);

{-------------------------------------------------------------------------------------------------}

Program to model the behaviour of a reed valve.
Copyright © 1992, Peter Collins, Oxford Brookes University

Purpose:    This program uses the procedure InitialCond 2ndOrder which solves an
            initial value problem - a second order ordinary differential equation with
            initial conditions specified - using the fourth order, two variable Runge
            Kutta formula. See Borland Numerical Toolbox.

Unit:       InitVal procedure InitialCond 2ndOrder

{-------------------------------------------------------------------------------------------------}

{$I-}                                   {Disable I/O error trapping}
{$R+}                                   {Enable range checking}

uses
InitVal, Dos, Crt, Common, Graph;

const
      no_of_reed_segments = 12;
      no_of_modes = 3;

type
      reed_div = 1..no_of_reed_segments;
      reed = array[reed_div] of real;
      modes = array[1..no_of_modes] of real;
      reed_modes = array[1..no_of_modes] of reed;

var
      LowerLimit, UpperLimit : Float;     {Limits over which to approximate X}
      InitialValue, InitialDeriv : Float; {Initial values at lower limit}
      NumReturn : integer;                {Number of values to return}
      NumIntervals, i, j : integer;       {Number of intervals}
      TValues : TNvector;                 {Value of T between the limits}
      XValues : TNvector;                 {Value of X at TValues}
      XDerivValues : TNvector;            {Derivative of X at TValues}
      Error : byte;                       {Flags if something went wrong}
      infile, infile1, outfile, outfile1 : text;
```

```
    p_up_str : real;                    {Upstream pressure at any time}
    p_down_str : real;                  {Downstream pressure at any time}
    sigma : modes;                      {Vibrational constant for clamped free
                                         beam}
    ar : modes;                         {Lambda(i) * length for clamped beam}
    ymod : real;                        {Youngs modulus for beam material
                                         N/(m*m)}
    secmomarea : real;                  {Beam second moment of area}
    mperl : real;                       {Mass per unit length kg/m}
    rdlentru : real;                    {Effective length of reed  (m)}
    rdwidth,rdthk : real;               {Reed width and thickness (mm)}
    rhord : real;                       {Density of reed material (kg/(m*m*m)}
    csard : real;                       {Reed cross sectional area}
    rdlenfree, original_rdlenfree : real;    {Free length of reed}
    modshp : reed_modes;                {Free vibration mode shape}
    rdlenmax,clamplen : real;           {Maximum and clamped lengths of reed}
    omega : modes;                      {Radiancy of vibration (rad/sec)}
    stiff : modes;                      {Vibration constant}
    r1 : modes;                         {Lamda(i)*l and Lambda(i)*x}
    r2 : reed_modes;
    freq : modes;                       {Natural frequency of vibration (Hz)}
    F : real;                           {Force on reed (N)}
    engspeed : real;                    {Engine speed (rev/min)}
    crangint : real;                    {Crank angle interval for pressure data}
    tim_for_crangint : real;            {Time taken to cover crangint}
    p_up_str_new,p_down_str_new,
    p_up_str_old,p_down_str_old : real;
    crang : real;                       {Total crank angle covered}
    lift : reed_modes;                  {Reed tip lift in each mode}
    total_lift : reed;                  {Resultant tip lift}
    reed_inc : real;
    reedlen : real;
    im : integer;
    x : modes;
    xderiv : modes;
    go : char;
    stop_radius : real;
    jx : integer;
    reed_stop : reed;
    hit_stop : boolean;
    damping : modes;

function cosh(x:real):real;

{Function to determine hyperbolic cosh}

begin
```

```
        cosh := 0.5*(exp(x)+exp(-x));
end;

function sinh(x:real):real;

{Function to determine hyperbolic sinh}

begin
        sinh:= 0.5*(exp(x)-exp(-x));
end;

procedure generate_parameters;

begin
        for im:= 1 to no_of_modes do
begin
        omega[im]:=ar[im]*sqrt(ymod*secmomarea/mperl/(rdlenfree*rdlenfree*
                rdlenfree*rdlenfree));
        freq[im]:=omega[im]/2.0/pi;
        stiff[im]:=sqrt(sqrt((omega[im]*omega[im])*csard*rhord/
                (ymod*secmomarea*1e-6)));
        r1[im]:=rdlenfree*stiff[im]*1e-3;
        sigma[im]:=(sinh(r1[im])-sin(r1[im]))/(cosh(r1[im])+cos(r1[im]));
end;
        reedlen := 0.0;
        for im:= 1 to no_of_modes do
begin
        reedlen:=0.0;
        for j := 1 to no_of_reed_segments do
begin
                reedlen := reedlen + reed_inc;
        r2[im,j]:=stiff[im]*reedlen;
                modshp[im,j]:=cosh(r2[im,j])-cos(r2[im,j])-(sigma[im]*
                        (sinh(r2[im,j])-sin(r2[im,j])));
end;
end;
end;

procedure get_reed_data;

{Reads reed data from data file, infile1, together with engine speed
 and crank interval from infile, writes data and calculates various
 constants}
```

```
var
        im : integer;

begin
        reset(infile1);
        readln(infile1,rdwidth,rdthk,rdlenmax,clamplen);
        original_rdlenfree:=rdlenmax-clamplen;
        rdlenfree := original_rdlenfree;
        assign(outfile,'c:\tpascal\work\jan19k3.out');
        rewrite(outfile);
        assign(outfile1,'c:\tpascal\work\j19k3xl.out');
        rewrite(outfile1);
        writeln(outfile,'Reed width : ',rdwidth:5:1,' mm');
        writeln(outfile,'Reed thickness : ',rdthk:5:3,' mm');
        writeln(outfile,'Reed length : ',rdlenmax:5:1,' mm');
        writeln(outfile,'Clamped length : ',clamplen:5:1,' mm');
        writeln(outfile,'Reed free length :',rdlenfree:5:1,' mm');
        writeln('Reed width : ',rdwidth:5:1,' mm');
        writeln('Reed thickness : ',rdthk:5:3,' mm');
        writeln('Reed length : ',rdlenmax:5:1,' mm');
        writeln('Clamped length : ',clamplen:5:1,' mm');
        writeln('Reed free length :',rdlenfree:5:1,' mm');
        readln(infile1,ymod,rhord);
        csard:=rdwidth*rdthk;
        writeln(outfile,'Youngs modulus :',ymod:10:0,' N/(m*m)');
        writeln(outfile,'Density of reed material : ',rhord:8:1,' kg/(m*m*m)');
        writeln(outfile,'Reed cross sectional area : ',csard:8:5,' (mm*mm)');
        writeln('Youngs modulus :',ymod:10:0,' N/(m*m)');
        writeln('Density of reed material : ',rhord:8:1,' kg/(m*m*m)');
        writeln('Reed cross sectional area : ',csard:8:5,' (mm*mm)');
        secmomarea:=(rdwidth*(rdthk*rdthk*rdthk)/12.0);
        writeln(outfile,'Second moment of area : ',secmomarea:8:5,'
                (mm*mm*mm*mm)');
        writeln('Second moment of area : ',secmomarea:8:5,' (mm*mm*mm*mm)');
        mperl:=rdwidth*rdthk*rhord*1e-6;
        writeln(outfile,'Mass per unit length : ',mperl:10:6,' (kg/m)');
        writeln('Mass per unit length : ',mperl:10:6,' (kg/m)');
        readln(infile1,stop_radius);
        writeln(outfile,'Reed stop radius : ',stop_radius:5:1,' (mm)');
        writeln('Reed stop radius : ',stop_radius:5:1,' (mm)');
        ar[1]:=3.52;
        ar[2]:=22.03364;
        ar[3]:=61.701;
        damping[1] := 0.38;
        damping[2] := 0.38;
        damping[3] := 0.38;
        jx := 1;
```

```
        rdlentru:=rdlenfree*1e-3;  {units (m)}
        reed_inc := rdlentru/no_of_reed_segments;
        generate_parameters;
        for im:= 1 to no_of_modes do
begin
        writeln(outfile,'Omega : ',omega[im]:8:3,' (rad/s)');
        writeln(outfile,'Frequency of free vibration : ',freq[im]:8:2,' Hz');
        writeln(outfile,'Stiff ',stiff[im]);
        writeln('Stiff ',stiff[im]);
        writeln(outfile,'sigma ',sigma[im]);
        writeln('sigma ',sigma[im]);
end;
        reedlen:=0.0;
        for j := 1 to no_of_reed_segments do
begin
        reedlen := reedlen + reed_inc;
        reed_stop[j] := stop_radius*1e-3*(1.0-cos(reedlen/stop_radius/1e-3));
end;
        for im:= 1 to no_of_modes do
begin
        for j := 1 to no_of_reed_segments do
begin
         writeln(outfile,'r2 ',r2[im,j]);
         writeln(outfile,'Mode shape ',modshp[im,j],'  Stop height
                reed_stop[j]*1e3:5:1);
        writeln('Mode shape ',modshp[im,j],'  Stop height ',
                reed_stop[j]*1e3:5:2);
end;
        writeln(outfile,'Mode shape : ',modshp[im,1]:8:3);
end;
        readln(infile,engspeed,crangint); {Engine speed and crank angle interval
                between readings}
        writeln(outfile,'Engine speed : ',engspeed:8:1,' (rev/min)');
        writeln(outfile,'Crank angle interval between readings : ',crangint:4:1,'
                (deg)');
        tim_for_crangint:=crangint/360.0/engspeed*60;
        writeln(outfile,'Time taken to cover crank angle interval :
                ',tim_for_crangint:8:6,' (sec)');
        close(infile1);
end;

{$F+}
function TNTargetF(T      : Float;
        X                 : Float;
        XPrime : Float)   : Float;

{-------------------------------------------------------------------------------------------------}
```

```
{This is the second order differential equation}
{-------------------------------------------------------------------------------------------------------------}

begin
        p_up_str := p_up_str_old + (p_up_str_new - p_up_str_old)
                /tim_for_crangint * T;
        p_down_str := p_down_str_old + (p_down_str_new - p_down_str_old) *
                T/tim_for_crangint;
        F := (+p_up_str - p_down_str-0.01)*((15.0-total_lift[12])/15.0)
                * rdlentru * rdwidth * 1e2;

{writeln('Time : ',T:8:6,' Force : ',F:8:6,' X :',X,' Xprime : ',xprime);}

TNTargetF := F/(rdlentru * mperl) - 2 * omega[im] * damping[im] * xprime
        - omega[im] * omega[im] * X;
end; { function TNTargetF }
{$F-}


procedure Initialize(var LowerLimit   : Float;
        var UpperLimit      : Float;
        var InitialValue    : Float;
        var InitialDeriv    : Float;
        var NumIntervals    : integer;
        var NumReturn       : integer;
        var Error           : byte);

{-------------------------------------------------------------------------------------------------------------}
{Output: LowerLimit, UpperLimit, LowreInitial, InitialDeriv,}
{NumIntervals, NumReturn, Error}
{                                                }
{This procedure initializes the above variables to zero}
{-------------------------------------------------------------------------------------------------------------}

begin
        LowerLimit := 0;
        UpperLimit := 0;
        InitialValue := 0;
        InitialDeriv := 0;
        NumReturn := 0;
        NumIntervals := 0;
        Error := 0;
end; {procedure Initialize}

procedure GetData(var LowerLimit    : Float;
        var UpperLimit              : Float;
        var InitialValue            : Float;
```

```
        var InitialDeriv          : Float;
        var NumReturn             : integer;
        var NumIntervals          : integer);

{-------------------------------------------------------------------------------------------------------}
{Output: LowerLimit, UpperLimit, InitialValue,}
{InitialDeriv, NumReturn, NumIntervals}
{                                                    }
{This procedure assigns values to the above variables}
{from keyboard input}
{-------------------------------------------------------------------------------------------------------}

begin {procedure GetData}
        LowerLimit:=0.0;              {Lower limit of integration}
        UpperLimit:=tim_for_crangint; {Upper limit of integration}
        InitialValue:=x[im];          {Initial X value}
        InitialDeriv:=xderiv[im];     {Initial Xprime value}
        NumReturn:=1;                 {Number of values to be returned}
        NumIntervals:=100;            {Number of intervals over which to solve
                                       equation}
end; {procedure GetData}

Procedure draw_reed(lift : reed);

var
        seg,mm,j,x,y : integer;

begin
        seg := GetMaxX div 20;
        mm := GetMaxY div 50;
        x := GetMaxX div 3;
        y := GetMaxY div 2;
        MoveTo(GetMaxX div 3,GetMaxY div 2);
        for j := 1 to No_of_Reed_segments do
begin
        x := x + seg;
        y := y + round(lift[j]) * mm;
        LineTo(x,y);
end;
end;

Procedure graphics;

var
        Graphdriver, GraphMode, ErrorCode : integer;
```

```
begin
        Graphdriver := Detect;
        InitGraph(GraphDriver, GraphMode, '');
        ErrorCode := GraphResult;
        IF ErrorCode <> grOK then
begin
        writeln('Graphics error: ',GraphErrorMsg(ErrorCode));
        writeln('Program aborted.');
        Halt(1);
end;
        SetColor (yellow);
        for j := 1 to no_of_reed_segments do
begin
        total_lift[j] := 0.0;
end;
        draw_reed(total_lift);
end;

begin {program InitialCond2ndOrder}
        assign(infile1,'c:\tpascal\work\reedsim.dat');
        {graphics;}
        hit_stop := false;
        crang:=0;
        numintervals :=1;
        for im:=1 to no_of_modes do
begin
         x[im]:=0.0;
         xderiv[im]:=0.0;
end;
        assign(infile,'c:\tpascal\work\j19k3.rdm');
        reset(infile);
        get_reed_data;
        readln(infile,p_up_str_old,p_down_str_old);
        readln(infile,p_up_str_new,p_down_str_new);
        Initialize(LowerLimit, UpperLimit, InitialValue, InitialDeriv,
                NumIntervals, NumReturn, Error);
        writeln(outfile,' ');
        writeln(outfile,' ');
        writeln(outfile,'Crank angle   Force    Tip Lift   Mid Lift',
                '          X              Xprime');
        writeln(outfile,'   (deg)       (N)       (mm)');
        jx := 1;
        repeat
        rdlenfree := original_rdlenfree - (jx - 1) * reed_inc;
        generate_parameters;
        for im := 1 to no_of_modes do
```

```
begin
        GetData(LowerLimit, UpperLimit, InitialValue,
        InitialDeriv, NumReturn, NumIntervals);

InitialCond2ndOrder(LowerLimit, UpperLimit, InitialValue, InitialDeriv,
        NumReturn, NumIntervals, TValues, XValues,
        XDerivValues,Error, @TNTargetF);
        x[im]:=XValues[1];
        xderiv[im]:=XDerivValues[1];
end;
        crang:=crang+crangint;
        {SetColor(black);
        draw_reed(total_lift);}
        jx := 0;
        for j := 1 to no_of_reed_segments do
begin
        total_lift[j] := 0.0;
        for im := 1 to no_of_modes do
begin
        lift[im,j]:= x[im] * modshp[im,j]*1e3;
        {writeln('lift ',lift[im,j]);}
        total_lift[j]:=total_lift[j]+lift[im,j];
end;
        if total_lift[j] > reed_stop[j]*1e3 then
begin
        total_lift[j] := reed_stop[j]*1e3;
        hit_stop := true;
        writeln('Hit stop');
        hit_stop := false;
        jx := j;
end;
        if total_lift[j] < 0.0 then
begin
        total_lift[j] := 0.0;
        for im := 1 to no_of_modes do
begin
        x[im] := 0.0;
        xderiv[im] := 0.0;
end;
end;
end;
        for im := 1 to no_of_modes do
begin
        if jx = no_of_reed_segments then xderiv[im] := 0;
end;
        writeln('Xderiv ',xderiv[1]);
        for j := 1 to no_of_reed_segments do
```

```
begin
        writeln('Total lift ',total_lift[j]);
end;
        writeln(' ');
        {SetColor(yellow);
        draw_reed(total_lift);}
        writeln(outfile,'  ',crang:5:1,'      ',F:5:2,'  ',
                total_lift[no_of_reed_segments]:8:5,'  ',total_lift[3]:8:5,
                '  ',X[1],' ',XDeriv[1]);
        writeln(outfile1,crang:5:1,'    ',total_lift[no_of_reed_segments]:8:5,
                '    ',F:5:2);
        p_up_str_old := p_up_str_new;
        p_down_str_old := p_down_str_new;
        readln(infile,p_up_str_new,p_down_str_new);
        until eof(infile);
        close(OutFile);
        close(infile);
        close(outfile1);
end. {program InitialCond2ndOrder}
```

Appendix III

Other equipment designed and constructed for this study:

descriptions and circuit diagrams

1. Power supplies

A fixed voltage dc power supply providing stabilised +12V was constructed. This used a non-switching design based upon a solid-state voltage regulator fed from a full-wave rectified and smoothed ac supply. The low voltage ac supply was generated by a step down transformer from the 240V ac mains supply. The output of the regulator contained a current limit and had thermal overload shutdown incorporated into them, making the power supply robust and safe.

2. Strain gauge amplifiers for silicon bridge pressure transducers

A two-channel instrumentation amplifier required for the pressure transducers was designed and constructed. This consisted of a split rail power supply and two differential amplifiers with null and gain adjustments. To be compatible with the microlink data acquisition system, the output was required to be between +/- 5V. An internal power supply generated this from a centre-tapped transformer. This was full-wave-rectified which generated +/- 8 volts with ripple. These supplies were regulated using 7805 and 7905 one amp power regulators to generate the stable supplies required by the amplifier. The regulators were decoupled, both on their inputs and outputs with classic high and low frequency decoupling networks, which were required to reduce ripple and eliminate oscillation. An advantage of having an internal power supply was that, although the rails themselves were not exactly + and - 5 volts, they would not require a nulling on every occasion that it was used.

Two instrumentation amplifiers were necessary and each was a three stage design using operational amplifiers (op-amp). The first stage formed a precision differential amplifier with a gain of ten providing the high common mode rejection ratio (CMRR) required. This cascaded into a variable gain dc amplifier with a null adjustment which allowed calibration to the required sensitivity of 200 mBar/volt with less than 1 mV offset error.

The final op-amp was configured as a unity gain buffer, which acted as a line driver. The simplest way to realise this circuit topology was to use a dedicated differential front-end amplifier, with a preset gain of ten. This was available as a custom package (INA106KP), and although it did not provide sufficient gain by itself, it generated a single-ended output with a high CMRR. This signal was then amplified by a classic two stage design with gain and null adjustments. The null was set up after the power supply and amplifier had been allowed to warm up with the amplifiers on full gain. This gave the best conditions for optimising the null adjustment.

To ensure the sensitivity of 200 mBar per volt, the amplifier was calibrated using a mercury manometer to set the maximum at 1 Bar. The gain was then adjusted to give an output of 5 volts. Having set full scale deflection, linearity was checked by taking 25 data points between 0 Bar and +1 Bar. The offset was re-checked with the pressure removed. This gave a straight line, with an error within the limits of the visual measurement of the manometer reading (1mm of mercury). Once set, the null control did not need adjustment as long as a five minute warm-up was possible. Maximum pre-warm-up error was less than 25 mV (i.e. 5 mBar).

1				2				3				4			
ISSUE	DATE	CHANGE	APPROVED	ISSUE	DATE	CHANGE	APPROVED	ISSUE	DATE	CHANGE	APPROVED	ISSUE	DATE	CHANGE	APPROVED
1	27.9.92	ORIGINAL													

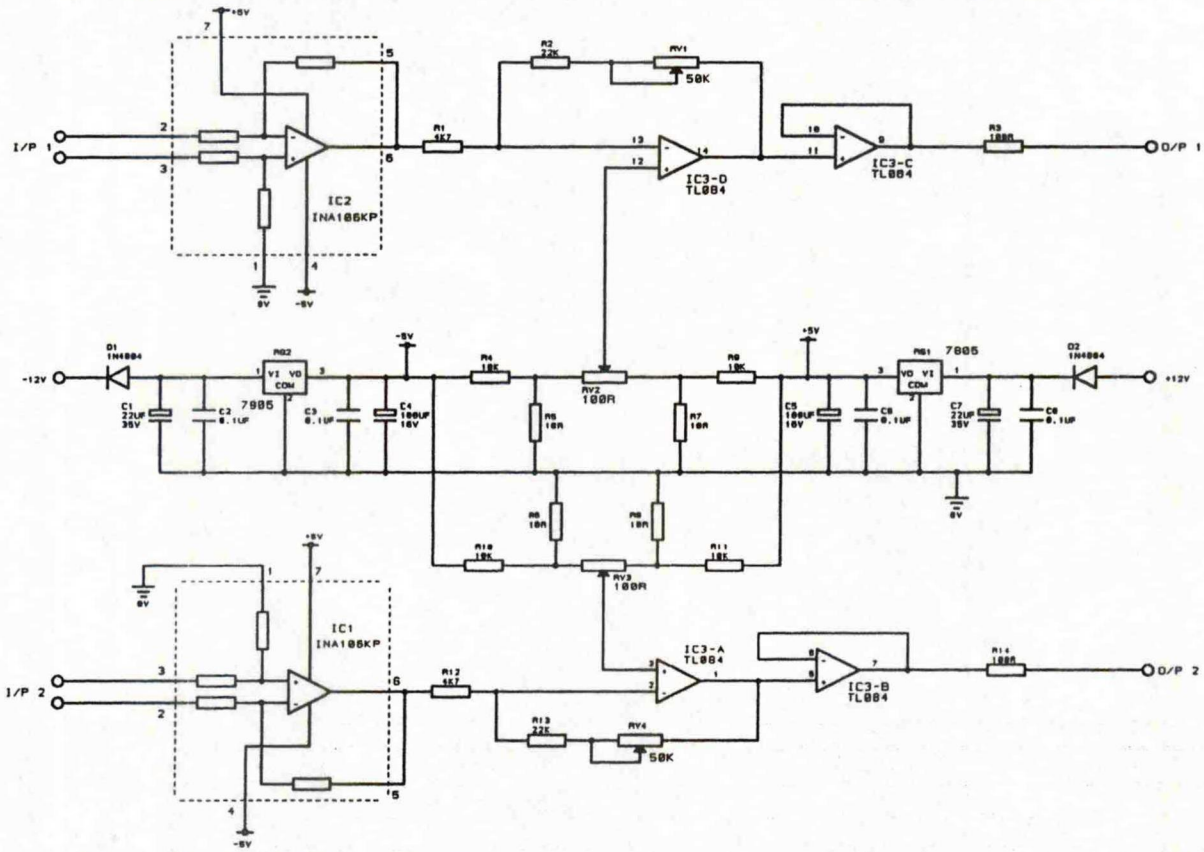

IC TABLE			
IC	DEVICE	POWER	-VCC
1	INA106KP	7	4
2	INA106KP	7	4
3	TL084	4	11

TITLE:
CIRCUIT DIAGRAM FOR :-
DUAL CHANNEL VARIABLE GAIN
INSTRUMENTATION AMP WITH OFFSET NULL

NEXT ASSY		DRAWN	P.COLLINS	TRACED	

DRAWING NUMBER

ASSEMBLY No

1				2				3				4			
ISSUE	DATE	CHANGE	APPROVED	ISSUE	DATE	CHANGE	APPROVED	ISSUE	DATE	CHANGE	APPROVED	ISSUE	DATE	CHANGE	APPROVED
1	27.9.92	ORIGINAL													

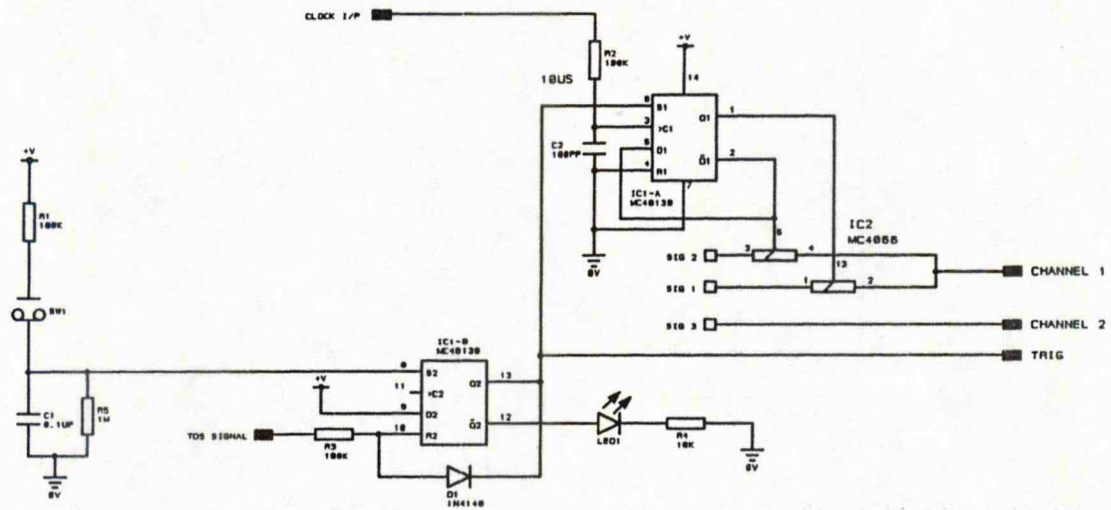

IC TABLE			
IC	DEVICE	POWER	GROUND
1	MC4013B	14	7
2	MC4066	14	7

TITLE:
CIRCUIT DIAGRAM FOR :-

CLOCK SEQUENCING & MULTIPLEXING UNIT

NEXT ASSY		DRAWN	P.COLLINS	TRACED	

DRAWING NUMBER

ASSEMBLY No

1				2				3				4			
ISSUE	DATE	CHANGE	APPROVED	ISSUE	DATE	CHANGE	APPROVED	ISSUE	DATE	CHANGE	APPROVED	ISSUE	DATE	CHANGE	APPROVED
1	20.9.92	ORIGINAL													

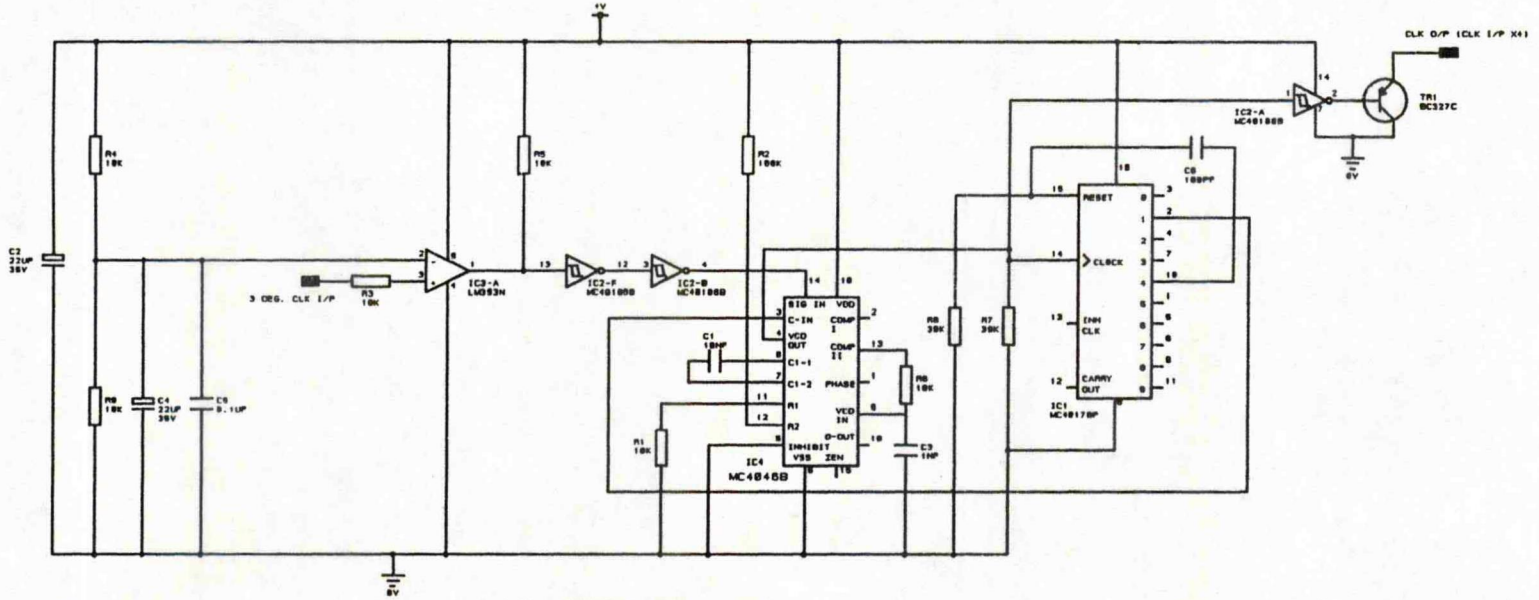

R,C, - FREQUENCY RANGE
R2 - FREQUENCY OFFSET

UNUSED GATES

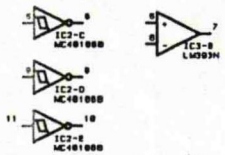

IC TABLE

IC	DEVICE	POWER	GROUND
1	MC4017BP	16	8
2	MC4011BBP	14	7
3	LM393N	8	4
4	MC4046B	16	8

TITLE:
CIRCUIT DIAGRAM FOR :-
PHASE LOCKED CLOCK MULTIPLIER (X4)
WITH OPEN EMITTER OUTPUT

NEXT ASSY		DRAWN	P.COLLINS	TRACED	

DRAWING NUMBER

ASSEMBLY No

Appendix IV

Modal response of the four reed types

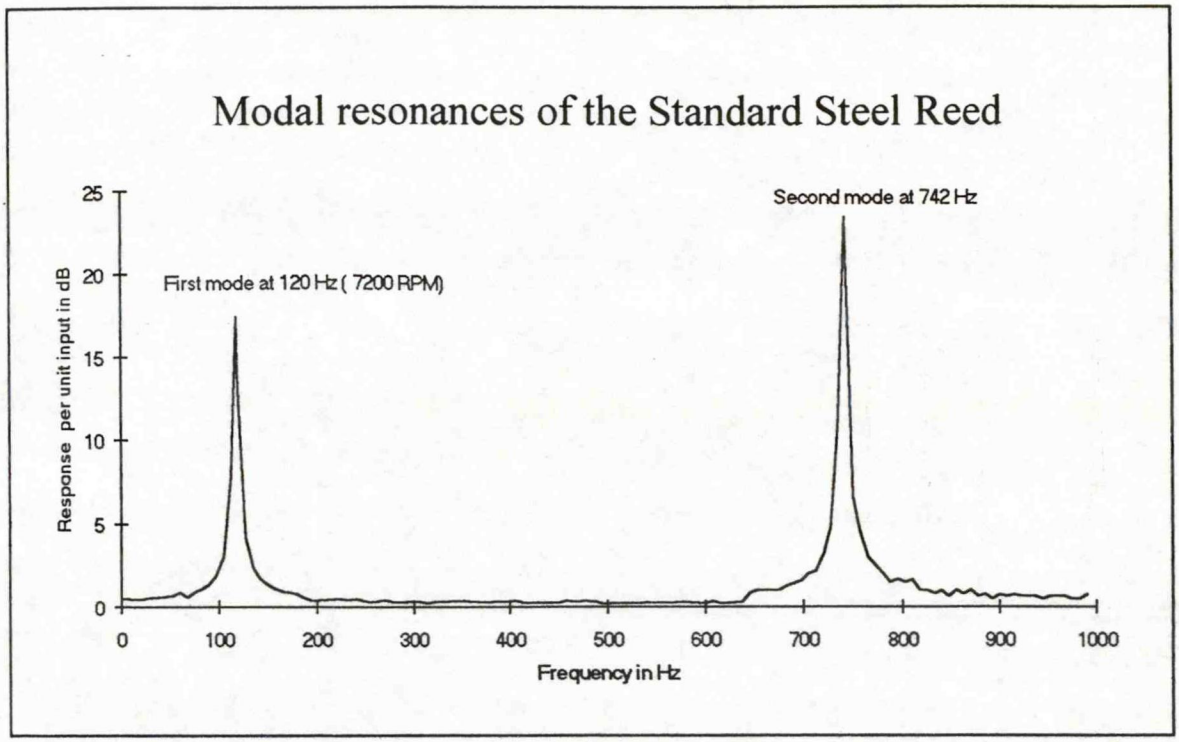
Modal resonances of the Standard Steel Reed
Second mode at 742 Hz
First mode at 120 Hz (7200 RPM)
Response per unit input in dB
25
20
15
10
5
0
0
100
200
300
400
500
600
700
800
900
1000
Frequency in Hz

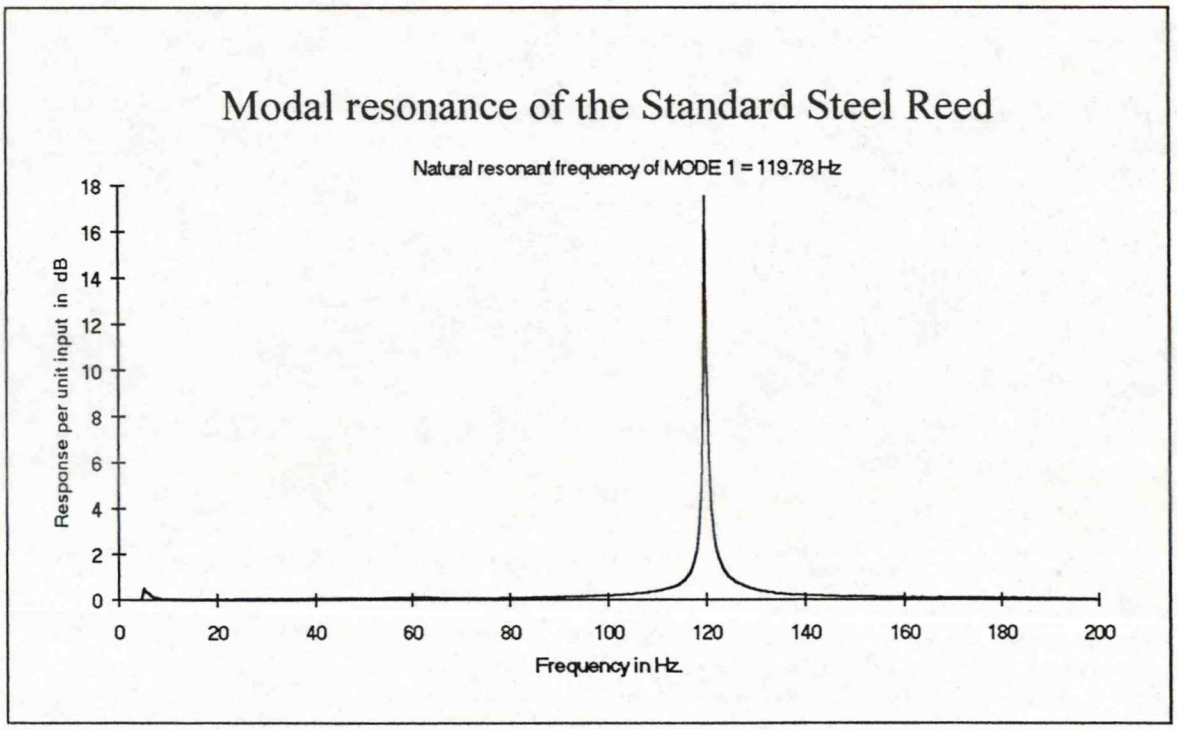
Modal resonance of the Standard Steel Reed
Natural resonant frequency of MODE 1 = 119.78 Hz
Response per unit input in dB
18
16
14
12
10
8
6
4
2
0
0
20
40
60
80
100
120
140
160
180
200
Frequency in Hz.

Modal resonance of the Proprietary Composite Reed.

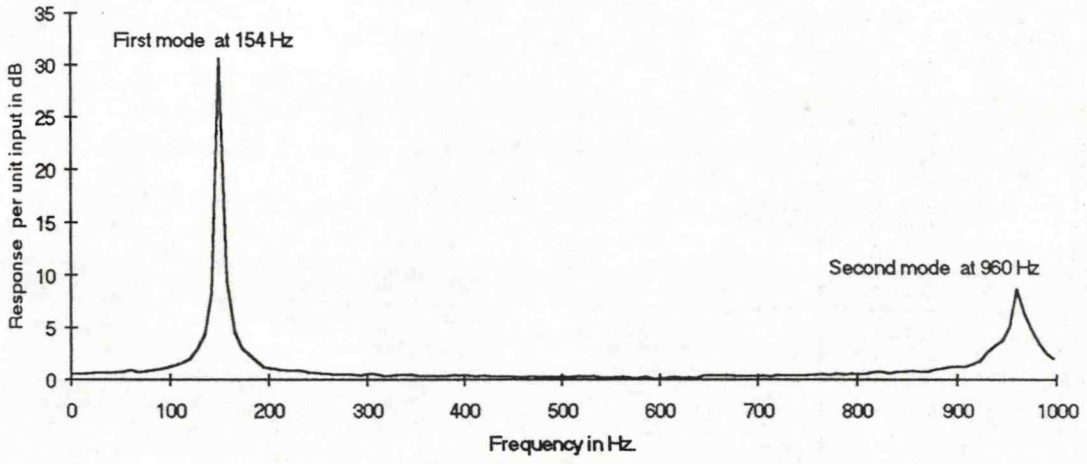

Modal resonances of the Tapered Steel Reed

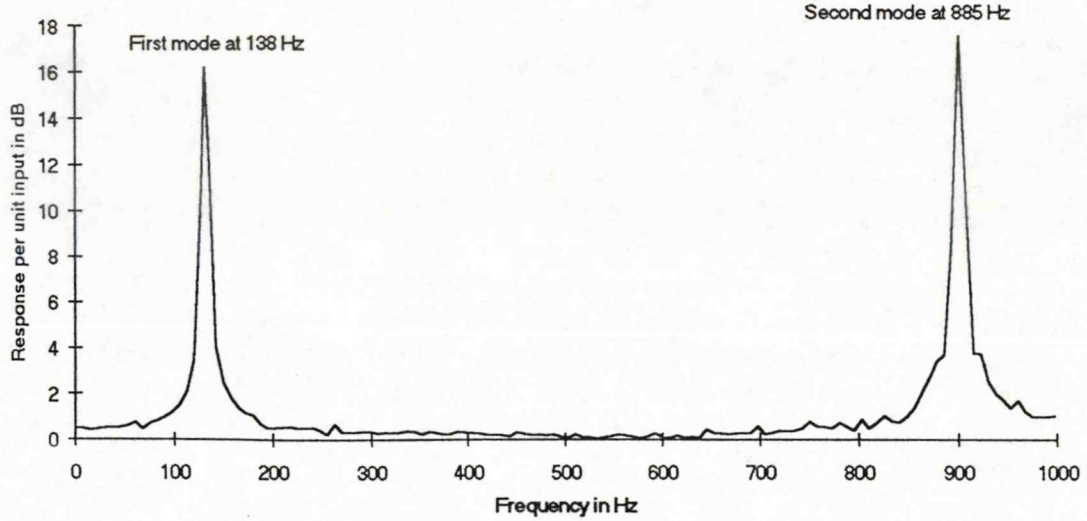

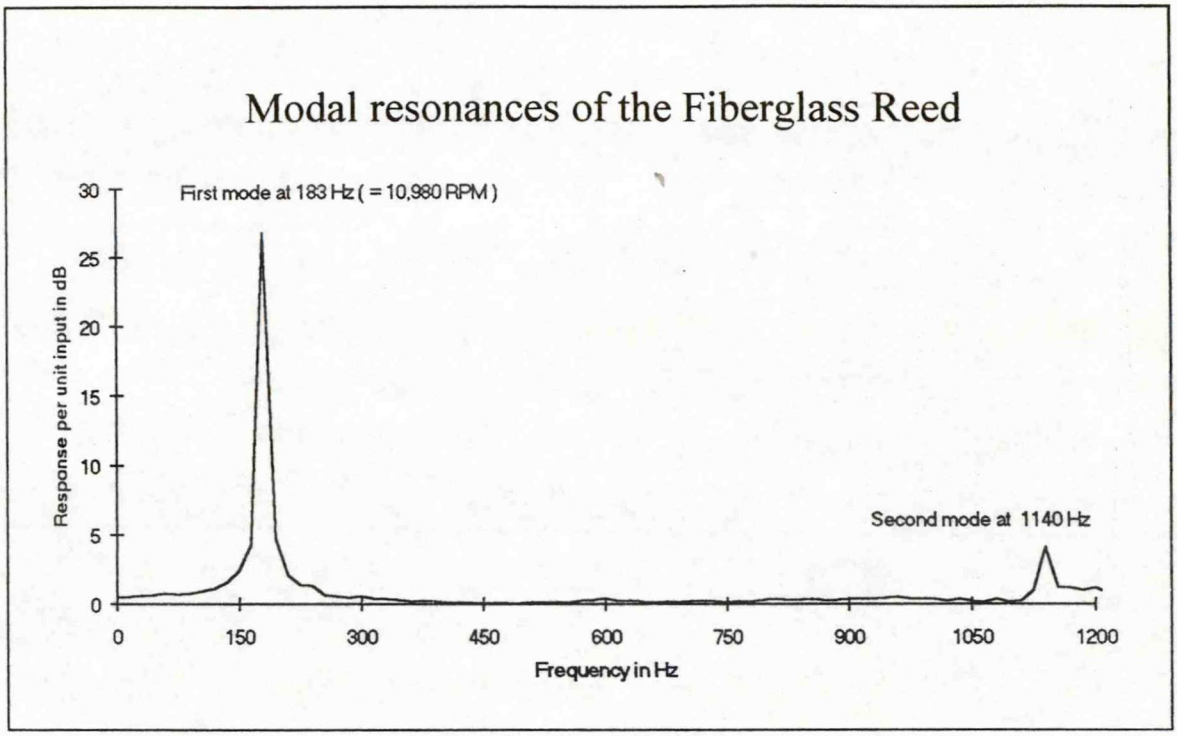
Modal resonances of the Fiberglass Reed
First mode at 183 Hz (= 10,980 RPM)
Second mode at 1140 Hz
Response per unit input in dB
Frequency in Hz
30
25
20
15
10
5
0
0
150
300
450
600
750
900
1050
1200